Design and fabrication of supercapacitors using 3D printing

A thesis submitted in partial fulfilment of the requirements of Brunel University for the degree of Doctor of Philosophy

by

Anan Tanwilaisiri

College of Engineering, Design and Physical Science
Department of Design, Brunel University

February 2018

Abstract

Supercapacitors, also known as electrochemical capacitors, have shown great potential as energy storage devices; and 3D printing likewise as a manufacturing technique. This research progressively investigates combining these two technologies to fabricate 3D-printed, electrochemical double-layer capacitors (EDLCs).

Small EDLCs were designed in a sandwich structure with an FDM-printed plastic frame and carbon electrodes. Inkjet printing was initially combined with FDM printing to produce a pilot sample with a silver ink current collector, however this performed poorly (Cs = 6 mF/g). Henceforth a paste extrusion system was added to the FDM printer to deposit the current collectors and electrodes, fabricating the entire device in a single continuous process. This process was progressively developed and tested, ultimately attaining specific capacitances of 200 mF/g.

The fully integrated 3D printing process used to manufacture the EDLCs was a novel approach. Combining the FDM printer with a paste extruder allowed for a high degree of dimensional accuracy, as well as simplifying the production process. This aspect of the design functioned successfully, without significant faults, and proved a reliable fabrication method.

The later designs used in this study provided the EDLCs extendable by incorporating connection jacks. This was to create the possibility to increase capacitance simply by connecting multiple EDLCs together. Tests of this feature showed that it worked well, with the extendable EDLCs delivering outputs very close to the theoretical maximum efficiency of the unit.

Carbon conductive paint was applied as a current collector and electrode for the 3D printed EDLCs in an exploration of metal-free 3D printed supercapacitors. These metal-free EDLCs were found to provide around 60% of the specific capacitance of the best performing EDLC variant produced (silver paint current collectors with activated carbon and carbon paint mixture electrodes).

Although considerable improvement is required to produce EDLC samples with comparable capacitances to existing commercial manufacturing techniques, this study

lays important groundwork in this area, and has introduces effective and innovative design ideas for supercapacitors and integrated 3D printing processes.

Acknowledgements

First and foremost, I would like to express my sincere appreciation for my supervisors, Dr Yanmeng Xu and Professor David Harrison for their valuable recommendations, support and encouragement. I am extremely grateful for their guidance throughout the whole period of my PhD study. I also would like to thank Professor John Fyson for his support and help. His professional advice and comments were very important in improving our experiments. I have no doubt gained great knowledge and experience through their supervision. This PhD thesis could not be achieved without their support and help.

I also would like to thank my colleagues, Mrs Ruirong Zhang and Mr Milad Arier. It is my pleasure to work with a group of excellent and helpful people. They suggested many useful ideas and helped me through our experiments. In addition, I would like to thank Dr. Esteban Schunemann who advised me on how to adjust and modify the 3D printing machine; and Mr. Thammarat Somthong who became my best friend and a good assistance through my PhD study. Special thanks are correspondingly due to the Brunel technician staff, especially Mr Douglas Rosario for his always helpful assistance.

Finally, I am also thankful to my beloved family: my father who passed away but always inspired me in memory; my mother, sisters and especially my wife, Miss Sarunyaphat Theeraumpaikul, who always encouraged and stood by me throughout this research study.

Table of Contents

Publication list

TANWILAISIRI, A., ZHANG, R., XU, Y., HARRISON, D. and FYSON, J., 2015. A novel manufacturing process for energy storage device using the combined techniques of 3D printing and inkjet printing, IMME 2015, International Conference on Intelligent Materials and Manufacturing Engineering on 2015, pp. 37.

TANWILAISIRI, A., ZHANG, R., XU, Y., HARRISON, D. and FYSON, J., 2016. A manufacturing process for an energy storage device using 3D printing, Industrial Technology (ICIT), 2016 IEEE International Conference on 2016, IEEE, pp. 888-891.

TANWILAISIRI, A., XU, Y., ZHANG, R., HARRISON, D., FYSON, J. and AREIR, M., 2018. Design and fabrication of modular supercapacitors using 3D printing. *Journal of Energy Storage*, **16**, pp. 1-7.

TANWILAISIRI, A., XU, Y., ZHANG, R., HARRISON, D., FYSON, J. and AREIR, M., 2018. A study of metal free supercapacitors using 3D printing. *International Journal of Precision Engineering and Manufacturing*, **(**accepted for publication on 10 April 2018)

Abbreviations

ABS	Acrylonitrile butadiene styrene
AC	Activated carbon
AM	Additive manufacturing
ASTM	American society for testing and materials
BPM	Ballistic particle manufacturing
CAD	Computer aided design
CMC	Carboxymethyl cellulose
CNTs	Carbon nanotubes
CV	Cyclic voltammetry
DOD	Drop-on-demand
EBM	Electron beam manufacturing
EDLCs	Electrochemical double-layer capacitors
EIS	Electrochemical impedance spectroscopy
ESR	Equivalent series resistance
FDM	Fused deposition modelling
KCI	Potassium chloride
KOH	Potassium Hydroxide
GCD	Galvanostatic charge-discharge
IJP	Inkjet printing
LED	Light-emitting diode
MJM	Multijet modelling

MWCNTs	multi-walled carbon nanotubes
NEC	Nippon Electric Company
NGP	Nano graphene platelet
LOM	Laminated object manufacturing
PANI	Polyaniline
PC	Propylene carbonate
PET	Polyethylene terephthalate
PLA	Polylactic acid
PPy	Polypyrrole
PRI	Pinnacle Research Institute
PVA	Polyvinyl alcohol
PVDF	Poly (vinylidene fluoride)
SWCNT	Single-walled carbon nanotube
SEM	Scanning electron microscopy
SFP	Solid foil polymerization
SLA	Stereolithography
SLS	Selective laser sintering
SLM	Selective laser melting
STL	Standard Tessellation Language
TEM	Transmission electron microscope
RP	Rapid prototyping
3DP	Three-dimensional printing

Nomenclature

A list of symbols is given with a brief description and units used

Symbol Definition and Units

C	Capacitance (F)
E	Energy (J)
P	Power (W)
Q	Stored charge (C)
$Qtotal$	Total supercapacitor's charge in coulombs
V	Voltage (V)
ΔV	Voltage of the discharge (V)
Δt	Discharging time (s)
I	Discharge current (A)
Cs	Specific capacitance of the electrode (F/g)
m	Total mass of activated carbon (g)

List of Figures

List of Tables

Chapter 2 Introduction

1.1 Research background

Energy has become a main focus for world powers and scientific communities. In particular, more efficient devices for energy storage have attracted great attention. One device, the supercapacitor, has increased in use significantly over the last decade and has the potential to bring about significant advances in energy storage [1-2]. Supercapacitors or ultracapacitors are capacitors that use electrode materials with a high surface-area to provide increased capacitance. Thus, supercapacitors are considered a promising development in the field of energy storage devices. The advantages of supercapacitors are their high power density, long life cycle and high reversibility. Because of these advantages, supercapacitors have been used in a wide range of applications such as for electric vehicles and portable electronics devices [2-6].

The construction of supercapacitors is similar to conventional capacitors except that the metal electrodes are replaced by electrodes made of porous material. There are three common types of supercapacitor: electrochemical double layer capacitors (EDLCs), pseudocapacitors and hybrid capacitors. In EDLCs, energy is stored by the formation of electric charges at the interface of the porous electrode material and the electrolyte. In pseudocapacitors, electrons are transferred between the electrolyte and the electrode through fast faradaic redox reactions in order to generate a current. Hybrid capacitors utilise a combination of the faradaic and non-faradaic process to store charge. One side of the electrode utilises a double-layer (carbon) material and the opposite side (positive electrode) uses a pseudo-capacitance material, such as nickel oxide [3, 5-7]. The mechanisms of three types of supercapacitor provide fast charge and discharge rates, and long cycle lives when compared with rechargeable batteries. In addition, the development of advanced nanostructured material offers the possibility of supercapacitors with a higher energy density [5-9].

Currently, several manufacturing processes for supercapacitors have been developed, including the additive manufacturing process that is generally applied in the rapid prototyping industry [9-14]. Additive manufacturing (AM), commonly referred to as 3D printing, is a method of manufacturing in which a Computer Aided Design (CAD) model is used to construct components on a layer-by-layer basis. 3D printing is considered a promising tool for the rapid production of 3D objects [15-18]. At present, the technologies of additive manufacturing are becoming increasingly capable and affordable. They have been applied to create different structures for many applications, and using several different materials [18-24]. Current research has focused on the development of new materials and the improvement of modern techniques to fabricate a wider range of 3D printed components [22-30]. Improvement in 3D printing techniques, enhanced by component placement and electrical interconnect deposition, can offer the ability to make electronic prototypes as shown in Figure 1.1. These developments provide integration of electronic components and interconnect into 3D printed devices. This 3D electronics integration is also known as 3D structural electronics or 3D printed electronics. 3D printed electronics can be designed with any form, providing a valuable improvement on conventional electronics processes [11-14, 18, 30-32].

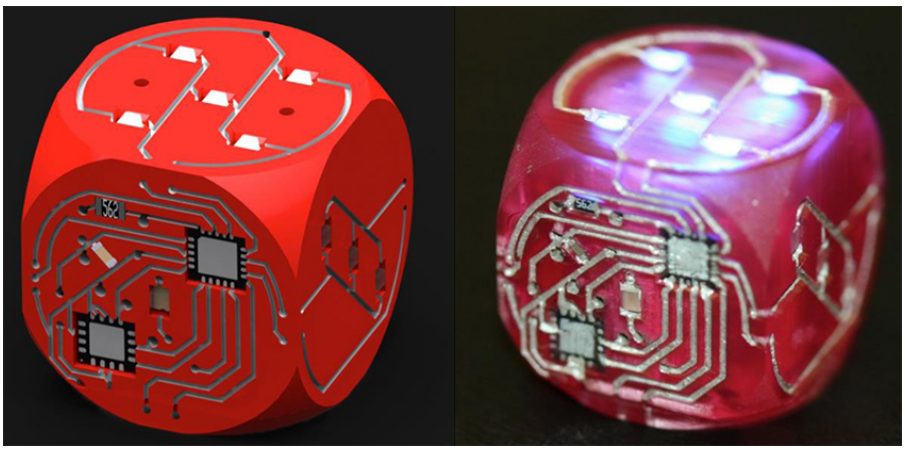

Figure 1.1 3D printing for the rapid prototyping of structural electronics [32].

In the last decade, many research groups have developed 3D printed energy storage devices, such as microbatteries and supercapacitors. Sun [31] introduced 3D interdigitated microbattery architectures (3D-IMA). For the anode and cathode materials of this 3D-IMA, $Li_4Ti_5O_{12}$ (LTO) and $LiFePO_4$ (LFP) were applied respectively. Ho

[89] also showed a zinc microbattery with an ionic liquid gel electrolyte using direct write dispenser printing. In this work, a developed dispenser printed a microbattery comprising of zinc and manganese dioxide electrodes which sandwich an ionic liquid gel electrolyte. Zhao [91] presented a 3D printed electrode for fabricating interdigitated supercapacitors using a Selective Laser Melting (SLM) method. In this research, pseudo-capacitors were produced using a 3D interdigitated Ti_6Al_4V electrode which is fine metal powder. Zhu [114] reported fabrication of 3D periodic graphene composite aerogel microlattices for supercapacitor using a direct-ink writing technique. In this study, the 3D-printed graphene composite aerogel (3D-GCA) was produced and fabricated as an electrode. Fu [154] introduced graphene oxide-based electrode inks for 3D printed lithium-ion batteries. In this work, highly concentrated graphene oxide (GO) was selected due to its excellent properties, for example a gel-like behavior and a high elastic modulus. The GO- based electrode inks with high viscosity were used to fabricate lithium-ion battery prototypes using extrusion-based 3D printing. In addition, Zhu [14] reviewed 3D printed functional nanomaterials for electrochemical energy storage. In this literature, manufacturing of batteries and supercapacitors using different types of 3D printing methods were reviewed and showed that 3D printing methods enable fabrication of functional nanomaterials with three-dimensional architectures.

From the above examples, it can be seen that 3D printing processes can be an effective method for manufacturing supercapacitors. 3D printing methods significantly expand the range of materials and designs which can be used to fabricate the electrodes. This is important since the electrical performance of supercapacitors is dependent on the material used, the component structure, and the assembly method.

1.2 Aim and objectives of the research

The manufacturing of supercapacitors can be accomplished using different methods, for example, a printing process, a coating process or a 3D printing process. In general, 3D printing techniques present several advantages over alternative manufacturing methods. First of all, 3D printing offers “freeform” design for all users. For example, complex geometries that cannot easily be manufactured using other methods can be created using 3D printing, because of the additive approach. Furthermore, functional parts with no requirement for assembly can be created with 3D printing. Recent developments in 3D

printing technology have provided the opportunity for many new applications and different types of material. These advantages of 3D printing lead to the broad research question: Are there ways in which to improve the design and manufacture of supercapacitors using 3D printing techniques?

This broad research question can be sectioned into three fundamental facets as follows:

- How to design and fabricate supercapacitors using 3D printing.
- How to manufacture extendable supercapacitors using 3D printing.
- How to characterise the electrical performance of these supercapacitors.

The aim of this research is to design and fabricate supercapacitors with a low-cost, environment friendly, additive manufacturing process. The distinct objectives of the research are as follows:

1) To design a functional shape and structure for 3D printed supercapacitors using computer aided design.
2) To fabricate the extendable supercapacitors using low cost and environment friendly materials.
3) To characterise the electrical performance of the supercapacitors.
4) To develop metal free supercapacitors.
5) To investigate factors that affected the performance of supercapacitors.
6) To improve the electrical performance and the manufacturing process of supercapacitors.

1.3 Chapter plan of the thesis

Figure 1.2 shows Methodology and thesis structure framework. This thesis consists of seven chapters described as follow:

Chapter 1 introduces the research background and importance of the research, including research questions, aims and objectives, and structure of the thesis.

Chapter 2 reviews relevant fundamental theoretical backgrounds of the supercapacitors and its components. It also outlines the principles of 3D printing and previous research

into 3D printed electronics. Knowledge gaps in the existing literature are identified and explored.

Chapter 3 describes the materials, experimental method and evaluation of electrical properties used in this study.

Chapter 4 presents the design, fabrication and characterisation of the first modular supercapacitor using a combination of inkjet printing and 3D printing. Inkjet printing in this study was selected to build the current collector on the EDLC sample. In addition, the combination of two 3D printing techniques is introduced. The casing for the device consist of two halves joined by a hinge. It can be printed in a single printing process and requires no assembly. The manufacturing process and characterisation of these supercapacitors are described in detail.

Chapter 5 describes the development in design and fabrication of extendable supercapacitors. It is explained how extendable supercapacitors were created in a single continuous process including a linking mechanism on the bottom of the supercapacitor, which offered the possibility for each frame to be directly connected. Electrode thickness, reproducibility and three different combination circuits are discussed in terms of electrical performance.

Chapter 6 investigates the different materials used to build current collectors and electrodes. Silver and carbon conductive paints were selected to be used as current collector materials. Different electrode materials (activated carbon and carbon conductive paint) were prepared as three different slurries and deposited to form the electrodes of the EDLC samples. Characterisations of the supercapacitors with different materials are described. In addition, the chapter investigates the possibilities of metal-free supercapacitors. Carbon conductive paint was used to form current collector and electrode of the supercapacitors. The concentration of carbon conductive paint, reproducibility and electrode thickness are analysed and evaluated.

Chapter 7 draws together the conclusions arising from this research investigation as well as providing recommendations of priorities for future research.

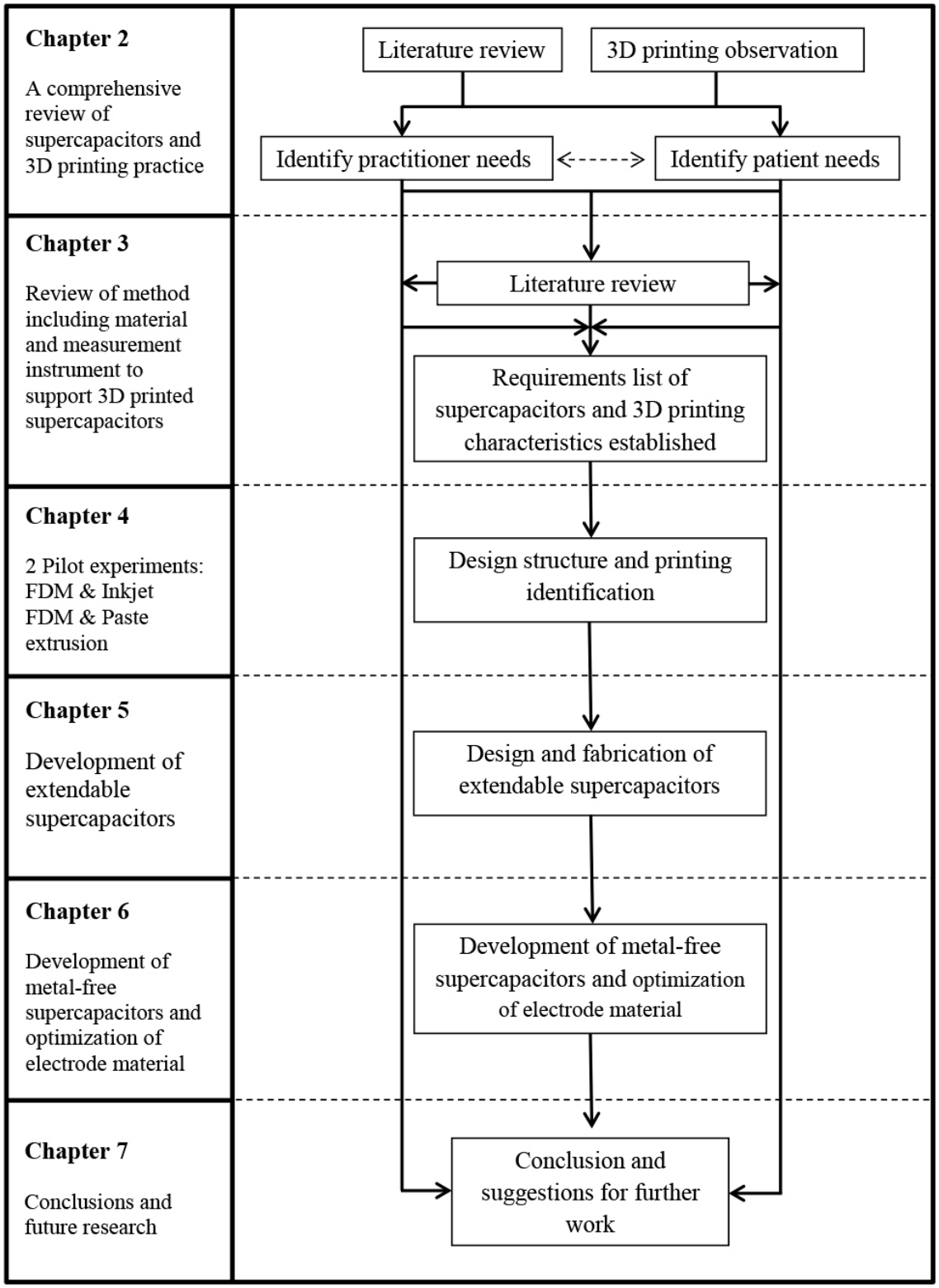

Figure 1.2 Methodology and thesis structure framework

Chapter 3 Literature review

2.1 Introduction

Supercapacitors, also known as electrochemical capacitors, have attracted great attention as energy storage devices. Supercapacitors have several advantages over batteries, such as higher power densities, longer life cycles and reversibility. They have been used as power sources in many applications, for example: portable electronic devices, electric vehicles, and emergency power supplies [1-5]. The fabrication methods of supercapacitors have been intensively researched and have successfully developed various techniques, such as dip coating [33-34], doctor blade coating [35], screen printing [36], and inkjet printing [37-38]. These fabrication methods rely on the application's requirement, for example the dip coating method is usually applied to fabricate flexible supercapacitors for wearable energy storage devices. 3D printing techniques are also one of the several methods that has been developed and used to manufacture supercapacitors. The 3D printing method differs from other methods due to its scientific theoretical backgrounds and methodologies of depositing behaviours. Thus, the scientific understandings of supercapacitor structure and materials, including fabrication techniques of 3D printing, are essential.

This chapter first reviews background and literatures of supercapacitors, after which the types of supercapacitors are discussed. The structure and materials used, including the manufacturing process of supercapacitors are then introduced, which precedes an overview of 3D printing technologies and an introduction to two 3D printing methods used in this study: fused deposition modelling (FDM), and paste extrusion system. Finally, knowledge gaps are identified and investigated with regards to how fabrication of supercapacitors using 3D printing methods are significant and why further research is required in this field.

2.2 Background of supercapacitors

Supercapacitors are currently known by various names: ultracapacitors, electrochemical capacitors, or electrochemical double-layer capacitors. The different names derive from their different manufacturers. Nippon Electric Company (NEC) were the first company to introduce the device into the commercial market, and ever since the term “supercapacitor” has been in common usage. Another word commonly used is “ultracapacitor”, which originates from the Pinnacle Research Institute (PRI), who provided these devices for the US military [3, 5, 8-9]. Within this thesis, the device is referred to either by the term “supercapacitor”, or “electrochemical double-layer capacitor” (EDLC).

The operational principle of supercapacitors is the same as for conventional capacitors. Conventional capacitors consist of two conductive materials insulated by a dielectric, as shown in Figure 2.1. Capacitors can be used to store energy by charging a voltage across the two electrodes, causing opposite charges to accumulate on the surface of each electrode. The dielectric functions as a separator that insulates the charge, so that an electric field is generated and stored [3-10].

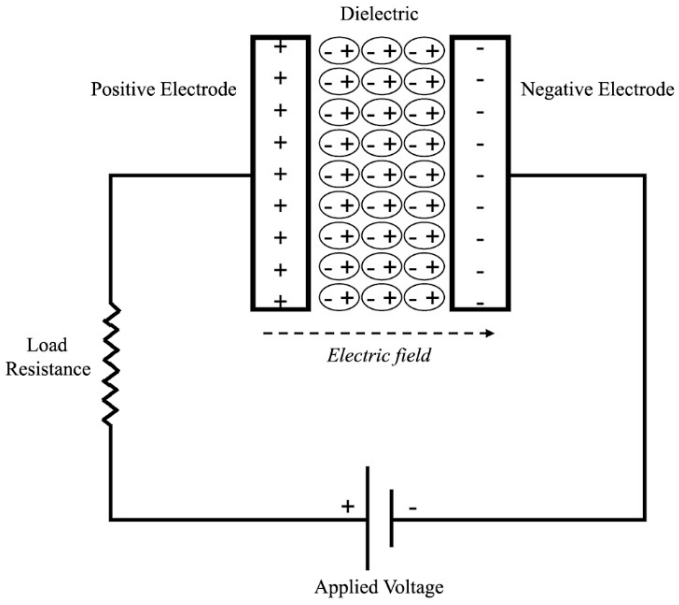

Figure 2.1 Schematic of a conventional capacitor [3].

Conventional capacitors offer low capacitance, and have been used as energy storage devices for almost a century, suitable for low power electronics devices, such as a component in an analogue circuit, or a short-term memory back-up supply [7-10]. Compared to other energy storage devices, such as electrochemical batteries or fuel cells, conventional capacitors provide high power density, but low energy density. Power density corresponds to the time that is required to deliver the energy, which means the conventional capacitors release energy quicker than a battery. On the other hand, conventional capacitors store less energy per unit mass or volume than electrochemical batteries (low energy density) [3, 8-10]. Research and developments in the past several decades have introduced novel materials and manufacturing techniques that have improved the electrical performance of conventional capacitors. Using high surface-area and low resistance material, and by improving the charge transfer process in the electric double-layer, high-power electrochemical capacitors can be fabricated that provide a higher energy density than regular capacitors, and a higher power density than standard batteries [8-10]. Despite these improvements, supercapacitors have been developed and governed by the similar basic principle as conventional capacitors. Nonetheless, EDLC uses high surface areas and thinner dielectrics, which decrease the distance between the two electrodes, resulting in increased capacitance [3, 7-10].

Supercapacitors employ thin dielectric layers and high surface area electrodes to deliver higher energy density than conventional capacitors. There is no strict measurable characteristic requirement distinguishing a capacitor and a supercapacitor, but generally devices termed supercapacitors should deliver an energy density of at least 0.2 Wh/kg, and normally several orders of magnitude higher than that.

Supercapacitors can be employed in a variety of energy capture and storage applications, either independently or in combination with batteries or fuel cells. Supercapacitors have advantages over conventional energy storage devices in terms of their large number of charging-discharging cycles, high power capability, and robust thermal operating range. Supercapacitors can store a large amount of charge that can be supplied at a higher power rating than rechargeable batteries, however the energy density of supercapacitors is lower than that of batteries and fuel cells. This necessitates coupling with batteries or other power sources for applications requiring an energy supply for longer periods of time. [7-10]

As shown in Figure 2.2, a supercapacitor consists of two current collectors, two electrodes, and a separator in the middle. The separator is an ion-permeable material which not only functions as an insulator preventing electrical contact between the electrodes, but also allows ions from the electrolyte to cross over to the other surface. Unlike conventional capacitors, which store charges in the dielectric layer, EDLCs store energy at the interface between the electrode material and the liquid electrolyte. The ions in the micropores of the electrode are transferred between the electrodes by diffusion through the electrolyte [6-10].

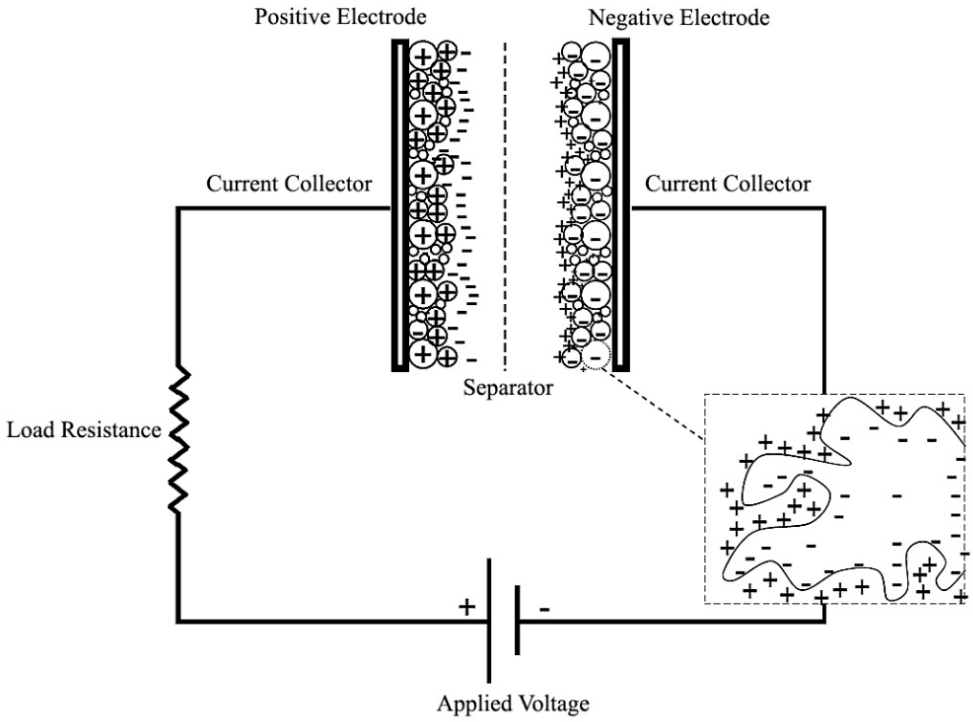

Figure 2.2 Schematic of an electrochemical double-layer capacitor [3].

The performance of typical energy storage devices can be represented in the form of a graph known as a Ragone Plot. This graph indicates the power density versus the energy density of different energy storage devices, as shown in Figure 2.3 [3, 5-10]. It can be seen from Figure 2.3 that EDLCs fill a considerable capability gap between conventional capacitors and batteries. EDLCs are in the position of providing better energy density than conventional capacitors and greater power density than batteries [9-10]. Furthermore, EDLCs not only bridge the capability gap between capacitors and batteries, but also may be used in combination with both energy storage devices to enhance their performance. For example, the combination of an EDLC with a capacitor might improve its performance in terms of energy density, or combining with a battery may enhance its performance in term of power density [5-7]. Moreover, supercapacitors are an attractive energy storage device because of their longer life cycle, since there is no, or insignificantly little, degradation caused by the small chemical charge transfer reactions. Most rechargeable batteries left in open conditions for months will degrade and become useless due to self-discharge and corrosion. In contrast, supercapacitors maintain their capacitance and thus are capable of being recharged to their original condition, although self-discharge over a long period of time can lead to a lower voltage. It has been reported that supercapacitors can maintain near full capacitance for many years in ambient conditions. Measuring degradation would be of interest but is difficult due to the length of time required to gather meaningful observations. [5-10]

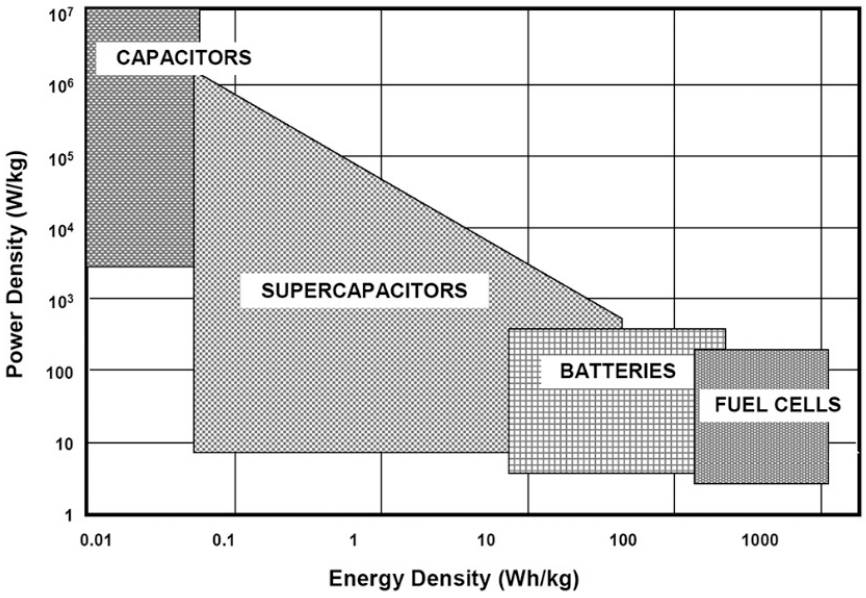

Figure 2.3 Ragone plot of various energy storage devices [3].

2.3 Types of supercapacitors

Based on the storage mechanisms, supercapacitors can be divided into three typical classes: electrochemical double-layer capacitors (EDLCs), pseudocapacitors, and hybrid capacitors, as shown in Figure 2.4. Each class presents a different mechanism for storing charges, which are: non-faradaic, reversible faradaic redox, and a combination of the two [3, 5-7].

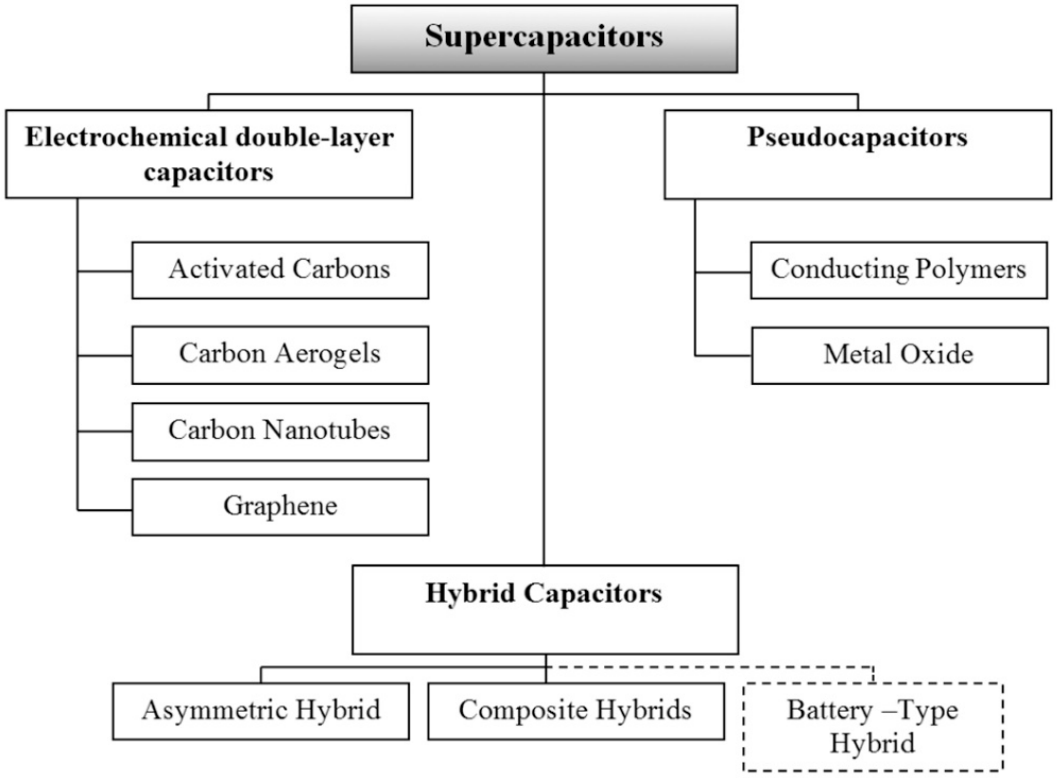

Figure 2.4 Types of supercapacitors [3].

2.3.1 Electrochemical double-layer capacitors (EDLCs)

In electrochemical double-layer capacitors, charge is stored in a double-layer construction. The energy storage is based on the formation of separated electric charges at the interface of a porous electrode material and an electrolyte. The charge storage process is non-faradaic and chemical oxidation-reduction (redox) reactions should not occur [3, 8-10].

To store energy in EDLCs, potential is applied so the charge accumulates on the electrode surface. Ions are diffused across the separator through an electrolyte solution

and enter the micropores of the electrode of the opposite charge. Each electrode can produce a double layer of charge because of the engineering of the electrode that prevents the recombination of the ions. The charge storage in EDLCs is highly reversible because the charge does not transfer between electrode and electrolyte. There is no chemical or composition conversion related to non-faradaic processes. For this reason, the high cycling stabilities EDLCs offer present the ability to operate with stable performance in application [5-10].

EDLCs are often known as 'carbon-based supercapacitors', because of the materials used to build the electrodes. A wide range of porous carbon materials have been employed in EDLCs, such as activated carbon (AC), carbon aero gels, carbon nanotubes, and graphene [5, 8-10].

2.3.2 Pseudocapacitors

In contrast, pseudocapacitors are based on several faradaic mechanisms, for example underpotential deposition, redox pseudocapacitance and intercalation pseudocapacitance. In underpotential deposition, a single layer of metal ion is deposited onto a different metal surface, for example the deposition of lead onto a gold electrode. In redox pseudocapacitance (as in $RuO_2 \cdot nH_2O$), electrons are transferred between the electrolyte and the electrode through a fast a faradiac redox reactions in the charge storage process. Intercalation pseudocapacitance arises from the intercalation of ions into the layers of redox-active electrode materials accompanied by a faradaic charge-transfer without generating phase change. In this regard they are unlike EDLC in that the electrons are stored at the electrode, or the electrolyte surface interface, by a simply physical process. Fast reversible oxidation/reduction reactions occur, providing 10 to 100 times the capacitance of pure carbon-based EDLCs [3, 5-10].

Ruthenium oxide is one of the comprehensively investigated materials for pseudocapacitors. This metal provides various redox stages, for example Ru (IV) / (III) and Ru (III) / Ru (II) in sulfuric acid (H_2SO_4), which can supply more electron transfer to increase the capacitance [5-8]. Although ruthenium oxide offers excellent electrical performance; its high cost and toxicity limit its practical application in supercapacitors. For this reason, how to improve less toxic and less expensive materials has been frequently studied. This has led to the introduction of different pseudocapacitor electrode materials, such as cobalt oxide, nickel oxide and conductive polymers. These

alternative materials can provide promising electrical performance, however they are still lacking in terms of long cycle stability [5-10].

Faradaic reactions are electrolytic reactions that obey Faraday's law of electrolysis: that the mass of the substance liberated at the electrode is proportional to the charge passed through the substance. Derivatives of these reactions may also be described as faradaic. Both faradaic and non-faradaic reactions can occur in electrode reactions. This is relevant to the difference between pseudocapacitors and EDLCs (two types of supercapacitor), because pseudocapacitors generate relatively more faradaic reactions.

2.3.3 Hybrid capacitors

Hybrid capacitors utilise a combination of the faradaic and non-faradaic process to store charge. One side of the electrode utilises a double-layer (carbon) material and the opposite side (positive electrode) uses a pseudo-capacitance material, such as nickel oxide [3, 5-7]. In addition, these supercapacitors can be assembled using different mixed metal oxides or doped conductive polymer materials. The hybrid capacitors can give higher energy densities than double-layer capacitors due to the electrochemical redox occurring at the faradaic electrode. However, employing faradaic materials for manufacturing electrodes in hybrid capacitors may decrease cycle stability [8-10].

To summarise, supercapacitors can be divided into three types according to their mechanisms. The electrochemical double-layer capacitor has presented several advantages such as high power density, long cycle stability and high reversibility. Electrode materials used to fabricate are reliant on carbon materials which provide easy processing, low costs, non-toxicity, higher specific surface area and good electronic conductivity. Based on these advantages of the device, including materials used, EDLC was selected to investigate further in terms of cell design and material used, including manufacturing techniques. This investigation focuses on the fabrication method of supercapacitors with the purpose of being environmentally friendly and cost-effective.

2.4 Supercapacitor components and materials

As mentioned above, the electrochemical double-layer capacitors are comprised of two current collectors, two carbon-based electrodes, an electrolyte and a separator. All components of supercapacitors need to be optimised in order to improve electrical

performance [5]. Selection of materials used in each part, such as electrodes, electrolyte, and conductive current collector, requires careful attention. Moreover, the manufacturing process of the supercapacitor also need be considered in terms of cost and safety [10].

2.4.1 Electrode materials

In EDLC, capacitance and charge storage heavily depends on the electrode materials used. The electrode materials in EDLC can be fabricated from different forms of carbon, for example activated carbon (AC), carbon nanotubes (CNTs), carbon aerogel, and graphene. All these carbon materials share common qualities such as large surface area, porosity, good surface wettability, high conductivity, and long cycle stability [39-47].

The wettability of a solid is the extent to which contacting liquids will tend to spread across its surface, and hence spread within a porous form of the material. The wettability of a solid is usually quantified by measuring the contact angle of a droplet of water placed on a flat surface of the solid material. The relationship between the wetting contact angle and the surface tensions or surface free energies at interfaces are described by the capillary equation of Young [186]:

$$\sigma_{sl} - \sigma_{sv} + \sigma_{1v} \cos\theta = 0$$

where σ_{sl}, σ_{sv}, σ_{lv} are the surface tensions for solid-liquid, solid-vapour and liquid-vapour interfaces, respectively, and θ is the contact angle. According to Young's equation, an increase in the surface tension of the solid-liquid and liquid-vapour interfaces is associated with a decrease in wettability.

The wettability of carbon material is of considerable importance in maximizing the access of electrolyte to the surface of porous carbon electrode. Selecting an activated carbon electrode with high specific capacitance is one of the primary focuses in the development of supercapacitors. Surface modification is believed to be an effective means to achieve this goal. A properly modified activated carbon can increase wettability, allowing electrolytes to readily penetrate the smaller pores [41].

1) Activated carbon (AC) AC can provide high surface area due to its complex porous structure, comprised of various particle sizes. AC, when utilised as the electrode in an

electrochemical double-layer, stores charges principally at the interface between the electrode and the electrolyte. Hence, the surface area of the carbon that can be accessible to the electrolyte is directly related to the capacitance. The specific capacitance of AC ranges between 50 and 200 F/g depended on electrolyte used [39-40].

There are many important factors that influence the electrical performance of carbon material: specific surface area, pore size distribution, pore shape and structure, and electrical conductivity. The most important factors, among these, are specific surface area and pore size distribution. In general, larger specific surface areas of AC possess a higher capability for accumulating charge at interface of the electrode/electrolyte [39-43]. In order to increase the specific surface area, many studies have investigated using different treatment techniques, such as heat treatment, alkaline treatment and plasma surface treatment with NH_3. By using these treatment methods, carbon surface can be efficiently made into micropores resulting in increases in the specific surface area [41-43]. Lota et al [137] have presented a simple method to re-activate a commercial AC using KOH at 850 ºC as shown in Figure 2.5. The results showed that the specific surface areas of the commercial AC were re-activated, which resulted in increasing the specific capacitance of the carbon material. The specific capacitance of the re-activated carbon material was three times higher than that of the commercial AC.

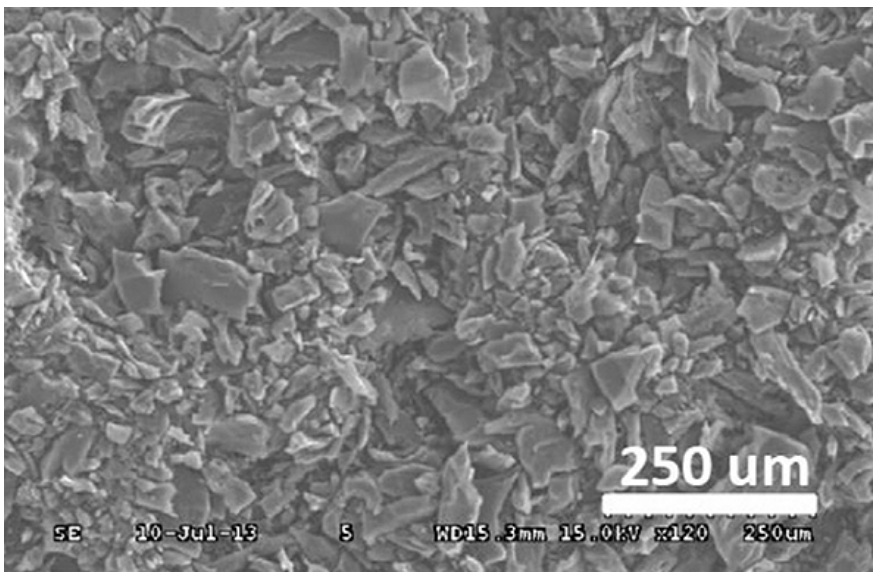

Figure 2.5 SEM of AC synthesized by heat treatment with KOH activation [138].

Even though specific surface areas are directly linked to the capacitance, for activated carbon material in practice, not all the increase in surface area translates to increasing the capacitance of the device. The pore size distribution is one of factors that directly affects electrical performance of EDLCs, because it affects the diffusion of electrolyte ions [40-44]. Pore size can be split into three categories: micropore (d <2 nm), mesopores (2 nm < d < 50 nm) and macropores (d > 50 nm). The analytical method, known as the Bruaver, Emmett and Teller (BET) technique, is usually employed to measure the surface area of the porous carbon material. In this method, gas that has no chemical reaction with the surface material is utilised to quantify the specific surface area of the porous material by calculating the total adsorbate gas relative to a monomolecular layer on the surface [113]. It is believed that electrolyte ions cannot permeate all micropores in the carbon electrode layer which causes some micropores to be unable to contribute to charge storage. As a result, the optimal pore size must be selected in relation to the size of the ions in the electrolyte solution [40-44].

There have also been studies into the pore distribution of different carbon. [113-114] For example, Grylewicx et al. [113] have reported the effect of pore size distribution of coal-based activated carbons on EDLC with an acidic electrolyte. The results indicated that a large surface area of AC, with the optimum range of mesopore content between 20% and 50%, was suitable for AC material in EDLCs.

An additional factor that should be of concern is the conductivity of the electrode, which affects the power density of EDLCs. Conductivity is related to the particle size of materials. Materials that have good conductivity typically have a large particle size which, because of the reduced surface area, decreases their potential for energy storage. Correspondingly, materials with high surface area generally have smaller particle sizes and thus higher electrical resistance. So, there is a trade-off. Power density of EDLCs can be enhanced by using activated carbons with larger pores, but this decreases its ability to store charge, because of the reduced surface area [41-47].

2) Carbon nanotubes (CNTs) CNTs are a form of engineered carbon that is attractive to use as a capacitor electrode material due to certain distinct and useful characteristics. CNTs are comprised of graphitic walls constructed in near one-dimensional (1D) cylinders as shown in Figure 2.6. CNTs offer superior properties, such as large area of exposed surface, several storage spaces for electrolyte ions, high electrical conductivity and also some highly desirable mechanical properties. CNTs can be divided into two classes: single-walled nanotubes (SWCNTs) and multi-walled carbon nanotubes (MWCNTs). The thickness of the tubes determines these classes. [3, 5, 122].

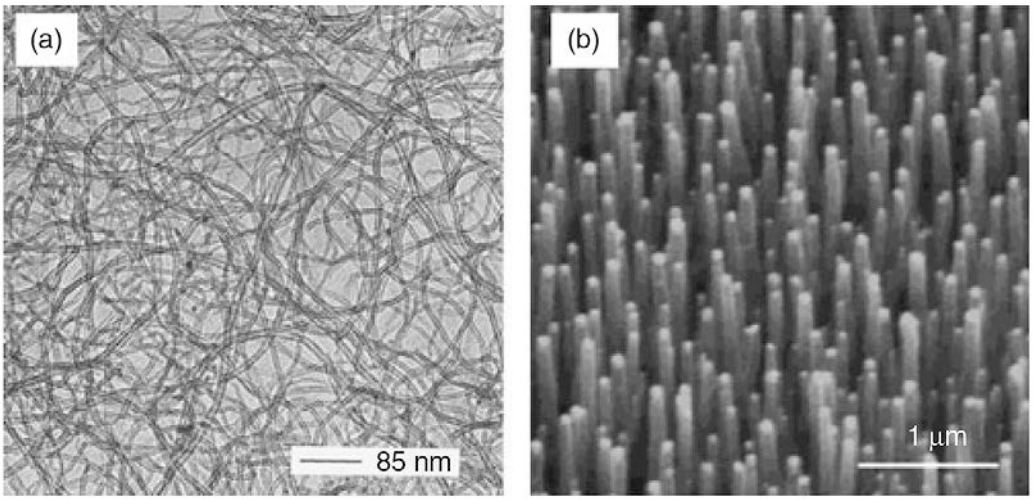

Figure 2.6 (a) Transmission electron microscope (TEM) image of catalytically grown carbon nanotubes. (b) Scanning electron microscope (SEM) image of a carbon nanotube forest [5].

Supercapacitor electrodes made from CNTs are generally grown as an entangled mat of carbon nanotubes, with an open and accessible network of mesopores. This causes electrolytes to diffuse more easily and helps decrease the equivalent series resistance (ESR). In addition, the connection between mesopores allows for the usage of almost all the available surface area, so the charge can be evenly distributed upon charging [3, 5].

The ESR of CNT electrodes can be further reduced using modern fabrication methods and preparation processes. For example, CNTs can be grown directly onto the current collector, or enhanced through heat-treatment. Chen [123] has reported on the method for CNTs electrode fabrication by growing the CNTs onto graphite foil. This method was shown to minimize the contact resistance between the current collector and the electrode material, and also simplified the process of electrode fabrication. The

maximum specific capacitance obtained was about 115.7 F/g at scan rate 100 mV/s in 1.0 M H_2SO_4 aqueous solution.

CNTs can store specific capacitance between 15 and 200 F/g depending on the morphology and purity. Chemical vapor deposition and carbon arc discharge are the currently implemented techniques for producing lab-scale quantities of high purity CNTs. Nonetheless, these methods require further research in order to scale up production and purification [5].

3) Graphene Graphene is an allotrope of carbon in the form of flat 2-D honeycomb monolayer sheets. It is the basic building block of all graphitic carbons, such as particle, 1-D CNTs, and 3D graphite as showed in Figure 2.7 [124, 127]. Graphene offers large surface area, as well as high thermal and electrical conductivity, chemical stability and mechanical strength.

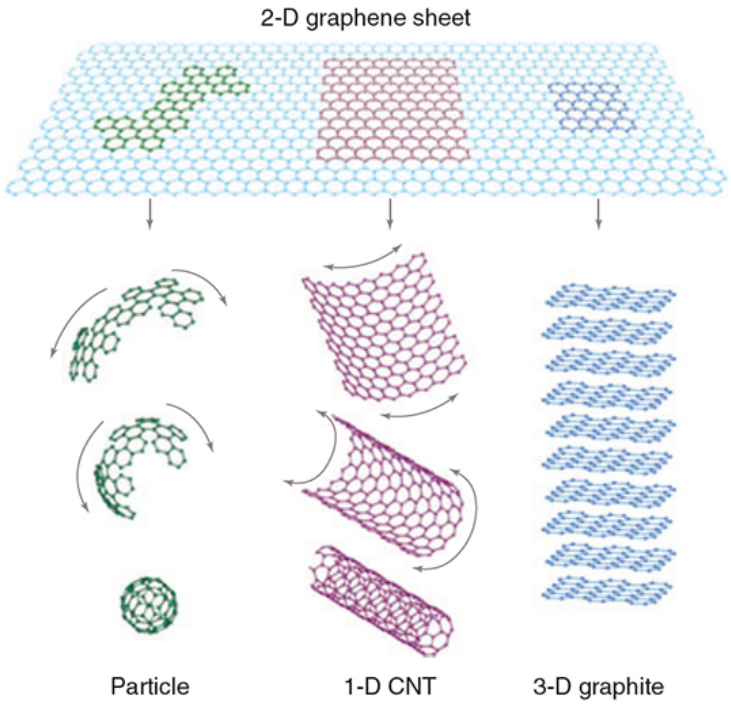

Figure 2.7 Illustration of 2-D graphene sheet as the basic construction units for other carbon materials such as particle, 1_D CNT, and 3-D graphite [5].

These properties distinguish graphene from other carbon materials and make it increasingly the most advanced material for supercapacitor applications [125-126]. There are several techniques used to produce graphene sheets, such as chemical exfoliation [128], epitaxial growth on SIC surface [129], mechanical exfoliation [130], unzipping carbon nanotube [131], and chemical vapor deposition [132]. These different production methods have a significant effect on the properties of the graphene produced. For example, while the highest quality graphene could be produced using a chemical exfoliation method, the chemical vapor deposition method could improve the productivity of the graphene [128, 132].

In theory, graphene may possess a maximum surface area of 2675 m^2/g, and hence a maximum capacitance of 550F/g when all the surface area is entirely employed. In practice however, the specific capacitance of graphene, especially graphene sheet, is usually limited to between 100 and 200 F/g due to agglomeration and restacking [5]. In order to reduce restacking, Wang [133] have introduced the use of a combination of CNTs as a spacer between graphene sheets as shown in Figure 2.8. This significantly expanded the capacitance to 318 F/g.

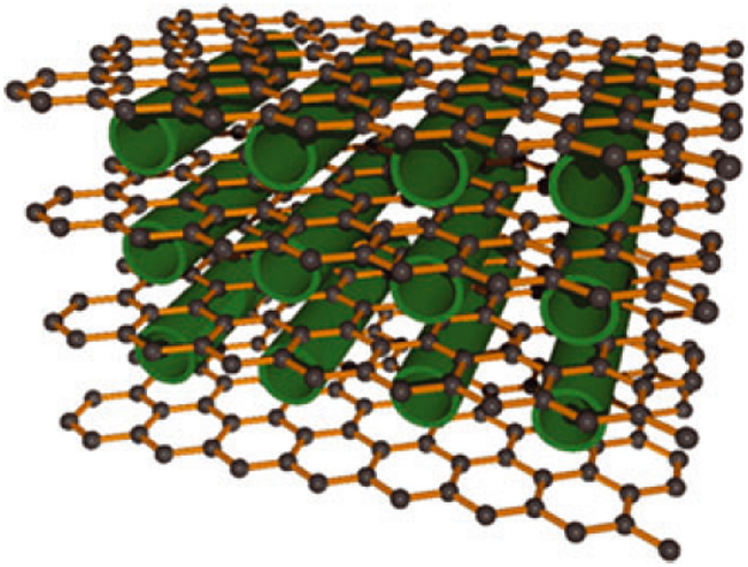

Figure 2.8 Model of graphene sheets separated by CNTs [133].

Other methods also have been demonstrated. Zhu [134] managed to extend the surface area of graphene using KOH-activated graphene. By exposing hidden graphene sheets and producing extra pores resulted in an increased surface area of up to 3100 m^2/g. Hassan [135] have tested a method to increase the electrical conductivity and promote graphene-ion interaction within the electrolyte. In this method, nitrogen atoms were doped with graphene planes to increase the capacitance to 194 F/g as shown in Figure 2.9.

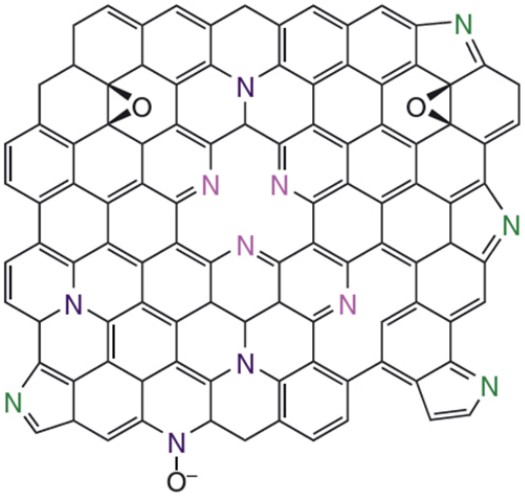

Figure 2.9 Nitrogen-doped graphene structure. [133].

Although graphene has been continuously studied as an electrode material for supercapacitors, practical applications have yet to be realised. This is due to the difficulty of manufacturing the material to a high-quality standard in a reliable and scalable approach [136]

In summary, activated carbon (AC) seems the ideal material for EDLC fabrication, as it is inexpensive, easy to process, non-toxic, and has a high specific surface area and good conductivity. In this study, AC (AR grade, 1375 μΩ·cm) purchased from Sigma-Aldrich was selected to build the electrode for the EDLC sample.

2.4.2 Current collector for EDLC

In EDLCs, both electrodes are generally formed on metal current collectors, such as aluminium foil and copper foil for the anode and cathode respectively. EDLC devices require the current collectors to be completely functional because conductivity of the

electrode is inadequate [5-6, 9-10]. The material used as current collectors in EDLCs must be electrically conductive, and resistant to chemical weathering caused by the electrolyte solution. Based on these requirements, the standard materials used for current collectors are aluminium, steel, and iron [48-49]. During the charge and discharge processes in a supercapacitor, current collectors allow the flow of charge carriers (electrons) through an external circuit between the active materials. Therefore, an effective surface contact between the current collectors and the electrodes is necessary to decrease the contact resistance. Otherwise, a high interfacial resistance can result from oxidation which arises from unstable electrochemical materials in both the current collectors and electrodes [5-6, 49-51].

Current collectors are an important component in terms of the performance of EDLCs. Efficiently designed current collection could achieve current densities around 30 A/g, energy densities around 40 Wh/kg, and a power density of 40 kW/kg. Deficiencies with the current collectors can see this performance reduce markedly however.

Creating firm, low resistance connections between the electrode and the collector is a particularly important aspect for maintaining the performance of the component materials. To improve the molecular contact between the electrode and the collector, electrode pastes or deposits can be applied or grown directly onto the collector. Examples of such methods include spin coat, drop coat, spray coat and electrode paste application. When combined with the use of a conductive coating very low resistances can be achieved. Alternatively, thin lead and gold films have been demonstrated to be effective in combination with graphene, and silver paste has been widely used to create an efficacious contact with roughly surfaced active materials. Connectivity becomes even more important when electrodes are free-standing, since contact is not fixed. When it is impossible to make a firm contact through a drying or annealing process, high pressure lamination is necessary to reduce resistance and maintain component performance.

As well as connectivity causing resistance, internal resistance can also be a substantial issue. Electrode pastes with poor conductivity or percolation can result in suboptimal conduction pathways through the electrodes and hence internal electrical resistance. The important factors to consider to limit internal resistance are the active materials used and the binding quality of the electrode fabrication. Substandard binding can not only cause internal resistance reducing the performance of the device, but also operational

failure. One method to reduce internal resistance is to apply a conductive carbon filler which may improve percolation by up to 20%.

Current collectors and conductive pastes also should be considered in terms of their mass. Since various performance measures are evaluated on a per gram basis, maximising performance must also involve minimising non-capacitive weight. Effective cell designs should use only thin and non-heavy collector metals, and minimal paste additives.

Degradation can also be a significant problem for current collectors, especially over a long cycle period. As well as the gradual loss of the electrode material to the electrolyte, metal current collectors can reduce in size. This results in a lower cycle life and capacitance of the device. Hence the combination of materials used must be carefully considered with expected operating temperatures in mind.

In addition, it is also important to consider how the current collectors will affect the efficiency of heat transfer. Metals with high thermal conductivity are ideal in this respect, as they allow heat to transfer quickly to the end plate for passive cooling via heat sinks. Amongst the most regularly used are aluminium foils. As well as good thermal transmission, they are also cheap, lightweight, and have good electrical conductivity.

Many researchers have reported different methods of improving the performance of current collectors in supercapacitors [48, 142-149]. Yu et al [142] reported to use stainless steel fabrics as the current collectors in order to fabricate graphene-based supercapacitors. Mehrabi-matin et al [143] presented a silver fiber fabric (SFF) and stainless steel foil as the positive and negative current collector, respectively. Portet et al [144], have introduced a sol-gel deposit of a conducting carbonaceous material for modification of an aluminium current collector surface. In this method, the film consisting of carbonaceous material powder in a polymeric sol was coated onto aluminium foil to use as a current collector in a supercapacitor system. Another study by Bo et al [145] presented vertically oriented graphene (VG) nanosheets covering a surface of nickel foam using the plasma-enhanced chemical vapour deposition (PECVD) process. In this study, the VG nanosheets were applied as a bridge to improve the connection between current collectors and active electrode material. There are also several studies of metal-free supercapacitors which attempt to prevent corrosion

problems of current collectors [48, 146-149]. In most of these works, current collectors were fabricated using graphite foil or carbon nanotubes using coating method on different thin films. Zhou et al [146] employed super-aligned carbon nanotubes as a nanoporous current collector. Super-aligned carbon nanotubes were produced that combine the advantages of carbon nanotubes and metal oxide nanoparticles and were made into a thin film applied to the current collector. Dyatkin et al [147] reported a green supercapacitor using environmentally friendly materials. In this study, three different carbon materials (carbon nanotubes, carbon fibre mat and graphite-foil sheets) were examined and the results showed that graphite-foil sheets have sufficient conductivity and are suitable for use as current collectors. Thin film supercapacitors in work by Liu et al [148] were created by combining all-carbon thin films with plastic paper and gel electrolyte. Current collectors in these supercapacitors were made from highly-conductive double-wall carbon nanotubes, (DWCNT) coated onto plastic papers. Also Xu et al [149] reported a supercapacitor with a high capacitance using a metal-free electrode material. In this research, polyaniline (PANI) and graphene composite monolith were constructed which showed a record high volumetric capacitance of over 800 F cm^{-3}. Moreover, there is another research in metal-free supercapacitors using an aqueous electrolyte and low-cost carbon materials introduced by Blomquist et al [48].

To conclude, when selecting the material for the current collectors of an EDLC, the material should have low volume resistivity, good conductivity, and chemical stability.

2.4.3 Electrolytes for EDLC

Aside from the electrode, performances of supercapacitors also rely on the electrolyte. The type of electrolyte is used to define the operational voltage window of a supercapacitor. For example, for EDLCs with an aqueous electrolyte, an operating voltage of 1.0 V is usually defined. Meanwhile, a supercapacitor with an organic solvent can achieve a working voltage in the range of 2 - 2.5 V [5-6, 9-10]. Moreover, the electrolyte affects the power density and energy density of the supercapacitor. While the resistivity of the electrolyte can limit the power density, energy density can also be limited by the ion concentration and operating voltage of the electrolyte [5-6]. In addition, it is believed that the resistance of the EDLC cell effectively relies on the electrolyte's resistivity and an appropriate ion size of the electrolyte related to the pores of the electrode particle. The electrolyte in EDLCs can be divided into two types: aqueous electrolyte and organic electrolyte [9-10].

1) **Aqueous electrolytes**, such as sulfuric acid (H_2so_4), potassium chloride (KCI), and phosphoric acid (H_3PO_4), are commonly used as aqueous electrolytes in research stages. They offer abundance, low cost, easy handling in an open environment, and low ionic resistivity. EDLCs with an aqueous electrolyte normally have a working voltage of about 1.0V, and they normally possess resistivity of about 1 - 2Ω·cm, which is lower than the resistivity of those with an organic electrolyte (20 - 60Ω·cm). Therefore, the pore size of electrodes in EDLCs using an aqueous electrolyte is required to be larger than for EDLCs using an organic electrolyte [6, 10].

2) **Organic electrolytes**, such as acetonitrile and propylene carbonate (PC), are usually employed in commercial supercapacitors. This type of electrolyte provides a wide range of operating voltage windows from 2.2 - 2.7V. This property allows the organic electrolyte to provide the energy density to the commercially required standard. By comparison, acetonitrile has a lower ion resistivity than PC, but it is toxic and flammable which causes an issue for practical safety [5, 9-10]. There are studies in effect of electrolyte in EDLCs which investigate the degradation of carbon electrodes in EDLCs when using an organic electrolyte. The results demonstrate that the pores of the electrodes are blocked by the decomposition of the organic electrolyte which decreases its capacitive performance and cyclic stability [52-53].

In conclusion, the operating voltage of a supercapacitor is dependent on the operating voltage of the electrolyte and this directly affects the energy density. Power density also relies on the electrolyte conductivity. To select an appropriate electrolyte, the size of electrolyte ions in relation to the pore size of the electrode particle should be considered. In this study, aqueous electrolyte (phosphoric acid, H_3PO_4) is selected because of its advantageous high conductivity, low cost and simple preparation at ambient conditions. The size of the ion is also suitable for the pore size of the electrodes used.

2.4.3 Separators

Most research in this area has attempted to discover ways to improve the performance of EDLC electrodes, however there is still limited research that investigates the engineering of separators. The separators used in supercapacitors can be made of polymers, glass, ceramics, or cellulose paper, depending on the type of electrolyte used and temperature of operation. The important function of the separator in a

supercapacitor is to prevent the incidence of electrical contact between both electrodes, and to provide ions transfer to the electrolyte [5-6]. A poorly designed separator can increase resistance in the cell and also, in the worst cases, cause a short circuit. To select an adequate separator, the following must be considered:

1) Nonconductive (electron cannot transport between electrodes)

2) The electrolyte ion permeability with low ionic resistance

3) The chemical resistance to both materials used as electrolyte and electrode

4) Easily wetted by electrolyte [5-6, 9-10].

A separator is usually a porous membrane/mat sandwiched between anode and cathode. Its main function is to physically separate the anode and cathode to avoid electrical short circuits, and at the same time provide a pathway for ionic charge carriers transport in liquid electrolyte throughout the interconnected porous structure. The wettability of separator can affect the internal ionic resistance and the electrolyte filling time during cell assembly. An optimal separator should absorb the electrolyte droplet instantaneously upon contact. Improving the wettability of the separator by means of the electrolyte contributes to decrease physical resistances caused by the separator for ions.

EDLCs with organic electrolytes typically use microporous polymers and cellulose paper separators, while the devices with aqueous electrolytes conventionally use glass, mica or ceramic separators. Paper-based separators are not appropriate for EDLC that operate in high temperature environments due to their poor mechanical strength [9]. Polyolefin-based separators, however, offer numerous advantageous properties, such as high porosity, flexibility, low cost, improved mechanical strength, and corrosion resistance. This material continues to displace natural materials, such as glass and cellulose fibres, due to its superiority in those properties. Polyolefin separators can also be employed in both electrolyte systems, although it does have a significant drawback when used with aqueous electrolytes: its hydrophobic effect complicates the wetting of the electrolyte. To overcome this difficulty, graft polymerisation can be used treat the polyolefin material to modify its surface properties and increase hydrophilicity [5, 9]

The structure of the separators can be classified into four types: microporous films, nonwovens, gel polymers, and solid polymers. Microporous films are usually made from nonwoven fibres, such as cotton, glass, polyester, polyolefins (PP and PE), or PVC. These films comprise of copious minute pores (5 to 10 nm in diameter) and are regularly utilised in lower temperature devices. In addition, microporous separators are generally used with both electrolytes (organic and aqueous electrolyte). Nonwovens present consistent thickness, weight, and degradation resistance, but they possess inefficient pore orders and are difficult to manufacture thinner than 25 µm. Nonwovens are commonly made from PTFE, PVC, PVdF, or a combination of polyolefins, and are the preferred separator for use in alkaline systems [9].

2.5 Manufacturing processes for supercapacitor

Supercapacitors can be fabricated using several techniques depending on application requirements [10]. The parameters in different manufacturing techniques differ between commercial products and research devices. The manufacturing process of supercapacitors has been studied and developed for several decades [10-14]. A wide range of fabrication techniques have been demonstrated, such as doctor blade coating [35], dip coating [33-34] including printing methods, such as screen printing [36], roll-to-roll printing [54], and inkjet printing [37-38].

2.5.1 Dip coating method

Dip coating is a method where a substrate is immersed with coating material in a suitable container, then retracted from the container. The wet coating material on the substrate is forced to dry to complete the coating layer as shown in Figure 2.10. This method is applied in a variety of industry for coating primer material on substrate or one-coat finish. The advantages of the dip coating method are simplicity, low cost, good coverage, and consistency [115].

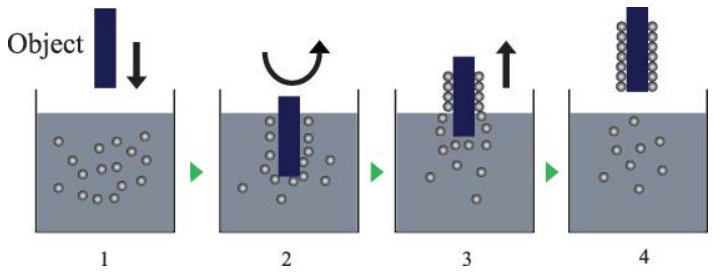

Figure 2.10 Schematic diagram of dip coating method.

The dip coating method can also be used to manufacture supercapacitors. Several researchers have applied this method to fabricate the electrodes or the electrolyte for EDLCs. For example, Harrison [116] has presented a coaxial single-fibre supercapacitor for energy storage. A stainless steel was coated with Chinese ink, gel electrolyte, active carbon, and silver conductive paint, using dip coating method. This fibre supercapacitor obtains the specific capacitance per unit area and length at 3.18 mF cm^{-2} and 0.1 mF cm^{-1}, respectively, for a 2.6 cm supercapacitor.

Alternatively, Yang [117] used a dip coating method to coat the electrolyte to fabricate a fibre-shaped supercapacitor. In this study, elastic fibre was dip-coated with electrolyte and then wrapped with carbon nanotube sheets to complete the structure of the supercapacitor. The maximum specific capacitance was 19.2 F g^{-1} with a thickness of 330 nm for the fiber-shaped supercapacitor.

2.5.2 Screen printing method

Screen printing is one of printing technologies that has been used for several years in electrode fabrication. This method provides a wide range of thickness of printed image depending on the thickness of the screen mesh. The thickness of a screen-printed image is usually in the range of several tens of microns to 100 µm with a single pass of printing. In screen printing, a squeegee is used to squeeze the ink or paste material through the mesh with low printing pressure as shown in Figure 2.11 [120].

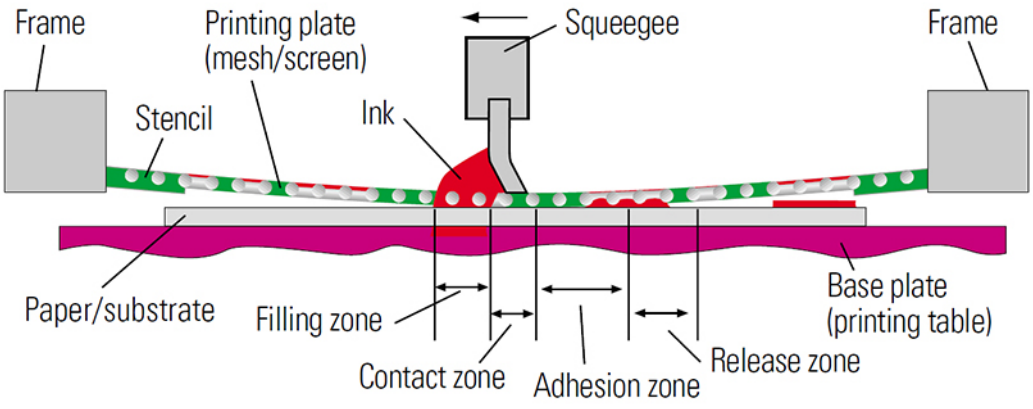

Figure 2.11 Schematic diagram of screen printing [112].

There are many studies that have used screen printing as a method to fabricate the supercapacitors. Xu [118] fabricates the thin film supercapacitor using screen printing. In this study, NGP/PANI inks with different weight ratios were used as electrode materials on a thin film. NGP/PANI $_{1:2}$ was found to be the most suitable material and showed the highest specific capacitance at 177 F g^{-1}. In addition, Tehrani [119] studied a large-area printed supercapacitor using the screen printing technique. In this research, the current collector, electrode, electrolyte materials, and adhesive were sequentially printed onto a polyethylene terephthalate (PET) substrate. The supercapacitor with thickness of 375 µm recorded a capacitance ranging from 50 to 400 mF.

2.5.3 Doctor-blade coating method

The doctor-blade coating method is a commonly used method for making thin films on large area surfaces. In this method, a sharp blade is used to spread the ink or slurry onto the substrate. As shown in Figure 2.12, the blade is set in a specific distance from the substrate to control the thickness of the coating material. This method can be applied with a stencil mask to create a specific pattern.

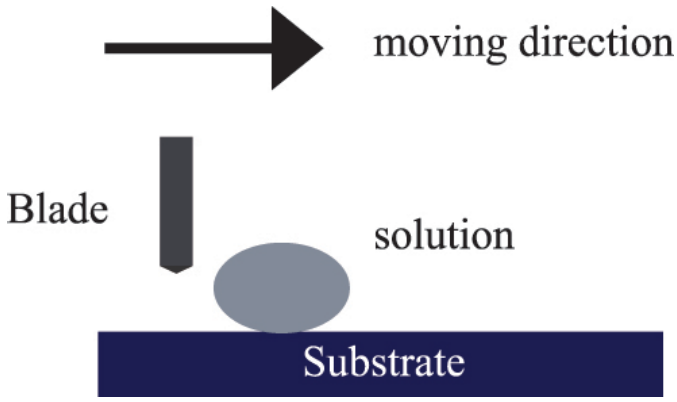

Figure 2.12 Schematic diagram of Doctor-blade coating method.

Doctor-blade coating method is commonly used to fabricate the electrode material of the supercapacitors. Tiruye [121] used this method to coat AC ink onto aluminium current collectors to manufacture solid state supercapacitors. Zhang [33] has also applied this technique to fabricate flexible strip supercapacitors. In this study, the AC slurry was coated on the stainless steel strip using a sharp blade. A slot in a component plastic sheet is used as a mark to control the thickness of the coated slurry.

2.5.4 Inkjet printing

Inkjet printing is a non-impact printing processes providing several advantages and is widely used for small-scale production (home and small office). In this process, an electronic signal sent to the print head is used to generate pressure and force droplets of ink onto the substrate. A commonly used variant of the inkjet method is the drop-on-demand (DOD) technique. As shown in Figure 2.13 and 2.14, the DOD technique can be classified further into thermal inkjet and piezoelectric inkjet.

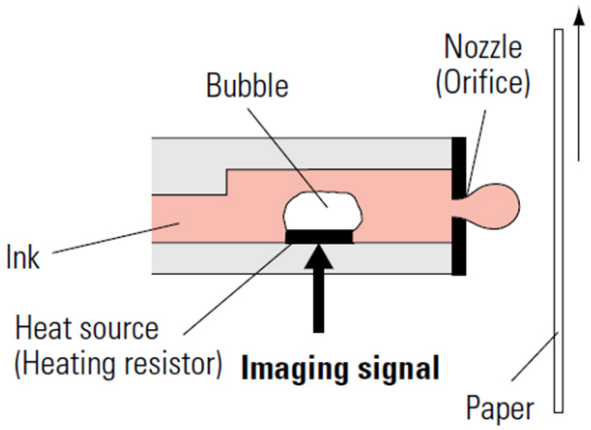

Figure 2.13 Functional principles for thermal inkjet [112].

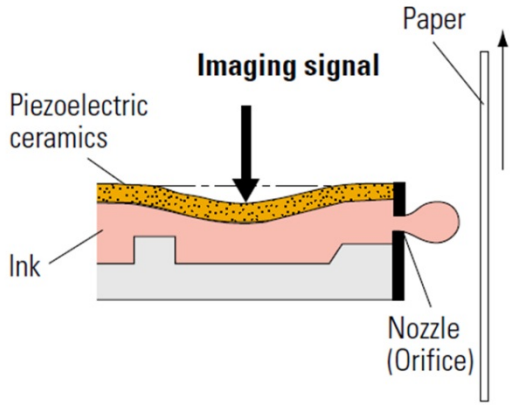

Figure 2.14 Functional principles for piezoelectric inkjet [112].

In recent years this printing process has increasingly been used in commercial printing and it is also attractive for particular manufacturing applications because of several advantages as follows:

1) It is a digital printing process. The deposited material can be delivered on an x-y grid and there is the potential to change the placement of droplet material in the real time if necessary. For example, when misalignment on the substrate occurs, each droplet can be adjusted in the real time to ensure that the pattern is in the correct position.
2) It is a non-impact printing process. It can deposit the image without contact to the substrates. This means fragile substrates can be printed that are not possible with other commercial printing processes.
3) It can print several different materials onto different surfaces. In addition, inkjet printing can combine with other manufacturing methods or integrate with 3D printing techniques [108-112].

In the past two decades, inkjet printing has been afforded great attention in scientific research. The inkjet process has been adapted to create different patterns using functional materials in the development of the printed electronics devices. This process enables the creation of line and space dimensions as small as 10 - 20 µm, which provides higher resolution of patterns than conventional printing such as screen printing. Nowadays, several electronic devices, such as flexible displays, radio frequency identification (RFID) tags, energy-harvesting sensors, and energy storage devices, can be manufactured using this process [95-107]. These printed applications are fabricated using conductive ink in order to create electronics function. The conductive ink can be based on different material such as silver [98, 103], copper [101], carbon nanotube, [96, 99-100] and conductive polymer [96, 105-106].

The conductive inks based on silver have received a great deal of interest due to their excellent conductivity and anti-oxidation properties. Jung et al. [98] have reported on the practicability of using the inkjet process for the fabrication of conductive ink in a printed circuit. The results indicated that samples sintered at 250 ºC for 20 minutes obtained a good resistivity.

The different resolution setups in this experiment significantly affected line creation due to the overlap of the dots. Nie et al. [103] have studied silver citrate conductive ink on a PET substrate using the inkjet process as shown in Figure 2.15. In this study, the conductive ink can be cured at relative low temperature due to the formation of silver. The ammine complex and the film, as shown in Figure 2.15, obtained the lowest resistivity of 17 μΩ when cured at 150 ° C.

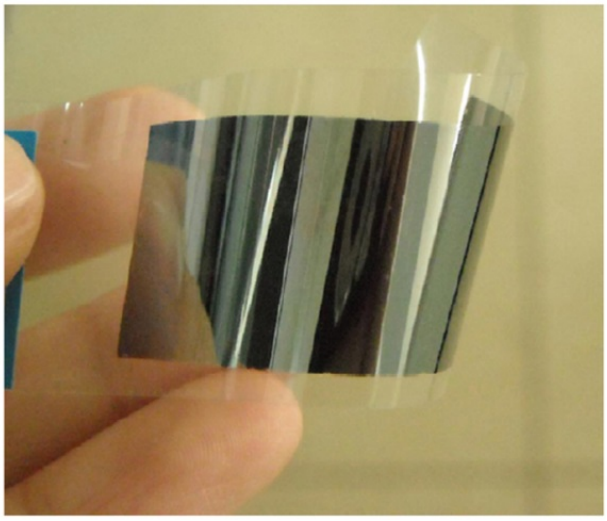

Figure 2.15 silver citrate conductive ink was printed in patterns of a 20 mm x 50 mm rectangle on PET substrate using inkjet printing [103].

In addition, a new technology has been introduced to fabricate multi-material freeform 3D objects, which enables the building of complete functional electronic devices [55-56]. This technology - known as additive manufacturing (AM), though more commonly referred to as 3D printing - is a method of manufacturing in which a model designed by Computer Aided Design (CAD) is captured and then subsequently constructed on a layer by layer basis [15-18]. With 3D printing, many researches have been able to investigate new materials and techniques to create energy storage devices, such as microbatteries and supercapacitors [11-14].

2.6 3D printing technologies for energy storage devices

3D printing or additive manufacturing (AM) was originally referred to as rapid prototyping. Rapid prototyping (RP) was the term used to describe the process of rapidly producing prototype specimens or parts from digital data before creating the

final product, which is regularly employed in a variety of industries. The development of RP machines has improved the quality of the output prototypes, so some parts created using these machines are now sometimes used in final products, therefore the term rapid prototyping was no longer appropriate. All RP technologies basically use additive approach in order to fabricate parts, so the term 'additive manufacturing' was adopted by the ASTM International Technical Committee. There are, however, several other terms that have been used to explain this technology, for example: Autofab, freeform fabrication, and most popularly, 3D printing.

2.6.1 Principles of 3D printing

Recent developments in manufacturing have been focused on 3D printing methods which can offer several advantages for rapid production of 3D objects. 3D printing is a term for a method of additive manufacturing of 3D objects directly from Computer Aided Design (CAD) files. From the digital file, 3D printing technology constructs 3D objects in a bottom-up manner on a layer by layer basis [17-19, 63]. 3D printing techniques present several advantages over traditional manufacturing methods. Compared to conventional manufacturing processes, 3D printing methods present unique capabilities as follows [19, 63]:

1) Design Flexibility: 3D printing enables the creation of practically any complex geometric shape. In conventional processes, the design of freeform specimens is limited because of the technical issues surrounding the need for mechanical fixtures, such as cutting in invisible zones or the possibility of collisions. 3D printing techniques also provide the ability to deposit multi-materials in precise positions according to the designed functionality of the objects.
2) Dimensional accuracy: The term "dimensional accuracy" refers to print tolerance, which determines the dimensional difference between the finished model and the digital design. In the early days of 3D printing development, the resolution and accuracy was not of great concern since it was largely being used to create prototypes; however, modern improvements to 3D printers facilitate more accurate print tolerance and can be expected to deliver completed finished parts.
3) Single-part assembly: Another possibility of 3D printing is the ability to create single-part assembly products that contain integrated mechanisms which would require multiple part assembly when manufactured using conventional methods.

In 3D printing, support material (called unbound/sintered powder) is applied to carry the parts and joints, then it must be removed after completing the printed part so that the single-part assembly can be completed.

4) Personal, on-demand fabrication: Because of the digital characteristics of the method, 3D printing offers the capability for products that require low-volume production or customisation, for instance home accessories or collectables.

Improvements in 3D printing technology offers the possibility of manufacturing a wide range of applications for many purposes. These developments also transform the 3D printing method to be applied to a low-cost, affordable, desktop printer, which opens it up to a wider user base that has access only to a small manufacturing platform [16-20].

2.6.2 The generic 3D printing process

There are a number of fabrication steps that transform the virtual designed object to the physical finished part. Products manufactured using 3D printing can be involved in different steps depending on the design. Prototype products may require fewer steps to complete the rough parts with lower resolution and high printing speed, while an actual product demands more steps of the process, for example surface preparation, careful cleaning, and post-processing before it is used. There are seven basic steps that engage in 3D printing as follow:

1) **Step 1: Design in solid modelling software.** The first step is to design the part using solid modelling software such as computer-aided design (CAD) software, for example, SolidWorks®. To design parts using these types of software, the geometry must be fully described and the output should be in 3D. Alternatively, optical scanning can also be used to create the digital design. Once the design has been finalised, a 3D model must be converted or exported to an STL file and almost all solid modelling software can export to this file format.

   STL (Standard Triangle Language) files are the industry standard file type for 3D printing. It uses a series of triangles to represent the surface of a solid model. For the last two decades, the STL file format has also been the industry standard for transferring information between design programs and the software specific to a given additive manufacturing hardware. An STL file contains information only about a surface mesh (digital geometry), and has no provisions for representing colour, texture, material, etc.

Several extensions to this remit have been proposed, but not widely accepted. The surface is represented by an unordered list of triangles, and each triangle is defined by 12 floating point numbers. A 3D surface normal is defined, followed by three coordinates that define the vertices of the triangle in three dimensions. Already, this contains redundant information, since the surface normal can be calculated from the order and location of the three vertices. By default, the right-hand rule is used to define the direction of the normal based on the order the points are encoded. Since each triangle is represented separately, each vertex must be written repeatedly for every triangle that shares that vertex (three or more times). This introduces leaks, where small rounding errors result in vertices that do not precisely line up, which make subsequent slicing algorithms ineffective without an intermediate "welding" step to repair these defects.

Also, the STL file has no provisions for defining the physical units intended. Even though pre-processing software can make an educated guess between inches or mm depending on the build size of the machine, there is still unnecessary ambiguity. An additional point of confusion regarding the STL file is that in fact there are two separate file formats that may be used: binary and ASCII. The ASCII version exists to make the format human readable, but the binary version is often used by mature programs to minimize storage space.

2) **Step 2: Conversion by slicing software.** The 3D printer requires the instruction for each layer to be built, and slicing software is used to achieve this. The slicing software takes a 3D model (in STL file format) and slices it in to thin layers to generate a G-code. This software is usually open-source or provided by the machine manufacturer, though commercial software is available. It needs to be noted that G-code is usually applied in fused deposition modelling and paste extrusion systems. Other technologies may use different programming language to control the machine. Nevertheless, slicing the design into thin layers is the basic technique commonly used by all 3D machines.
3) **Step 3: Transfer to 3D printer.** After the STL is converted into thin layers, it must be transferred to the 3D printer. In general, the slicing software can be directly transferred to the machine, while some technology requires saving the file to an external card to be inserted into the machine.

4) **Step 4: Printer set up.** Before printing**,** the 3D machine must be set up in accordance with the required printing parameters, e.g. the height of extrusion head, material constraints, etc.
5) **Step 5: Printing.** Construction of the part is an automated process. The printing time relies on printing parameters, such as speed of printing, infill density.
6) **Step 6: Removal.** When the part is completely built, it must be removed. With some 3D techniques, the part can be ready to use without post-processing.
7) **Step 7: Post-processing.** Post-processing is the step required for cleaning up the part which may involve applying a cleaning solution. Supporting materials are also removed as part of this process, so that the part is ready for use [63].

2.6.3 Classification of 3D printing processes

A broad range of 3D printing processes have been classified by researchers depending on the implemented machining approach, as shown in Figure 2.16. The difference between each process is the method of depositing the material to create parts, the principles of the operating system, and the material that can be deposited. Some techniques operate by melting the materials to construct the layers, such as selective laser sintering (SLS), selective laser melting (SLM) and fused deposition modelling (FDM); whereas other methods can directly extrude the material to build an object, e.g. paste extrusion system. Each method has its advantages and drawbacks, so the main considerations made for selecting a 3D printer are generally dependent on the designed object, its function, and the material used [18-20, 62].

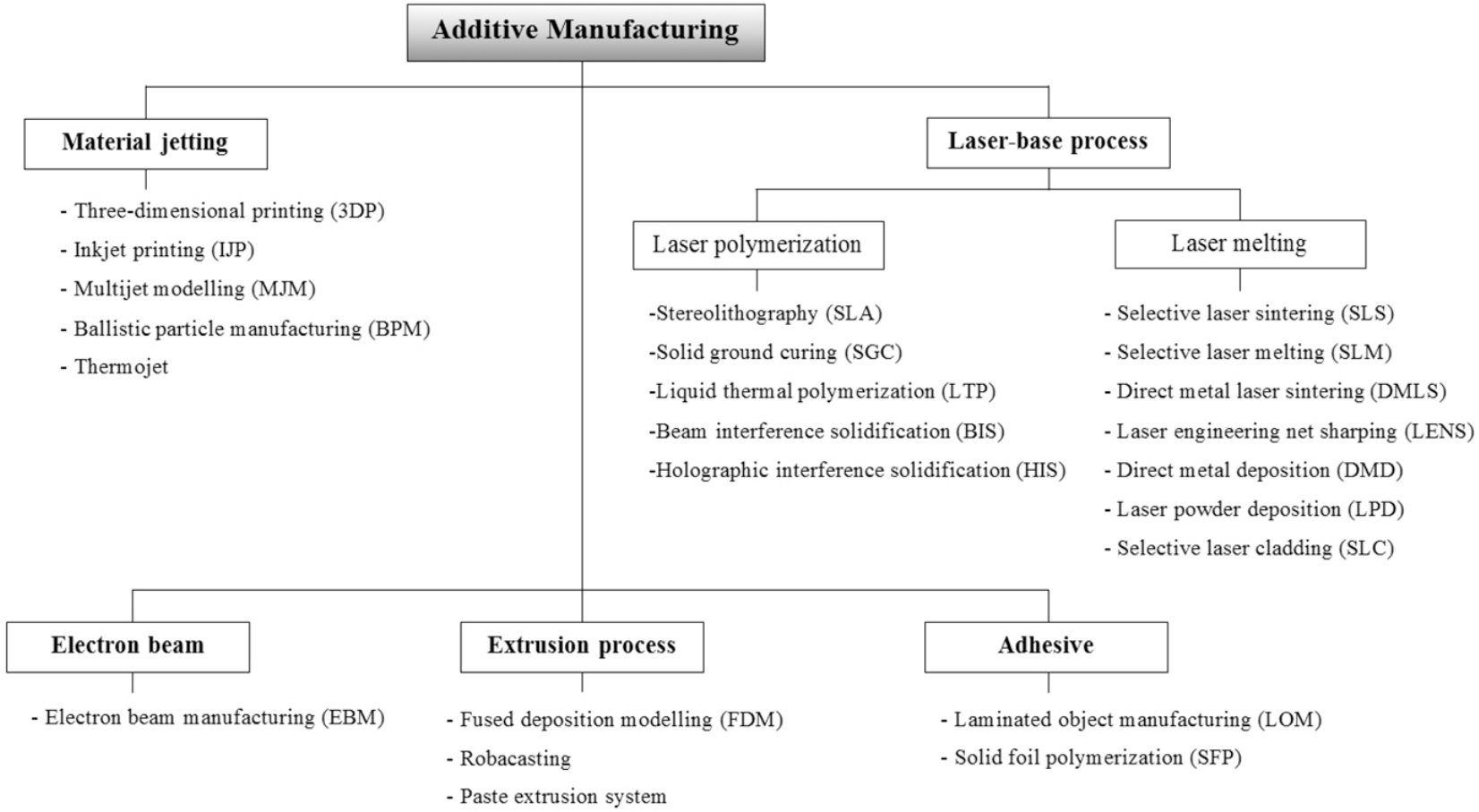

Figure 2.16 Classification of 3D printing process adapted from Bikas [17]

1) **Laser-based processes.** In this technology, low to medium power lasers are used to melt, solidify, or cure the material as shown in Figure 2.17. The laser-based processes can be classified in two sub-categories: laser polymerization and laser melting. This classification derives from the phase change mechanism. In the laser polymerization process, photosensitive resin is used as the material. This process allows the material to be cured through exposure to UV radiation, which is supplied by a low-power laser source. In the laser melting process, the powder material is directly delivered via nozzles to the processing head. The material is melted by the laser, then cooled and solidified to form the part. Examples of specific laser-based processes are stereolithography (SLA), selective laser sintering (SLS), and selective laser melting (SLM).

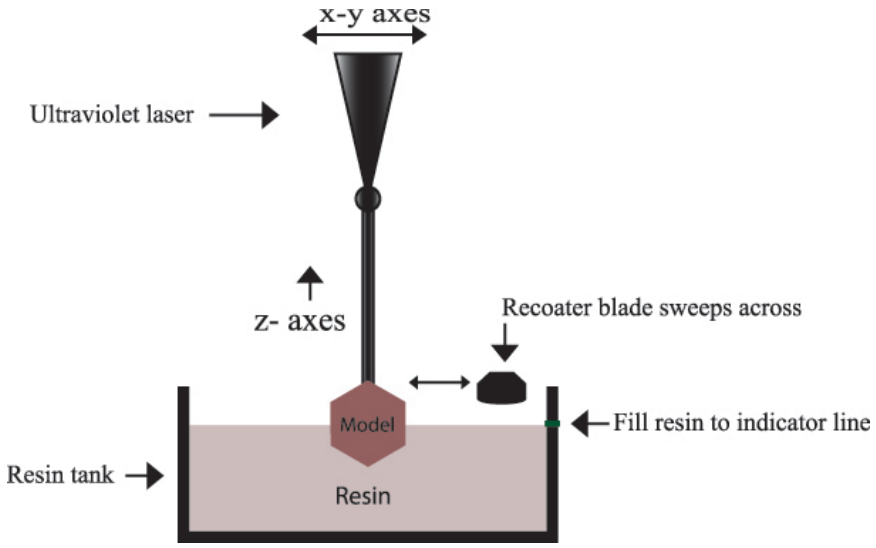

Figure 2.17 Schematic diagram of the stereolithography (SLA) process.

2) **Material jetting.** Material jetting processes employ two steps to build the 3D object. Firstly, thin nozzles spray the material, and then molten material, or commonly a binder, is used to bind the powder in order to create a solid part. The operating principle of these processes is similar to the laser-melting processes, but the differences are: 1) no phase change arises and 2) the powder particles are held by a binder. There are five applied technologies categorised as

material jetting processes: three-dimensional printing (3DP), inkjet printing (IJP), multijet modelling (MJM), ballistic particle manufacturing (BPM), and thermojet. Figure 2.18 shows the schematic diagram for inkjet printing (IJP).

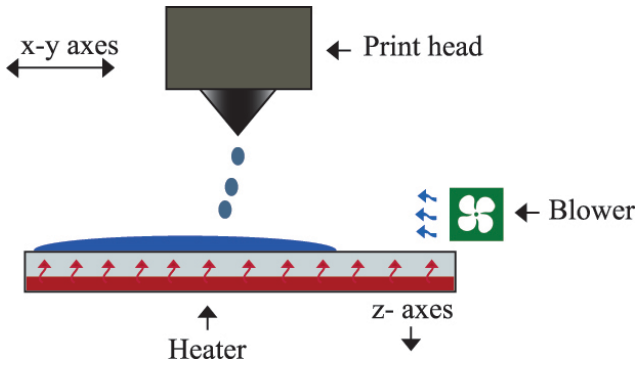

Figure 2.18 Schematic diagram of the inkjet printing (IJP) process.

3) **Adhesive-base processes.** These processes can be divided into two technologies: laminated object manufacturing (LOM) and solid foil polymerization (SFP). In recent years, these processes have fallen out of favour. To build the part, adhesive-coated film, made from plastic, paper or metal laminate, are cut using a laser to the designed dimensions. Then the film is pressed down and heated by a heated compactor to form a layer as shown in Figure 2.19. Each layer is bonded by activating a heat curing adhesive to create the part.

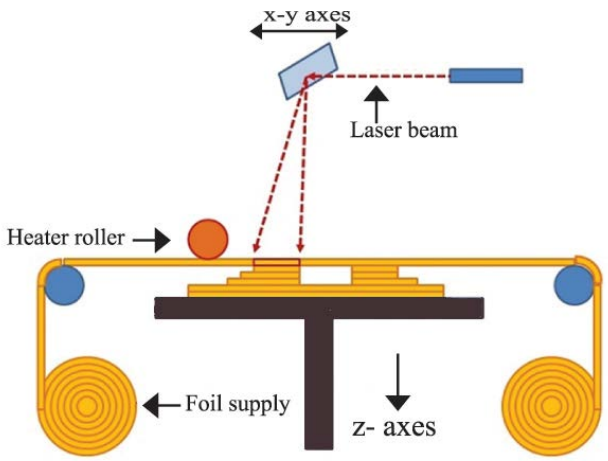

Figure 2.19 Schematic diagram of the laminated object manufacturing (LOM) process.

4) **Extrusion processes.** Extrusion processes refer to the method that melts or softens a plastic material using a heated extrusion nozzle, and then deposits it on the substrate. The deposited layer is then cooled to form the final part geometry. The extrusion process can be classified into two technologies: fused deposition modelling (FDM) as shown in Figure 2.20 and robocasting. New technology in the extrusion process offers the possibility to deposit paste material without requiring a heating process. The paste material can be extruded through the nozzle to build the part. This operating method is also known as paste extrusion system.

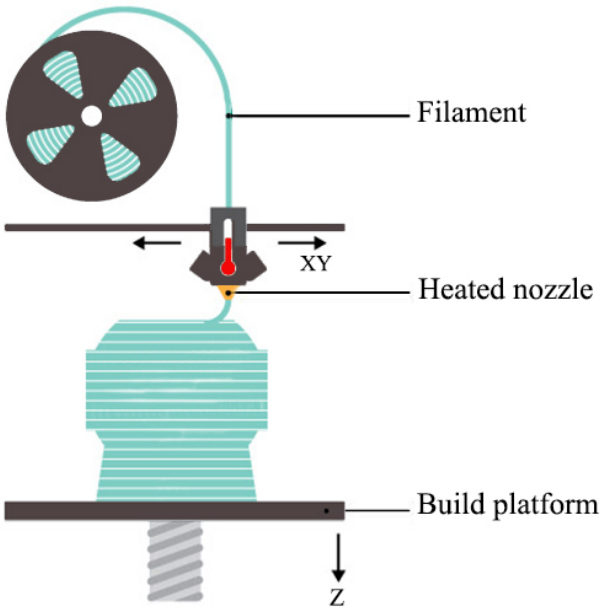

Figure 2.20 Schematic diagram of the fused deposition modelling (FDM) process.

5) **Electron beam process.** Electron beam manufacturing (EBM) utilises the same basic principle as the laser-melting process, except it uses an electron beam as the energy source to sinter or melt the material. This process is designed to build the part with metallic materials. The process uses a high-voltage electron beam, contained within a vacuum chamber to prevent oxidation problem [18-20, 62]. Figure 2.21 shows the schematic diagram for the electron beam process.

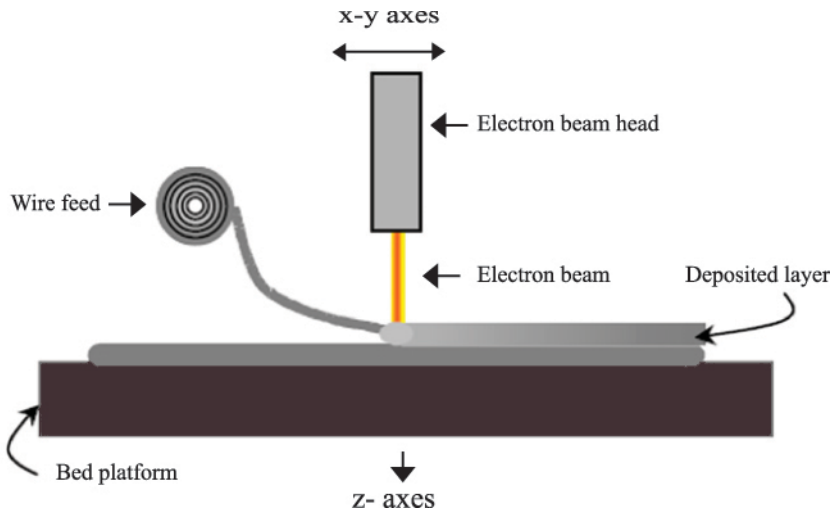

Figure 2.21 Schematic diagram of the electron beam manufacturing (EBM) process.

In summary, 3D printing techniques generally present several advantages over traditional manufacturing methods. First of all, 3D printing offers “freeform” design for users, for example, complex geometries that cannot be easily manufactured by other methods can be created by 3D printing because of the additive approach. Furthermore, functional parts with no requirement for assembly can be created using 3D printing. The development of 3D printing technology recently has provided an opportunity for many new applications and using different types of materials.

In this thesis, typical extrusion processes are of interest and selected to be used to fabricate the supercapacitors. As mentioned above, the extrusion process can be categorized into two main technologies: fused deposition modelling (FDM) and paste extrusion system. Both methods have presented a simple fabrication method, suitable to

create a supercapacitor frame using FDM machine, and all other components using the paste extrusion system. The specific details of these 3D printing technologies are given below.

2.6.4 Fused deposition modelling (FDM)

Fused deposition modelling (FDM) was developed by Stratays, USA and became the most common extrusion-based 3D printing technology. FDM technology has been developed and presented a rapid growth in 3D printing technology due to its capability to create functional parts requiring complex geometry. Recently, different manufacturers, such as MakerBot, Cube, RepRap, Fab@home and Ultimaker have developed FDM techniques to be used in low-cost desktop 3D printers and offer widely accessible individual product fabrication that corresponds to individual designs [62-66].

As shown in Figure 2.22, the FDM printer works by feeding the thermoplastic filament material off a feedstock spool using two rollers. The filament is heated and transformed into a semi-molten polymer via a small temperature-controlled extruder which then deposits it onto the build platform on a layer by layer basis. To fabricate the object, the heated extruder moves on an x-y plane to deposit the semi-molten filament according to the layer design. After each layer is complete, the build platform is lowered and the next layer is deposited, and so on until object is entirely built. The build platform is also able to control the temperature to facilitate the rapid hardening of thermoplastic filament [62, 64-66].

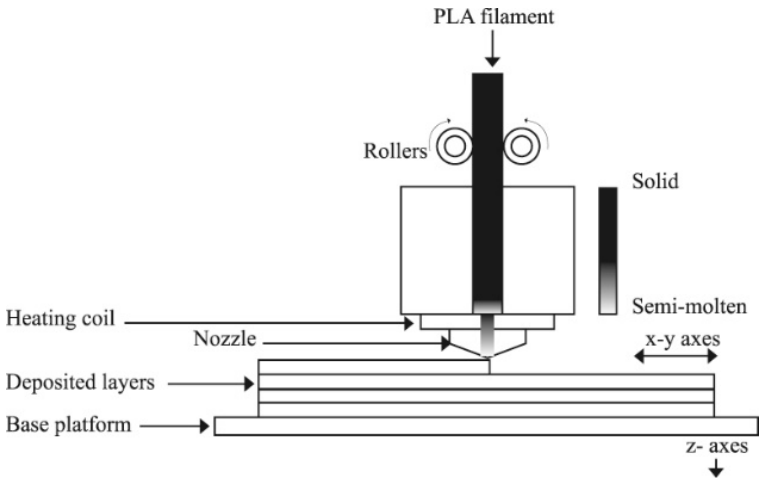

Figure 2.22 Schematic diagram of the extrusion and deposition of FDM process.

There are also disadvantages of FDM printers in term of build speed and accuracy. For the most expensive, so presumably the most advanced, FDM printer, the thinnest layer thickness printable is 0.078 mm, and it significantly increases the build time. The build speed of FDM machines is also dependent on the feed rate and depositing speed. The feed rate relies on the capacity to deliver the filament material and the speed at which the heat chamber can melt the filament and feed it through the nozzle. In terms of accuracy, the nozzle is generally circular and so not able to create sharp external or internal corners or edges, which causes functional problems for some applications. Furthermore, desktop FDM machines employ belt drives to move the printing head resulting in reduced accuracy due to flexing in the belts [62-68].

The development of FDM machines has provided a wide range of potential fabrication materials allowing the creation of parts with various effective mechanical properties. Parts created using FDM technology are the strongest in comparison with any other polymer-based 3D printing processes. Desktop FDM printers mainly use either acrylonitrile butadiene styrene (ABS) or polylactic acid (PLA) as building materials. Both materials have subordinate thermostability, when ABS is heated above 250 ºC, it can decompose into acrylonitrile-monomer, butadiene-monomer, and styrene-monomer. These monomers are highly toxic. In contrast, the PLA is much safer in this respect, as it decomposes into H_2O, CO_2 and humus. Moreover, PLA is “greener”, because it produced from renewable resources such as cassava and corn, and is biodegradable. Unlike ABS, the PLA filament also offers low-cost, low-melting point (around 160 ºC) and good mechanical properties. As a result of these advantages, the PLA filament is increasingly used for FDM printing by industrial and general users [64-75].

2.6.5 Paste extrusion system

The paste extrusion process (also referred to as direct-write technology) applies pressure to deposit paste or fluid materials thorough a nozzle to control the composition onto the substrate [62]. This process varies from FDM in requiring no heating of the material before deposition. The main advantages of this process are the ability to deposit several paste materials on to different substrate surfaces and a simpler fabrication method [11-14, 62]. Due to these advantages and improvements in material deposition technology, it is possible to print electronic components onto or within complex three-dimensional objects [76-80].

As shown in figure 2.23, the paste extrusion system consists of a stepper motor, a syringe connected to a plastic tube and a nozzle at the end of plastic tube. To extrude the paste material, the stepper motor is driven to rotate the screw underneath the syringe plunger. After the plunger is pushed, the paste material flows through the plastic tube into the nozzle, and the material is then deposited in the desired position.

Paste extrusion machines differ in nozzle and pump design. The nozzle design determines the size and shape of the deposited material. In addition, the nozzle is designed according to the viscosity and particle size of the material used. The pump design affects the volumetric control and repeatability of dispensing, the accuracy of the start-stop deposition process, and the speed of deposition [62, 77-80].

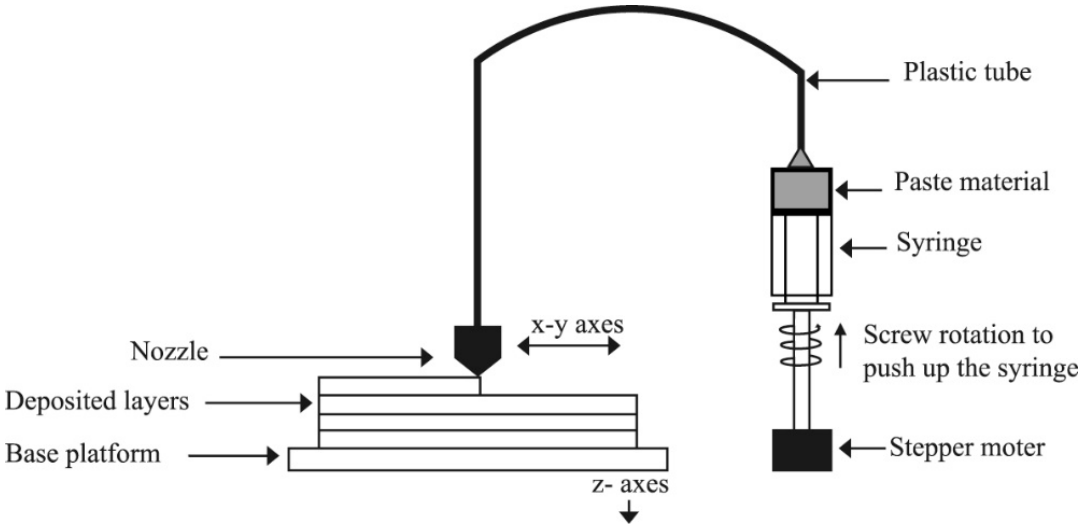

Figure 2.23 Schematic diagram of the extrusion of paste extrusion system.

2.6.6 Current research in 3D printing technologies for energy storage device.

Current research into 3D printing focuses on widening the range of materials which may be printed and the improvement of newer techniques in order to fabricate a wider range of applications for many purposes [22-30]. Improvement in 3D printing techniques, enhanced with component placement and electrical interconnect deposition, offers the potential to make electronic prototypes. These developments allow integration of electronic components with 3D printed devices. This type of 3D electronics integration is also referred to as 3D structural electronics or 3D printed electronics. 3D printed

electronics can be designed to any form providing a unique advantage over conventional electronics systems [81-86].

In the last decade, many research groups have developed 3D printed electronics, such as sensors, interactive devices, and energy storage devices. These developments create the components and electrical interconnect using 3D printed structures [84-85]. For example, Palmer [58] initiated research on a 3D printed embedded structure with conductive ink using Direct Printing (DP), which was later expanded by Medina and Lopes [87-88]. In their research, two different 3D printing techniques were integrated: stereolithography (SLA) and a dispensing system. The commercial stereolithography (SLA) was integrated with direct-write (DW) technology to manufacture electrical circuits for the SLA-manufactured parts. A simple multi-layer SLA part with embedded circuitry was fabricated and the hybrid system has presents the potential to fabricate a functional 3D structural electronics device. This method was also applied to print simple circuits, as well as for a demonstration construction of simple prototype temperature sensors.

To manufacture an energy storage device using 3D printing technologies, Ho et al. have experimented with a zinc microbattery using direct-write dispensers [89]. In this research, zinc and manganese dioxide were prepared and applied as electrodes. The electrolyte used was an ionic liquid gel. All materials were made into slurry and printed in stacked configuration using a direct-write dispenser as shown in Figure 2.24. The electrode was printed with a thickness between 80 and 120 μm, then dried on a hot plate at 60 ºC for 20 min. The ionic liquid gel electrolyte was deposited and dried on hot plate at 60 ºC for 20 min. In this experiment, the zinc slurry functioned as the electrode and current collector on one side, and the electrode made from manganese dioxide used a nickel foil as the current collector on the other side.

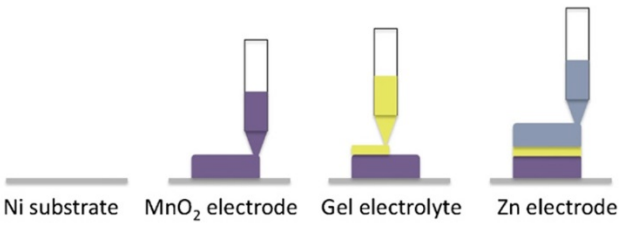

Figure 2.24 Process schematic for the printing of a zinc-metal oxide stacked microbattery [89].

This microbattery was further improved by Wang et al [90], who developed an integrated energy-harvesting prototype which combined thermoelectric energy harvesting and electrochemical energy storage, both of which were fabricated using direct-write dispenser technology. Further to that, 3D interdigitated microbattery architectures (3D-IMA) have been studied by Sun et al [31]. In this work, $Li_4Ti_5O_{12}$ (LTO) and $LiFePO_4$ (LFP) materials were applied as anode and cathode, created using direct-write technology on a glass substrate. As shown in Figure 2.25, the 3D-IMA used gold (Au) as the material for the current collector. The dimensions of the electrodes were 960 µm x 800 µm x 60 µm, spaced 50 µm apart. A packaging frame of 3D-IMA was made from plastic using laser machining applied to contain the microbattery and electrolyte. The microbattery in this study obtained 9.7 J cm^{-2} at a power density of 2.7 mW cm^{-2} and can be applied in autonomously powered microelectronics.

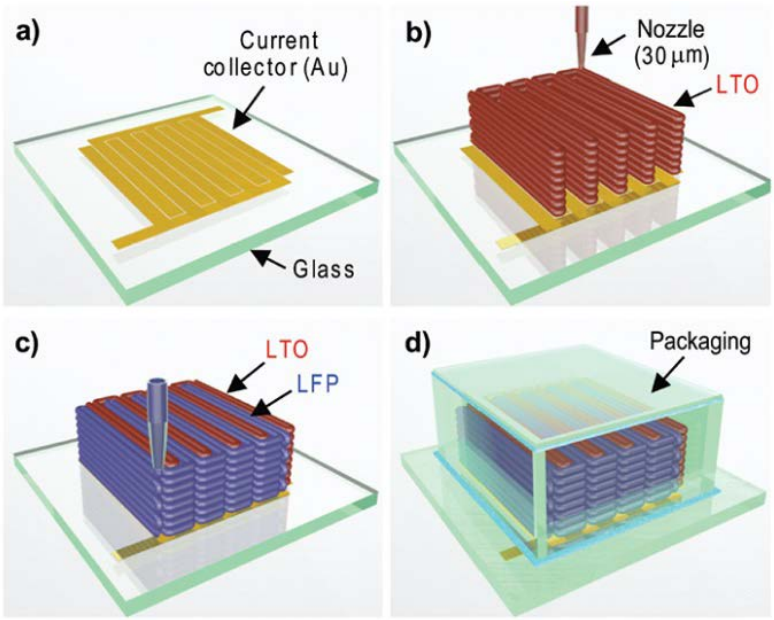

Figure 2.25 Schematic illustration of 3D interdigitated microbattery architectures (3D-IMA) fabricated on (a) gold current collector by printing (b) Li 4, Ti 5, O 12 (LTO), and (c) LiFePO 4 (LFP) inks through 30 µm nozzles, followed by sintering and (d) packaging [31] .

Furthermore, Zhao et al [91] have applied Selective Laser Melting (SLM) and demonstrated how a 3D printed electrode can be used to fabricate interdigitated supercapacitors as shown in Figure 2.26. The electrodes used in this study were Ti_6Al_4V and the electrolyte was polyvinyl alcohol (PVA)-H_3Po_4 polymer electrolyte. The SLM method operated using a high-power laser beam on a build plate of fine metal powder to create free-form metal parts. After the Titanium alloy electrodes were printed, they were removed from the bed using a wire electrical discharge machine (WEDM machine), and cleaned using Milli-Q water and ethanol. An organic polymer, polypyrrole, was used to coat the metal electrode before assembling the pseudocapacitors, then the supercapacitor was immersed in an electrolyte solution (PVA- H_3Po_4) for 2 hours. The electrolyte filling was done under vacuum and dried in a fume hood for 12 hours.

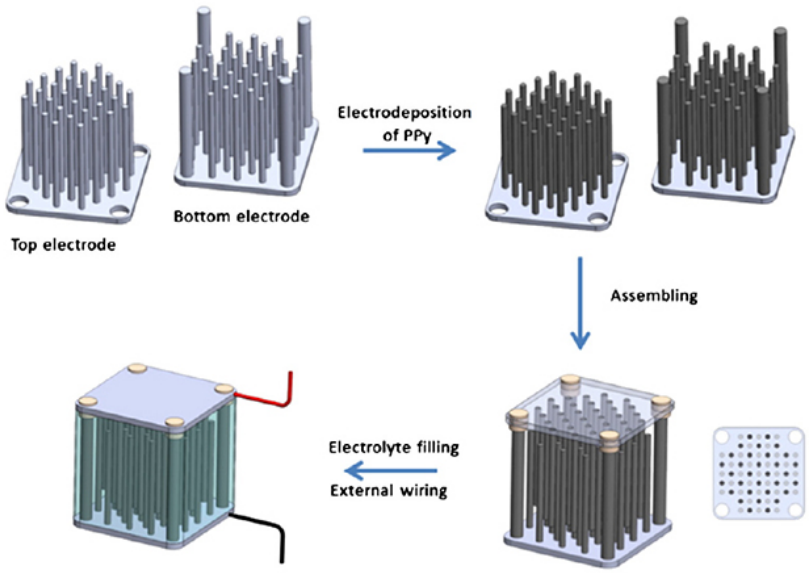

Figure 2.26 Schematic procedures used to fabricate interdigitated supercapacitors.[91]

Zhu et al [114] have introduced a 3D-printed graphene composite aerogel (3D-GCA) for EDLCs. Graphene oxides (GOs), graphene nanoplatelets (GNP) and silica fillers are prepared as a printable ink, which is designed to be printed on an extrusion-based 3D printer equipped with a micronozzle. After printing is complete, post processing is required using heat treatment in nitrogen atmosphere and silica fillers etching.

Ambrosi et al [92] have designed and fabricated 3D-printed pseudocapacitors using the SLM technique. In this research, helical steel electrodes were tested in different sizes, as shown in Figure 2.27. Testing exhibited that the electrodes maintained normal metal conductivity despite their distinctive geometry. When the electrodes were coated with IrO2, they presented superior capacitive properties. Moreover, they also exhibited excellent catalytic and sensing properties. These results indicate that 3D printing techniques can be employed to create complex shape designs, and that there are advantages to developing electrochemical energy storage devices using 3D printing.

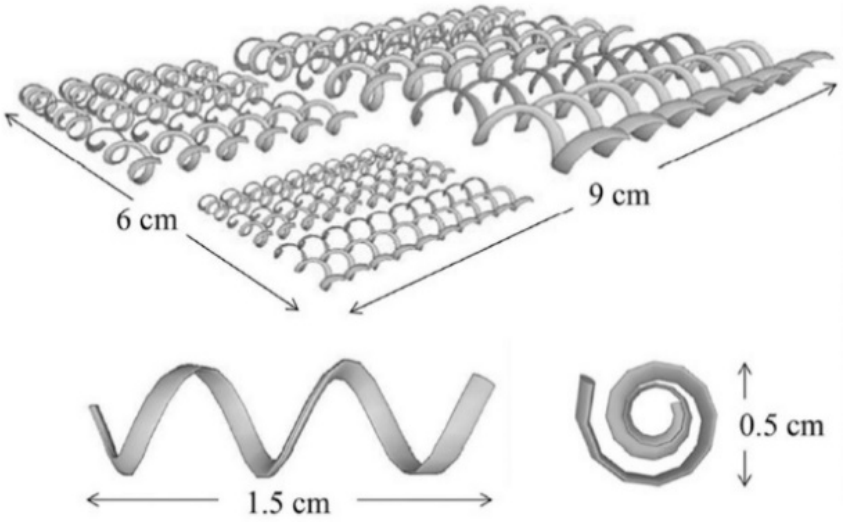

Figure 2.27 Schematic of the helical-shape electrode design for 3D printing, and dimensions of the electrode [92].

Other researches into the development of pseudocapacitors using 3D printing have been undertaken by Liu et al [93]. They used a direct metal laser sintering system to fabricate 3D-printed stainless steel scaffolds. In this process, the laser power and scan speed were used to control the porosity of the metal scaffolds in order to optimize the electroactive surface area.

From the above examples, it can be seen that 3D printing processes can be an effective method for manufacturing supercapacitors. 3D printing methods significantly expand the range of materials and designs which can be used to fabricate the electrodes. This is

important since the electrical performance of supercapacitors is dependent on the material used, the component structure, and the assembly method. [11]

2.7 Research gaps and literature review summary

In this chapter, the principles of conventional supercapacitors including classification of supercapacitors, supercapacitor structure and materials were summarized. Furthermore, previous studies in manufacturing of supercapacitors were reviewed and it was outlined why future developments of manufacturing of supercapacitors are focussing on applying 3D printing technologies. 3D printed electronics is a comparatively new subject of scientific interest, and is attracting attention in the field of energy storage devices. Existing research on 3D printed electronics for energy storage devices, including supercapacitors, were also summarized. Most studies into the manufacturing of 3D printed supercapacitors have focused on the development of new materials that can be used in 3D printing methods.

To identify the research gaps, and thus the issues that require investigation through this research:

- The manufacturing of supercapacitors using 3D printing techniques has already been developed using 3D printing methods such as Selective Laser Melting (SLM). In this thesis, two small desktop 3D printing methods, fused deposition modelling (FDM) and paste extrusion system, will be integrated and applied to fabricate EDLCs. These techniques are selected because of their simple application, and their ability to deposit several different suitable materials for the fabrication of EDLC.
- As mentioned previously, the manufacturing of EDLCs using some 3D printing methods requires post-processing and assembly. In this thesis, new designs will be investigated to fabricate EDLCs in a single continuous process, without the need for post-processing. In addition, an investigation into the design of EDLC packaging frames will be included to explore the possibility of wirelessly stacking multiple EDLC cells to create a more capable unit. These will provide a novel method to manufacture 3D-printed EDLCs.

- Previous studies into materials used to fabricate the electrodes of supercapacitors have been limited to nanomaterial and metal. This thesis will identify and investigate different materials for fabricating current collectors and electrodes. The material used will be examined and evaluated in terms of their cost, preparation difficulty in ambient conditions, and environment friendliness. The investigation will hopefully identify possible ways to develop a metal-free supercapacitor.

It is believed that this study into 3D printed supercapacitors using 3D printing methods will contribute to fill the research gap in this research field and empower the further development of 3D printed supercapacitors.

Chapter 4 Experimental materials and measurement Methods

In this chapter, the general materials and measurement instruments used in this thesis are explained in detail. In addition, evaluation of electrochemical properties is described.

3.1 Materials and equipment

3.1.1 Chemical and reagents

Polylactic acid (PLA) filament with a diameter of 2.89 mm. obtained from 3dgbire Ltd was used to build packaging frame of supercapacitors. Silver conductive paint obtained from RS Components Ltd, (the volume resistivity is 0.001 Ω·cm when fully hardened), was used for creating current collector layer. Activated carbon (AC) (AR grade, 1375 μΩ.cm), Sodium carboxymethyl cellulose, CMC ($C_{28}H_{30}Na_8O_{27}$, MW: 250,000), ethanol (≥ 99.8%, ACS grade) were obtained from Sigma-Aldrich. AC and CMC were used as material for electrode fabrication. Carbon conductive paint (Bare Conductive Electric Paint) obtained from RS Components was used as current collector and electrode. Phosphoric acid (H_3PO_4) and polyvinyl alcohol, PVA (MW 146,000-186,000, > 99% hydrolysed) were also obtained from Sigma-Aldrich and used as gel electrolyte. Postlip filter paper (d= 127 mm, the thickness is 130 $\pm$ 1μm) were manufactured by Evans Adlard & Company limited and used as separator. All the materials above were used without further purification.

3.1.2 Equipment

Preparation of materials and electrochemical performance measurement were completed using general equipment as follow: The oven was manufactured by BINDER GmbH

Company (Germany). The hot plate & Magnetic stirrer (model, JENWAY 1000) was manufactured by Bibby Scientific Limited. The weight scale (model, PM2000MC) was manufactured by Mettler - Toledo Inc.

Electrochemical performance measurement was carried out using Versa-STAT3 electrochemical workstation as shown in Figure 3.1. The Versastat was set up in two electrode mode as a potentiostat or galvanostat as required. The VersaStudio v2.20.4631 was the software controlling the Versastat and installed in a Samsung laptop with Window 7 operation system. The capacitance and specific capacitance of all samples were defined by this measurement instrument.

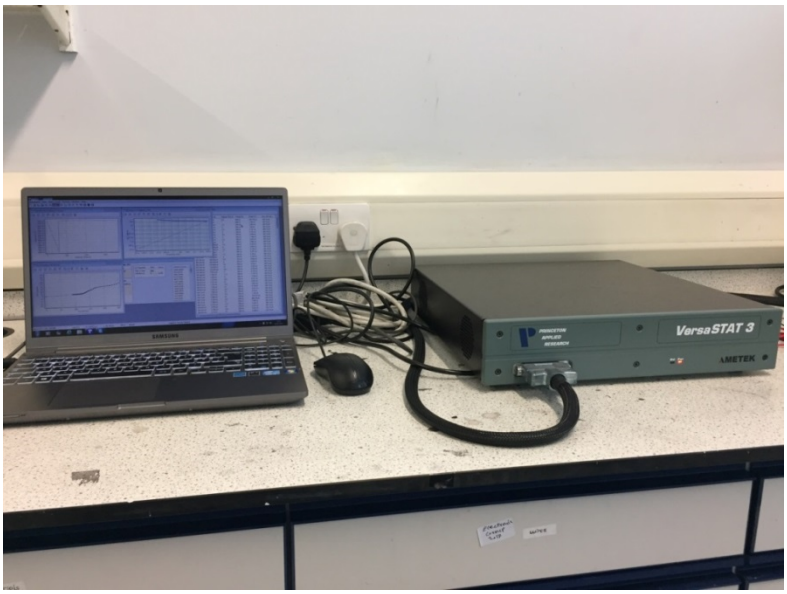

Figure 3.1 Versastat 3 electrochemical workstation with the operating software.

Capacitance (C) is the ability of a component or circuit to collect and store energy in the form of an electrical charge, and is the standard measure of energy storage for capacitors and supercapacitors. Capacitance is expressed as the ratio of the electric charge on each conductor to the potential difference (voltage) between them. The SI unit for capacitance is the farad, named after English physicist Michael Faraday, and is equivalent to one coulomb per volt. A farad is a large quantity of capacitance. Most household electrical devices include capacitors that produce only a fraction of a farad, often a thousandth of a farad (or microfarad, μF) or as small as a picofarad (a trillionth, pF). Supercapacitors, meanwhile, can store very large electrical charges of thousands of farads.

Devices with larger electrodes and current collectors will inevitably store more charge. Specific capacitance (Cs), measured in farads per kilogram, is the capacitance divided by the mass of the active material. This is commonly used to compare the performance of devices of different sizes.

In addition, a scanning electron microscopy (SEM) was applied to study the physical characteristics of the material as shown in Figure 3.2. In SEM method, the surface of solid specimens was characterised using a variety of signals generated by a focused beam of high-energy electrons. The characteristics of the sample revealed by these signals were external morphology (texture), chemical composition, crystalline structure and orientation of material making up the sample. After data was collected over a selected area of the sample's surface, a photo image was captured which demonstrates spatial variations in these properties. Conventional SEM techniques offer characterisation of areas ranging from approximately 1 cm to 5 microns in width. These conventional SEM methods provide magnification ranging from 20X to approximately 30,000X, and spatial resolution of 50 to 100 nm.

Figure 3.2 A typical SEM instrument, showing the electron column, sample chamber and visual display monitors.

In this thesis, a Zeiss scanning electron microscope (Model SUPRA 35 VP) was used to characterise the physical properties of the carbon material, which was conducted at an acceleration voltage of 15 kV. During the examination, the samples were attached to a metal stud using a double-sided conductive adhesive tape as shown in Figure 3.3.

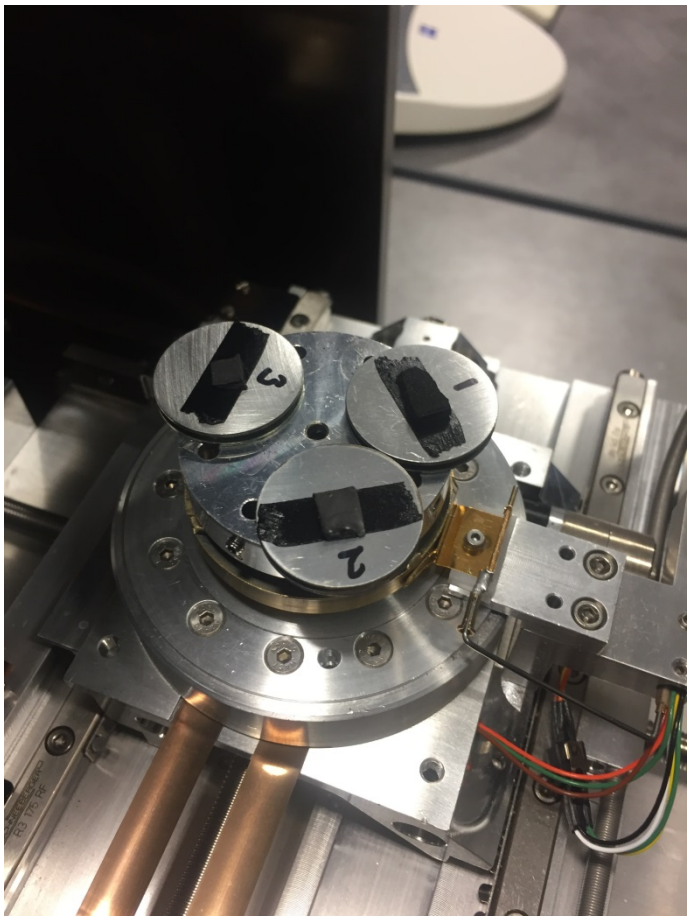

Figure 3.3 Three different types of carbon were attached to a metal stud in SEM measurement.

3.2 Evaluation of electrochemical properties

In this study, the electrochemical performance of the supercapacitors was studied by cyclic voltammetry (CV) and galvanostatic charge/discharge (GCD) using a Versa-STAT3 electrochemical workstation. The CV and GCD testing results were applied to calculate the electrical capacitance of the supercapacitors. All the measurements were conducted at room temperature (20 $\pm$ 4 ºC).

3.2.1 Cyclic voltammetry

When an electric potential is applied between the two electrodes in an EDLC, opposite ion charges accumulate on the surfaces of the electrodes. An ion-permeable separator is placed between the electrode in order to avoid short-circuit and therefore an electric field is created between the two electrodes to form the function of storing energy.

Cyclic voltammetry (CV) is an effective method in the area of electrochemistry. It has been applied to characterize the performance of several electrical energy storage devices, for example batteries and supercapacitors. CV tests are performed by applying a linear potential sweep to the working electrode. A positive (charging) voltage sweeps in a specific voltage range (0 ~ 0.8 V) and then reversing (discharging) voltage sweep immediately after the maximum voltage is reached. The electrochemical behavior of the supercapacitor can be assessed from the current response against the applied voltage.

In CV measurement, there are two important parameters that have to be adjusted in the VersaStudio as shown in Figure 3.4. Firstly, the operating voltage range set up in the CV measurement method relies on the electrolyte used in the supercapacitor. There are two different types of electrolytes used in this study. Supercapacitors with an aqueous electrolyte are regularly applied with the working voltage of 0.8 -1.0 V. Another type of electrolyte is organic solvent which can be specified with a rated voltage of 2.5 V. In this study, organic solvent (a mixture of tetrabutylammonium tetrafluoroborate ($C_{16}H_{36}BF_4N$) with propylene carbonate ($C_4H_6O_3$) was used in manufacturing the first trial 3D printed supercapacitor with the working voltage at 2.4 V. Manufacturing of extendable supercapacitors and metal free supercapacitors used water-based electrolyte (H_3PO_4 and PVA gel electrolyte) with the working voltage at 0.8 V.

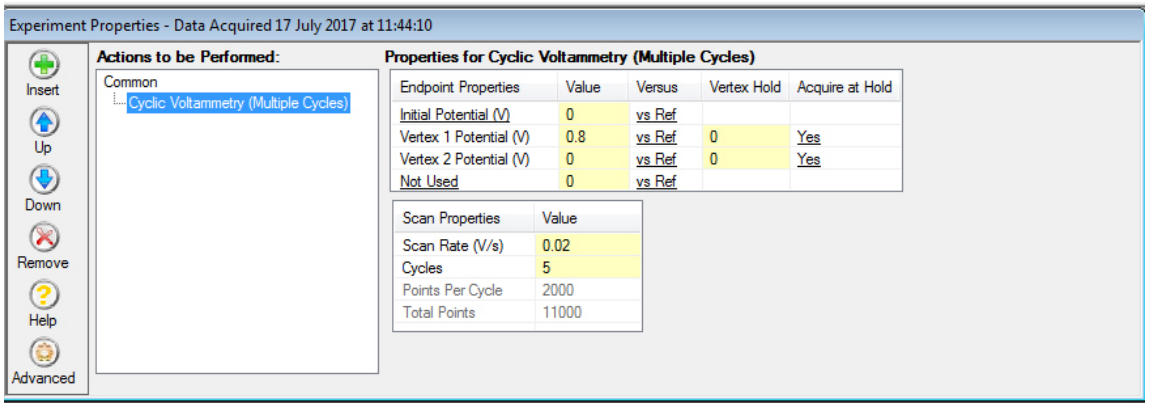

Figure 3.4 Typical set up window of CV measurement using the VersaStudio.

Secondly, adjusting of scan rates (V/s) is also required. The scan rates have significant effects on measurement of capacitance. The performance of supercapacitor can be characterized by capacitance measured at different scan rates. At lower scan rate (e.g., 0.005 mV/s), CV curve exhibit a rectangular shaped curve as an ideal capacitor. However, when scan rates increase, the ideal rectangular CV curve is deformed as shown in Figure 3.5.

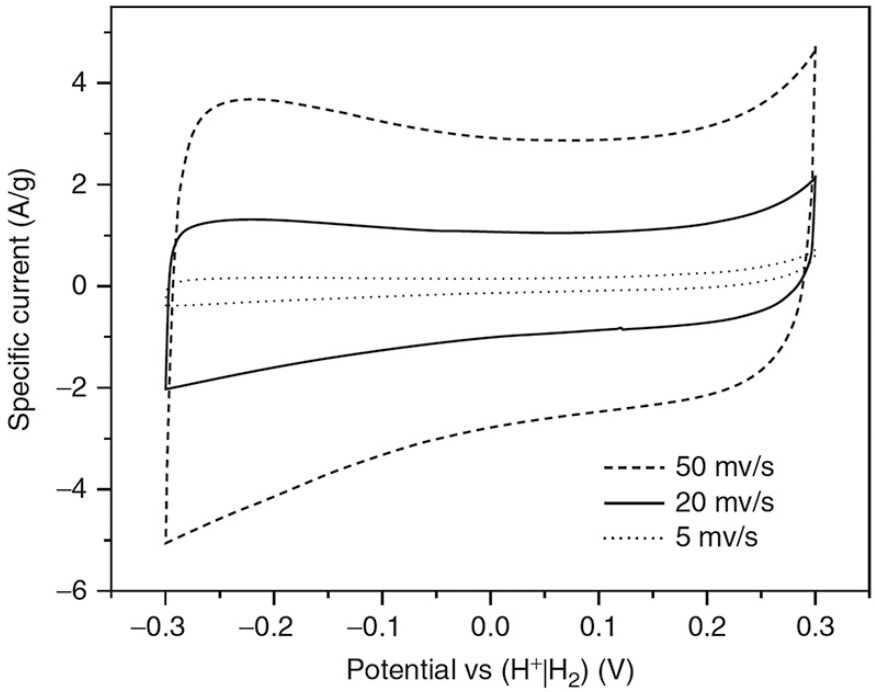

Figure 3.5 Cyclic voltammograms (CVs) of ordered graphitic mesoporous carbon at different scan rates [5].

As shown in Figure 3.6 [94], the electrochemical behaviour of a composite supercapacitor is assessed based on the CV measurement. Measurement of electrochemical behaviour of the supercapacitor can be calculated from the current response against the applied voltage. The capacitance, C1, of an EDLC can be calculated by the following Equation (3.1) [3, 5]:

$$C_1 = \frac{Q_{total}}{2\Delta V} \qquad (3.1)$$

Where, Q_{total} is the average integral area of CV curve obtained from the VersaStudio software which represented the total supercapacitor's charge in coulombs. This value was measured from the CV response curve. ΔV is the voltage change between the device's terminals in volts (V)

The specific capacitance is the fundamental capacitance of the active material normalized by the mass of the electrode of EDLC sample. The specific capacitance can be calculated as the equation (3.2):

$$Cs_1 = \frac{C}{m} \qquad (3.2)$$

Where Cs_1 is the specific capacitance of the electrode, C is the measured capacitance for the two-electrode cell calculated from equation (1), *m* is total mass of the active material in both electrodes.

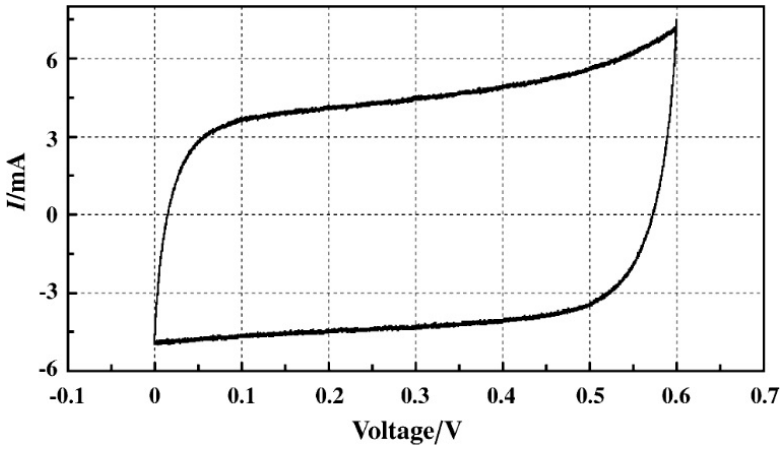

Figure 3.6 A typical CV curve of a supercapacitor recorded at the scan rate of 5 mV/s [94]

3.2.2 Galvanostatics charge/discharge

Galvanostatics charge/discharge (GCD) is an alternative method used to evaluate the performance of the supercapacitors under controlled current conditions. This method is the most preferred DC (direct current) test and is not only used in a laboratory but also in industry. The GCD process is measured by the responsive potential with respect to time unlike CV test, which evaluates data correlating to electrochemical phenomena arising in the electrode material. The measurement is completed in two steps: 1) a

constant current charges a supercapacitor then 2) discharge in a specific voltage range or charge/discharge time [94], As shown in Figure 3.7, an EDLC presents a triangle shape due to the voltage changing linearly as times increases.

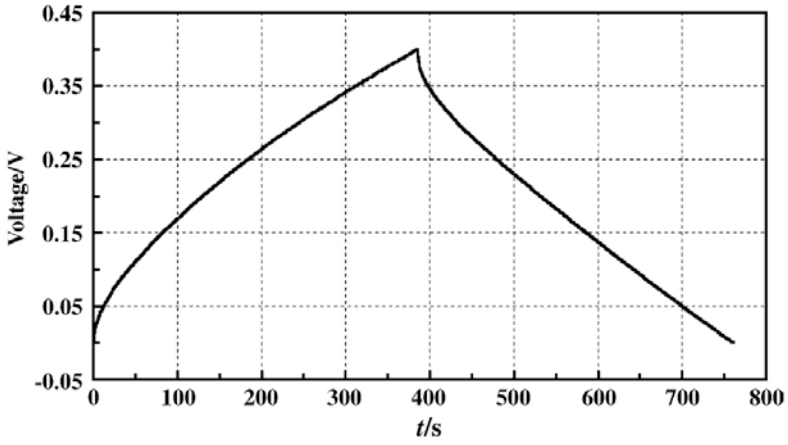

Figure 3.7 A typical GCD curve of a supercapacitor recorded at the current of 2 mA [94].

The GCD method is different from the CV technique because in GCD method, the working voltage is measured under controlled current. In GCD measurement, the potential established relies on the operating voltage of electrolyte used. The currents of charge and discharge have significant effects on measured capacitance. Increasing the charge and discharge current decreases the capacitance. Figure 3.8 shows a typical set up window of GCD method using the VersaStudio.

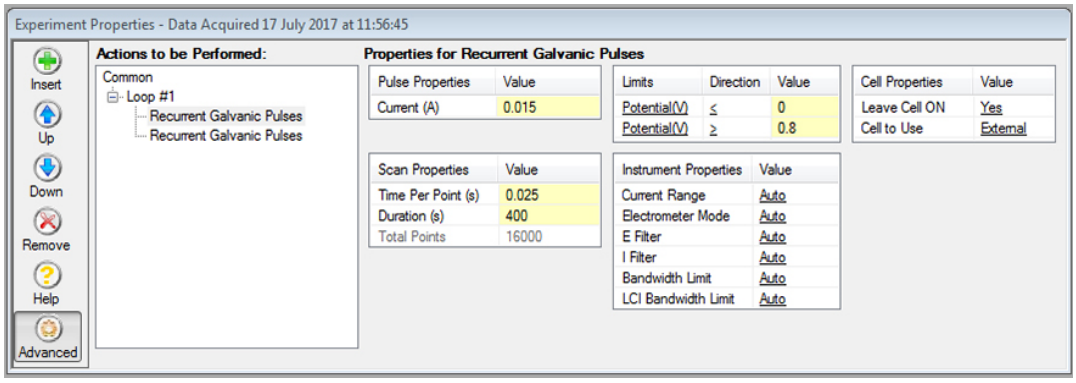

Figure 3.8 Typical set up window of GCD measurement using the VersaStudio.

The capacitance C_2 of an EDLC can be calculated by the following equation [8-9]:

$$C_2 = \frac{i \times \Delta t}{\Delta v} \qquad (3.3)$$

Where, i is the discharge current in amperes (A), Δt is the discharging time (s) and ΔV is the voltage of the discharge excluding iR drop (V).

In addition, specific capacitance (C_s) and single-electrode specific capacitance can be calculated from a galvanostatic charge-discharge curve by the following equation:

$$Cs_2 = \frac{i.\Delta t}{m.\Delta V} \qquad (3.4)$$

$$Cs_3 = 4.Cs_2 \qquad (3.5)$$

Where i is current in amperes (mA), Δt is the charging/discharging time (s), m is the total weight of active materials of two electrodes (g) and ΔV is the voltage of the discharge (V).

In this study, each sample were measured using the Versastat workstation and then the data were used to calculate capacitances using equations (3.1) and (3.3) given above. Specific capacitances were also calculated using equations (3.2) and (3.4).

As mentioned above, the GCD method has been used to observe the reaction in potential relating to time during charging and discharging. The GCD technique also can be used to determine the equivalent series resistance (ESR) using IR drop value. The term iR drop is used to refer to a voltage drop which occurs at the initial discharge. The iR drop is caused by uncompensated resistance or resistive component of impedance as shown in Figure 3.9

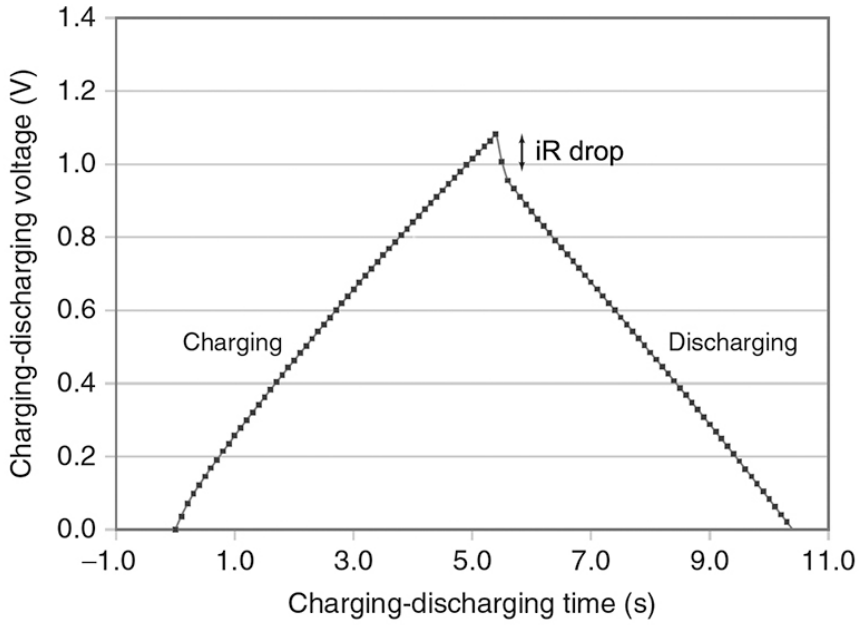

Figure 3.9 A GCD curve of the supercapacitor with the iR drop [5].

iR drop can be calculated from the difference of the electrical potential between the two ends of a conducting point through a current flow. In addition, iR drop can be increased when the high current is applied. In EDLC, the iR drop occurs when potential needs to move ions through the electrolyte solution. The factors that influence the iR drop are the position of electrode and conductivity of the electrolyte solution. Furthermore, the higher iR drop can be caused from the use of low conductivity of the electrolyte.

The ESR can be calculated from the GCD method using the iR drop value divided by double the potential used. This calculation method can be applied in both system of EDLC (three electrode or two electrode system) [8-9].

3.2.3 Electrochemical impedance spectroscopy (EIS)

Electrochemical impedance spectroscopy (EIS) is a method providing further study insight about the electrical characteristics of supercapacitor and also applied to measure and calculate the equivalent series resistance (ESR). The ESR can be used to determine resistance of cell component such as contact resistance between current collectors and electrodes and electrolyte resistance. In this method, an electrochemical supercapacitor sample is tested using a small alternating current (AC) over a different range of frequencies (0.01 Hz to 1 MHz). The result of measurement derives from changes in current caused by the impedance of the sample and is used to draw on a Nyquist plot which charts imaginary resistance (Z") against real resistance (Z). From the format of Nyquist plots, the plot typically displays information about the capacitance, ion-diffusion, and resistance of the device. Information about the resistance is contained within the high-frequency region; information about the ion-diffusion properties in the mid-frequency region; and information about the capacitance in the low frequency region. A perfect supercapacitor would be represented by a straight line parallel to the imaginary axis (the Y-axis) of the Nyquist plot.

The ESR is corresponded to the intersection of the impedance curve at the x-axis in the Nyquist plot. Examples of both (a) ideal capacitors and (b) supercapacitors have the same ESR as shown in Figure 3.10. However, it can be seen that an impedance response of a supercapacitor differed from the ideal capacitor at low frequencies. This difference is caused by the equivalent distributed resistance (EDR). The EDR corresponds to the ionic resistance of electrolyte within the pores of the electrodes. Therefore, an elevated EDR can be induced by increasing the number of pores in an active electrode [3, 5].

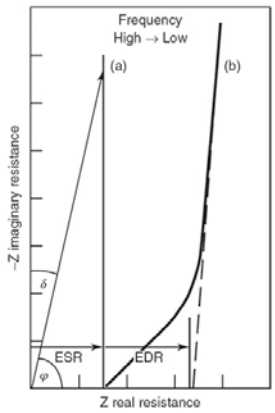

Figure 3.10 Schematic representation of the Nyquist plot of (a) an ideal capacitor and (b) a supercapacitor [6].

Chapter 5 Pilot Experiments: FDM & Inkjet, and FDM & Paste Extrusion

4.1 Introduction

This chapter details the tests of two prototype supercapacitors manufactured using 3D printing methods. For the first sample, an FDM printer was used to manufacture a frame designed for the current collectors to be printed on using an inkjet printer. The supercapacitor was then completed by blade-coating carbon electrodes, before affixing the two halves with an electrolyte-soaked paper separator in between. The second sample was an attempt to improve on the design of the first sample. Instead of printing the current collector with an inkjet printer, a paste extruder was employed to reduce the fabrication time. Other improvements to the frame design, manufacturing procedure and separator electrolyte were also incorporated.

At time of writing, there is no prominent published research that has attempted to integrate inkjet printing and 3D printing, or FDM and paste extrusion, to fabricate supercapacitors. Inkjet printing has been widely used in electronic devices in recent years, although more commonly to print circuitry or electrodes than current collectors. Paste extrusion is yet to be investigated as a means to manufacture current collectors. Although the designs of the two samples tested are very simple, the concept is that more complicated designs could be manufactured using the same process, which may have the potential to improve functional performance, or to create cost-effective bespoke devices for small-scale production.

As detailed in the literature chapter, FDM can deposit two different types of plastic, ABS and PLA. ABS has greater strength and durability, but PLA is more environment friendly. It was resolved to test both as the frame material: ABS in the first sample and

PLA in the second. Silver ink was the material of choice for the current collector because of its conductivity and resistance to chemical weathering. Activated carbon (AC) seemed the ideal electrode material as it is inexpensive, easy to process, non-toxic, has a high specific surface area, and good conductivity. Phosphoric acid was selected as electrolyte for its suitable ion size, low cost and simple preparation at ambient conditions. The separator was required to be nonconductive, have low ionic resistance, and be easily wetted by the electrolyte, thus filter paper was chosen.

Inkjet printing was selected to fabricate the current collector for the first sample as it was considered to be more accessible, lower cost and involve a simpler manufacturing procedure. However, inkjet printing would prove overly time consuming to print the iterations required to build a sufficiently thick current collector, and the resulting sample, although functional, failed to deliver a satisfactory level of performance.

It was surmised that using a paste extruder to build the current collector could be less time consuming. A paste extruder would be able to print silver paint, as opposed to the silver ink which the inkjet printer dispensed. Because silver paint is more viscous, it may be dispensed in thicker layers than ink and dry more easily, thus reducing the time taken to build it to the required thickness. Silver paint is less durable than silver ink, but otherwise this change was not expected to have a significant impact on performance.

In addition to altering the design of the current collector, other improvements were attempted:

1) The overall size of the sample was increased to accommodate changes to the frame design and improve performance.
2) A hinge was added to the frame to allow for simplified assembly.
3) The frame material was changed from ABS to PLA in order to test both materials
4) Drying times for the electrodes were altered to prevent cracking.
5) To further simplify the manufacturing process, the electrolyte was changed from 1 molar phosphoric acid (H_3PO_4) solution to a gel electrolyte, 1 molar tetrabutylammonium tetrafluoroborate ($C_{16}H_{36}BF_4N$) with propylene carbonate ($C_4H_6O_3$) solution.

Testing such a new manufacturing process, clearly the capacitance was never expected to be comparable to commercial EDLCs. Although the second sample performed

considerably better than the first, and it was clear much improvement was needed to the design and implementation of the manufacturing process.

4.2 Pilot sample 1: FDM & Inkjet Printing

4.2.1 Design and manufacturing procedure

1) Design

The supercapacitor was designed in two halves, which were to sandwich an electrolyte-soaked, filter paper separator. The two halves of the frame were designed as upper and lower parts, with four slots on the upper part designed to fit four protrusions on the lower part to ensure accurate assembly. These two parts were to be plastic, printed by the FDM machine. A silver ink current collector would then be printed directly onto each frame before each carbon electrode was built on top using a blade coating method. Finally, the separator was to be prepared and placed between the two halves as they were slotted together to form the completed sample. Figure 4.1 shows the schematic of the lower part of the supercapacitor, which is identical to the upper half, except that the upper part has slots where the lower part has protrusions. Figure 4.2 demonstrates how the two halves combine, and the design dimensions and technical drawing of designed sample was presented in an appendix A.

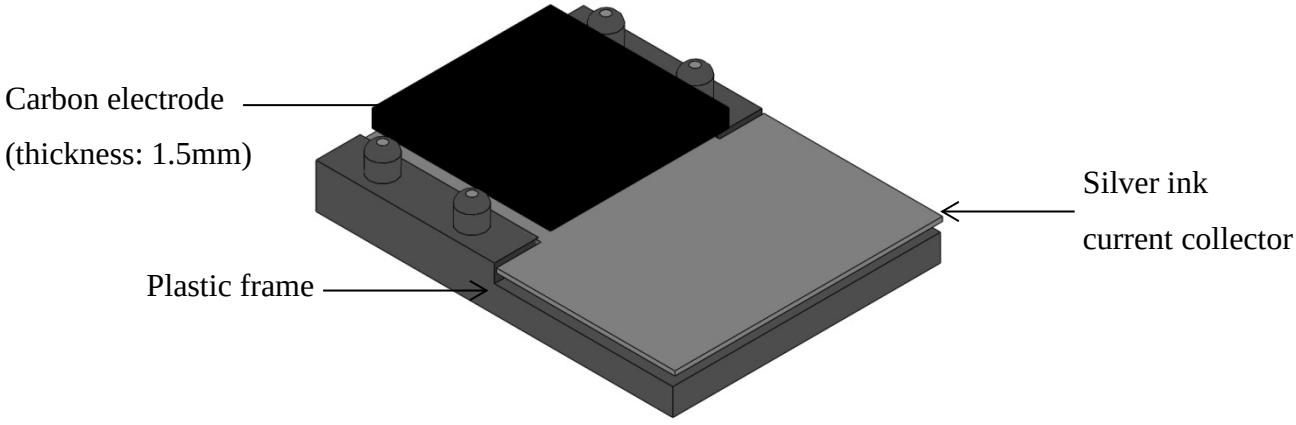

Figure 4.1 Schematic of lower part of supercapacitor.

**identical to upper part save protrusions on frame*

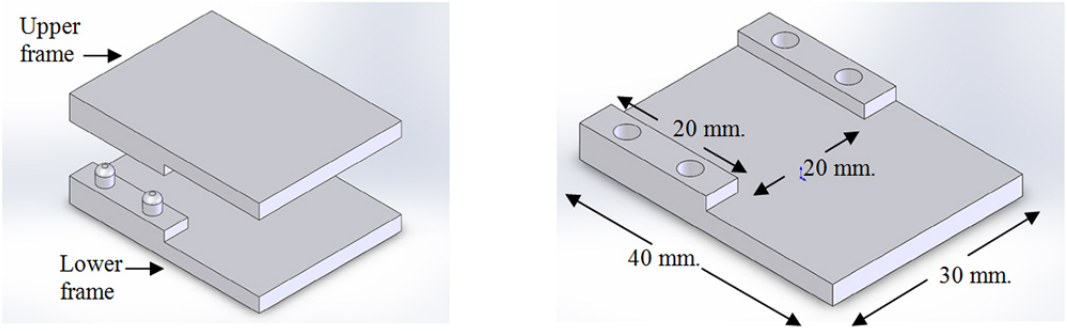

(a) **(b)**

Figure 4.2 (a) Designed assembly and (b) dimensions of EDLC

2) Printers, software and materials

The 3D printer used in this work was a fused deposition modelling printing machine (FDM Dimension SST 768 FDM Printer) as shown in Figure 4.3. The FDM printer has two cartridges containing the part-material and the support-material. The support material applied in this work was P400SR Soluble Support comprised of 99% butadiene-styrene copolymer (manufacturer information); the part-material is ABS-P430 Model composed of 70-75% butadiene-styrene-acrylonitrile-methyl methacrylate copolymer and 25-30% styrene/ acrylonitrile copolymer (SAN) (manufacturer information). These two materials were purchased from Stratasys Inc. The software used to design the frame for the FDM printer was Solidworks®.

Figure 4.3 The FDM printer (FDM Dimension SST 768 FDM Printer).

The inkjet printer (Dimatix, DMP-2800) has 16 nozzles, each nozzle delivering drops of 1-10 picolitres of ink with a resolution of 1270 dot per inch (dpi) as shown in Figure 4.4. Silver conductive ink purchased from Sun Chemical was used as the current collector material in this study. The dispersion viscosity of the silver ink was 10-15 cps at 23 ºC.

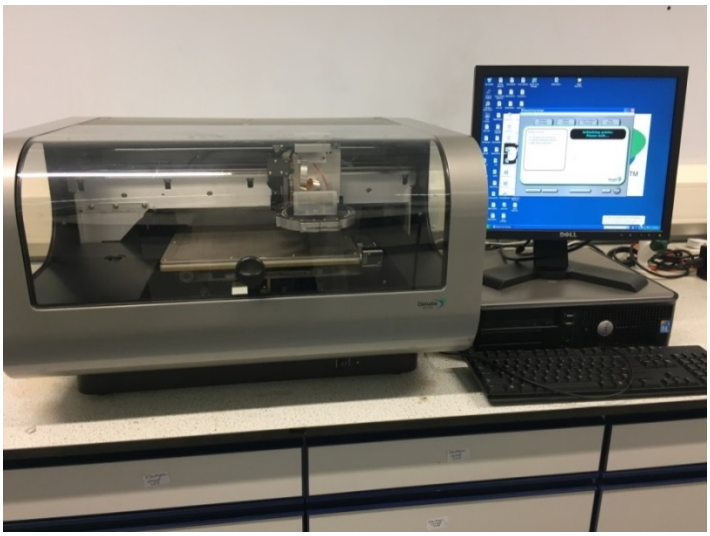

Figure 4.4 The inkjet printer (Dimatix, DMP-2800).

The software used to control printing parameters was the Dimatrix drop manager. This software was also used to design the current collector patterns for this experiment as shown in Figure 4.5. Two different patterns were used with sizes 20 x 20 mm and 20 x 30 mm respectively.

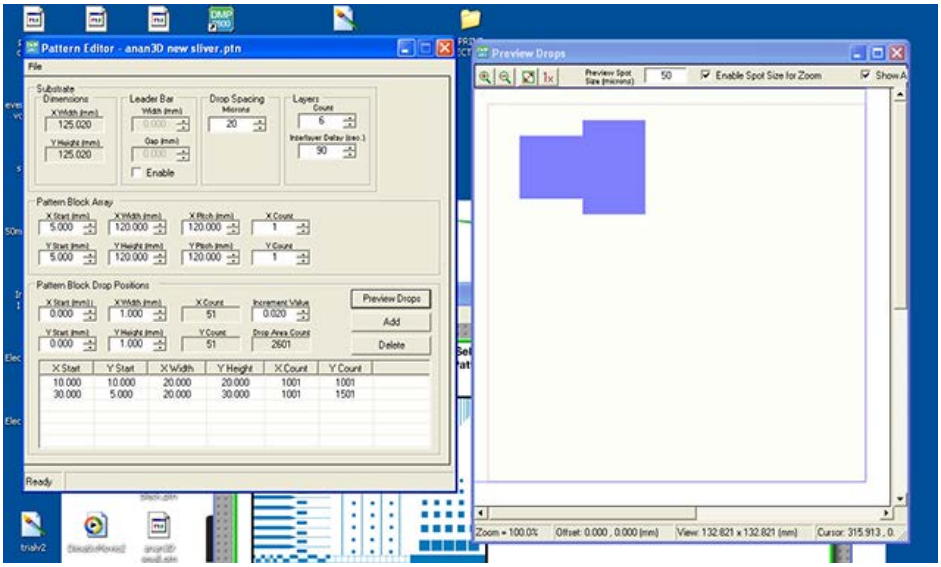

Figure 4.5 Patterns creation using the Dimatrix drop manager software.

The electrode material used for the supercapacitor was activated carbon. The activated carbon was made into a slurry and mixed with the carbon material using carboxy methyl cellulose (CMC) as a binder. The CMC binder was prepared by mixing a certain amount of CMC with distilled water at room temperature. It was stirred overnight using a magnetic stirrer. The concentration of CMC was fixed at 5wt% based on the total mass of AC and CMC. Then 0.5 g activated carbon was added to the CMC binder solution. In order to obtain a uniform slurry, it was stirred for 8 hours.

The electrolyte applied in this experiment was 1 molar phosphoric acid (H_3PO_4) solution, and filter paper was used as the separator.

3) Frame – FDM printing process

The 3D frame structure of the supercapacitor was fabricated by the extrusion heads of the printer. Initially, the machine deposited support-material, which was removed after the printing which acts as scaffolding. The thermoplastic part material was then heated and became semi-liquid. Then it was deposited layer by layer in ultra-fine beads along the extrusion path. Finally, the support-material was dissolved and removed and then the final 3D frame object for the supercapacitor is ready to use as shown in Figure 4.6.

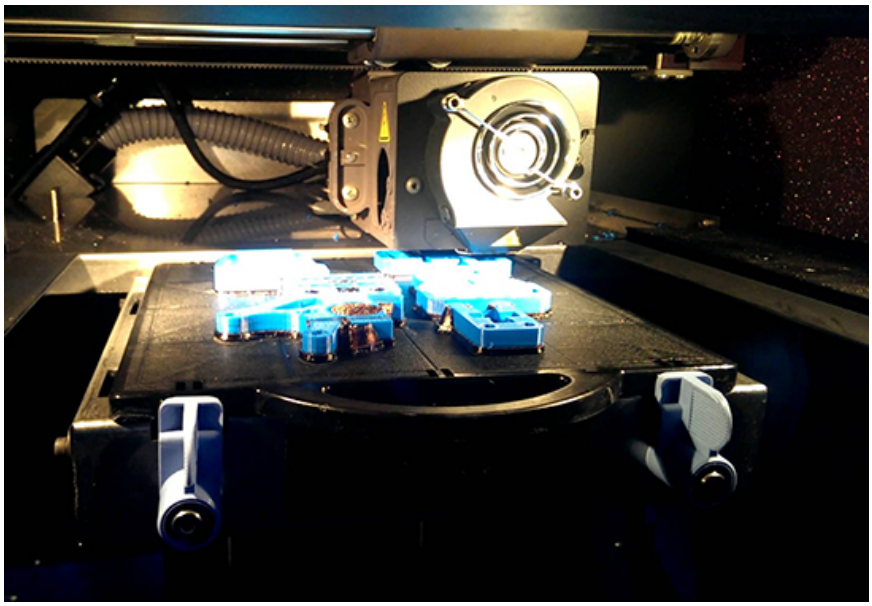

Figure 4.6 Printing the frame using FDM machine.

4) Current collectors – inkjet printing process

Having constructed the EDLC frame, an inkjet printer (Dimatix, DMP-2800) was used to print the current collector onto the 3D samples. The silver conductive ink was prepared in the ink cartridge. This inkjet printer contained 16 nozzles and each nozzle can be adjusted in terms of its firing voltage, which was set as shown in Figure 4.7. The firing voltage determines the drop velocity of the printed material and should be adjusted depending on the physical characteristics of the material and the condition of the nozzles.

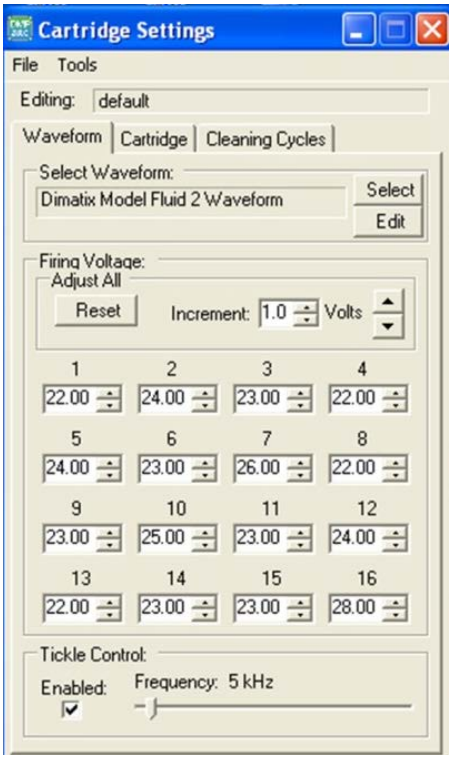

Figure 4.7 Cartridge setting for adjusting the voltage of 16 nozzles.

The 16 nozzles were tested in terms of ability to jet the liquid using the software's "drop watcher" function to determine the ideal print setup. This function provides direct viewing of the jetting nozzles, the actual amount of jetted ink, and the surface of the plate surrounding the nozzles as shown in Figure 4.8. It was determined that only six nozzles, in the middle of the nozzle row, should be used for printing due to inconsistency exhibited by the other nozzles in the quality control process.

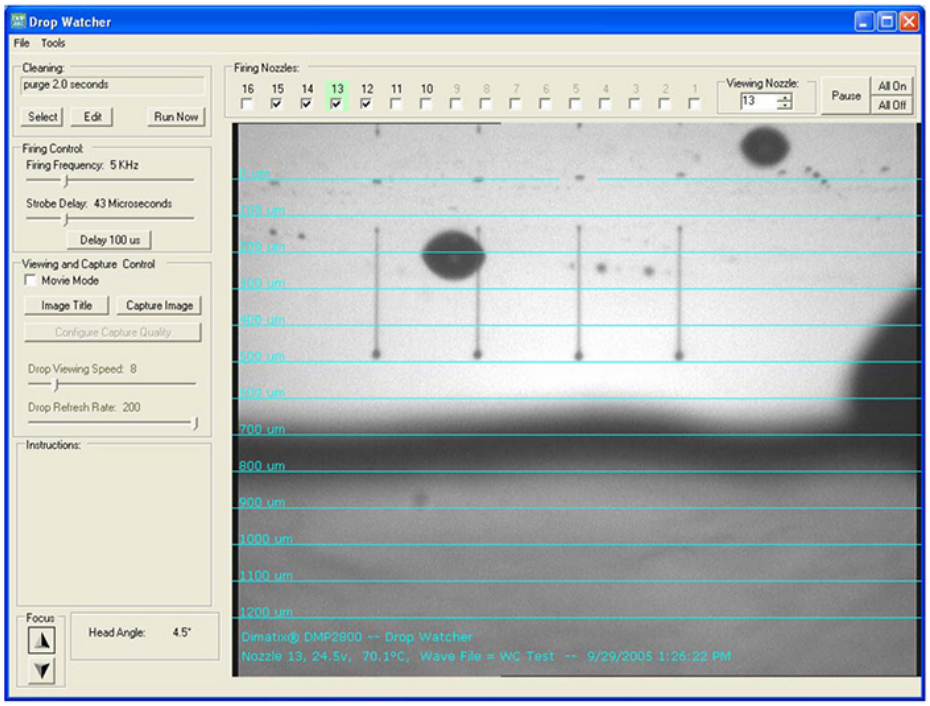

Figure 4.8 Testing of the actual jetting of the ink using the drop watcher function.

The 3D packaging frames were printed with silver conductive ink. Firstly, the silver ink was printed with a size of 40 x 20 mm on each of the 3D frame objects in order to build the conductive current collector layer. The frame was printed about 20 times to produce a suitably thick current collector, which took around one hour to complete. The samples were then dried in an oven at 90^{o}C to enhance the adhesion of the carbon slurry layer to be coated on it, as shown in Figure 4.9.

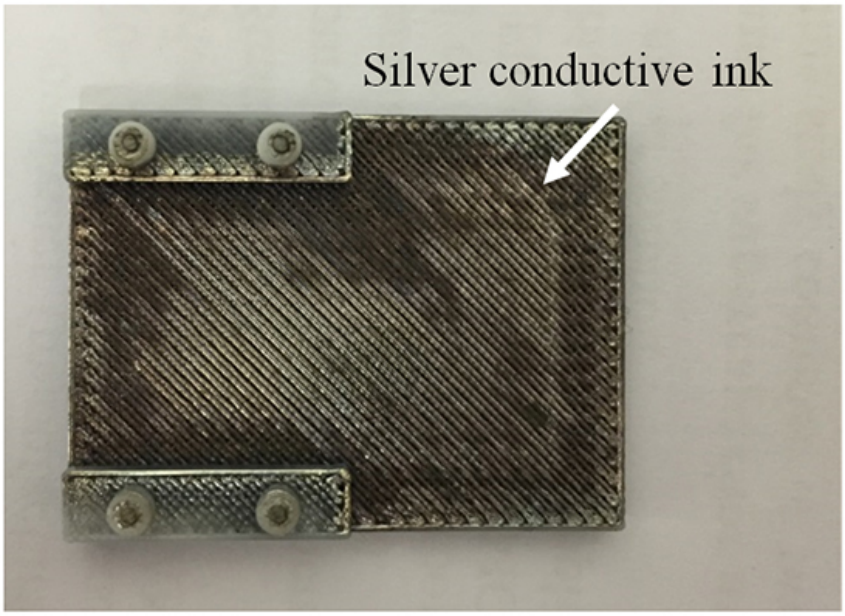

Figure 4.9 Inkjet prints the silver conductive ink on 3D packaging frame structure.

5) Electrodes – blade coating process

To build the electrodes, the carbon slurry was deposited using a blade coating method over the silver conductive ink with a size of 20 mm x 20 mm. It was coated in five layers positioned as shown in Figure 4.10 (a). The final thickness of each electrode was 1.5 mm.

6) Separator – electrolyte preparation and assembly

A filter paper was soaked in the electrolyte and used as the separator. The filter paper separator was placed on the electrode of the lower part of the EDLC before the upper half was affixed on top. This completed the fabrication process of the sample electrochemical as shown in Figure 4.10 (b).

(a) (b)

Figure 4.10 The coating process for making the final electrochemical supercapacitor.

(a) Showing the slurry coated on 3D object after printed the silver conductive ink
(b) Cross section of 3D supercapacitor.

4.2.2 Performance evaluation

The electrochemical properties of the prototype supercapacitor were assessed using an electrochemical workstation–VersaStat 3. Figure 4.11 shows the cyclic voltammogram (CV) curve of the prototype with a scanning rate of 0.02 V/s. The curve shape shows that the device operated as a supercapacitor. This experiment has shown that inkjet printing is at least a possible method for fabricating the current collector of an EDLC sample. The main drawback of inkjet printing was found to be its time-consuming nature. Approximately twenty iterations of printing were required to build a current collector of sufficiently low resistance. This might be a reason for applying other techniques to form the current collector.

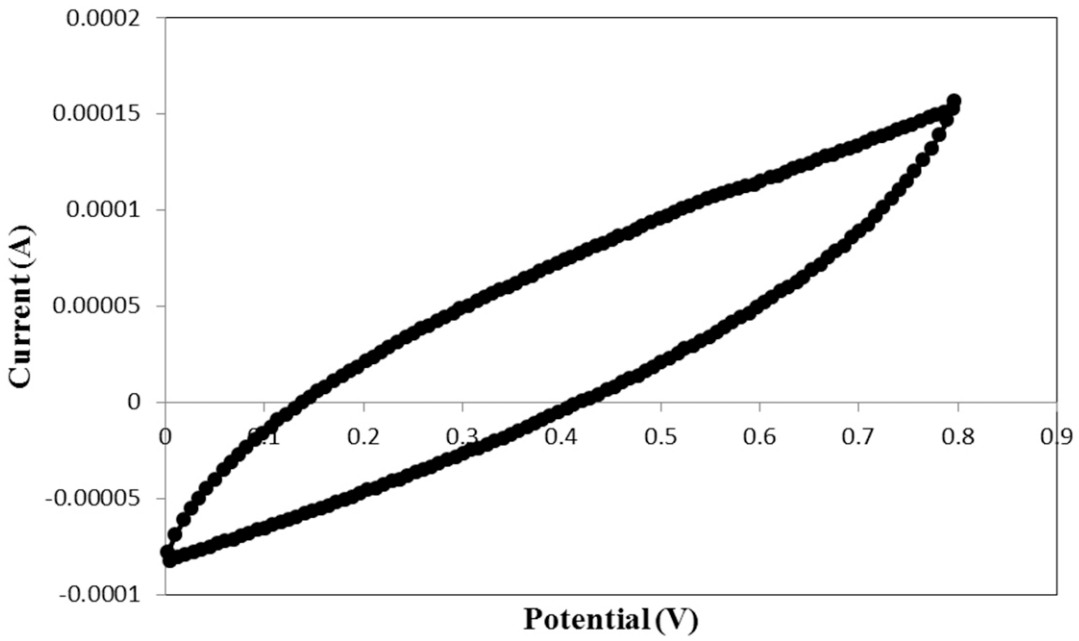

Figure 4.11 CV curves of the EDLC samples at the scan rate of 0.02 V/s.

The capacitance and specific capacitance from the CV measurement were calculated using equation (3.1) and (3.2). The capacitance calculated was 6.29 mF and the specific capacitance of the supercapacitor was 53.83 mF/g. A GCD test was also applied to evaluate the capacitance of the sample.

Figure 4.12 showed the GCD curve of the EDLC sample with the IR drop at 0.44 V. It can be seen that the IR drop was high because of high internal resistance. The capacitance calculated from the GCD was 6.51 mF and the specific capacitance of the supercapacitor was 59.23 mF/g. Both the capacitance and specific capacitance were calculated using equation (3.3) and (3.4).

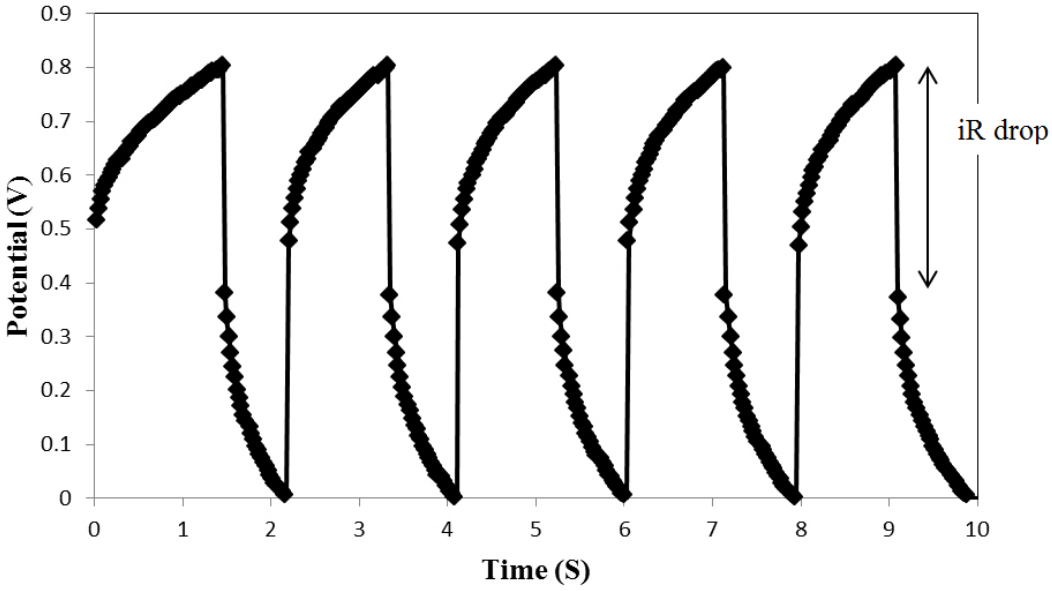

Figure 4.12 Galvanostatic charge/discharge curves recorded at a charging current of 0.015 A.

The capacitance was not high as expected because there were small cracks in the electrodes surface, causing internal resistance. It is possible that the layers of carbon slurry were afforded too long to dry between layers which led to the cracks.

4.3 Pilot sample 2: FDM & Paste Extrusion

4.3.1 Design and manufacturing procedure

1) Design

The supercapacitors designed for this study comprise of two electrodes and a separator layer soaked in electrolyte, as shown in Figure 4.13. The 3D frame for the supercapacitor was designed using Solidworks® software and created using the FDM printing machine. A view of the frame is shown in Figure 4.14. The 3D frame for the supercapacitor was designed similar to a hinge with a size of 30 x 50 mm dimensions and technical drawing of designed sample was presented in an appendix A. It can be printed in one printing event and requires no assembly. This design makes it easy to form the supercapacitor when all layers are finally printed. Given a suitable separator could not be 3D printed with current technology, efforts were made to simplify the assembly requirements as far as possible. The hinge ensures the two sides will be precisely folded together without the need for additional apparatus. The hinge design was deemed to work well, thus there were no suggestions for optimisation.

A living hinge, being flexible, would not likely provide the same degree of precision as the barrel hinge, so may result in the assembler folding the two sides together askew.

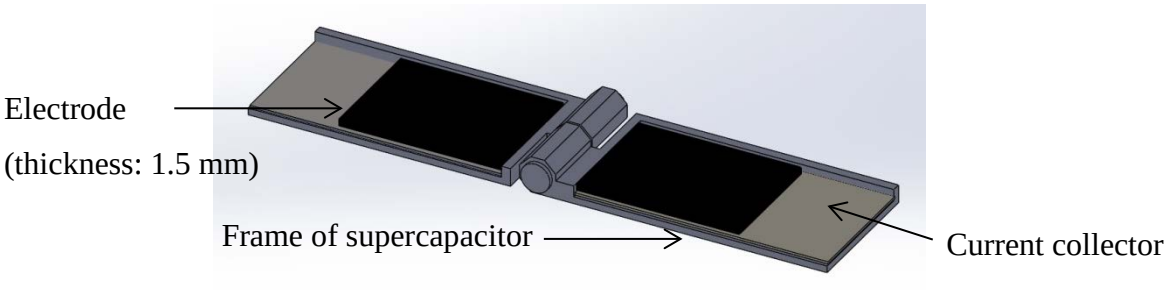

Figure 4.13 Schematic of design structure of supercapacitor.

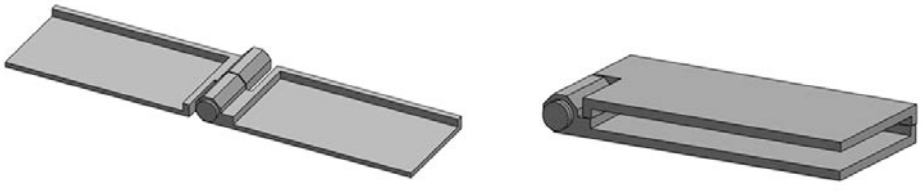

Figure 4.14 The 3D frame for the supercapacitor

2) Printers, software and materials

For this experiment, an FDM printer (Ultimaker 2®) and a Paste extrusion printer (Discovery®) were integrated in order to create the supercapacitors. The two 3D printing technologies were developed to capitalise on each of the particular processes, and provide the possibility to develop unique electrochemical devices. The FDM printer was used to create the frames and the paste extrusion printer was used to build the current collector and the electrode. Figure 4.15 shows the schematic diagram of the combination of the two 3D printing techniques. Figure 4.16 shows the setting of dual extrusion. The distance between the FDM extruder and the paste extruder was 37 mm. The paste tip extrusion was lower than the FDM extruder by around 26 mm. Because of this, the build platform required readjusting between printing the FDM and the paste materials.

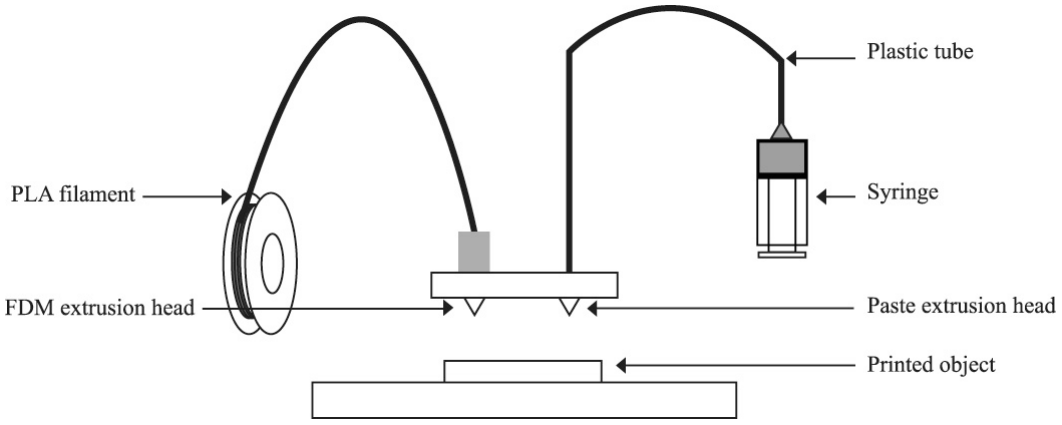

Figure 4.15 Schematic of a combination of two 3D printing techniques.

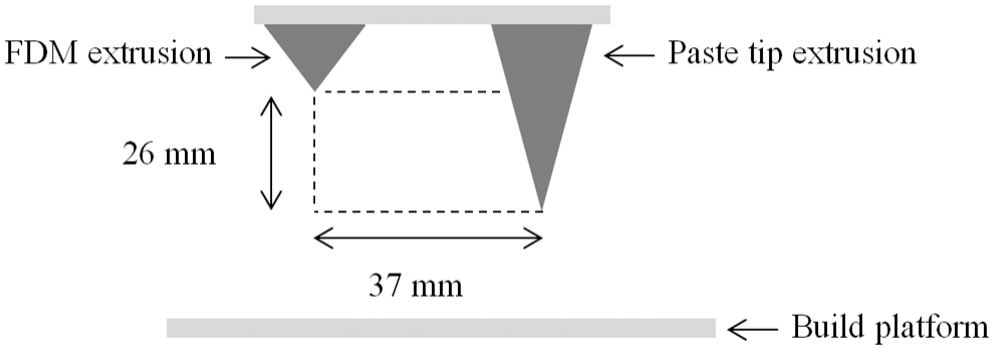

Figure 4.16 Setting of dual extrusion.

The operating method of the fabrication process was adjusted via CURA open source software, which is compatible with both the FDM and the paste extrusion system. The CURA software also transforms the STL file to G-code which is used in machine automation. The G-code files created in this study control the printing parameters for the FDM and paste extrusion system, such as printing speed, layer height and fill density. Figure 4.17 shows the combination of 3D printers for manufacturing the supercapacitor with software used.

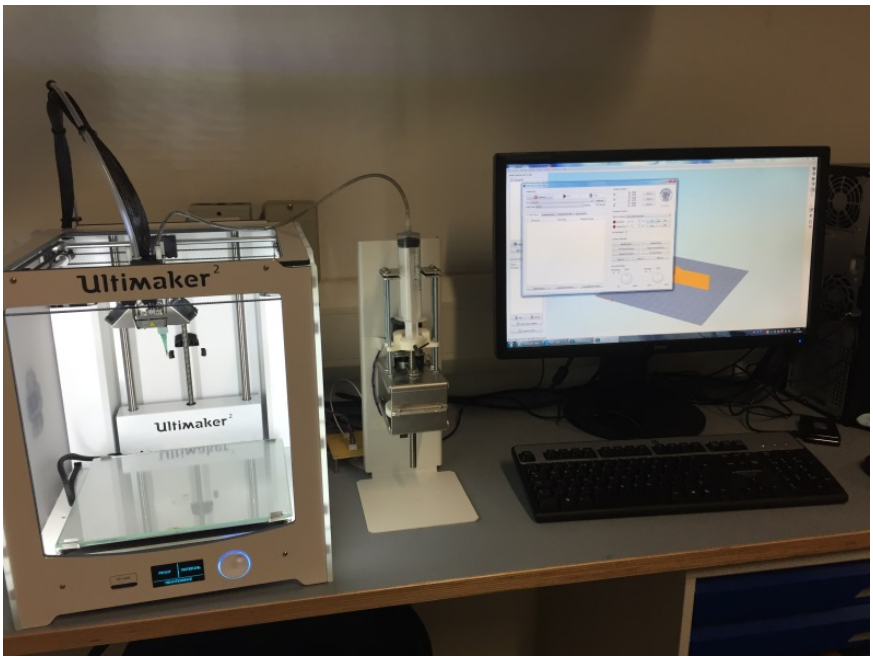

Figure 4.17 The combination of 3D printers for manufacturing the supercapacitor.

Figure 4.18 shows print setup of the FDM machine using the CURA software. The STL file exported from Solidworks software was loaded into the CURA software in order to set the print parameters and transform to G-code. The print parameters were layer height, shell thickness and print speed. After all settings were correctly set, the CURA software was used to transform these settings to G-code and save to an SD card. Note that the temperature control for the nozzle head and the bed platform of the FDM were adjusted at the printer.

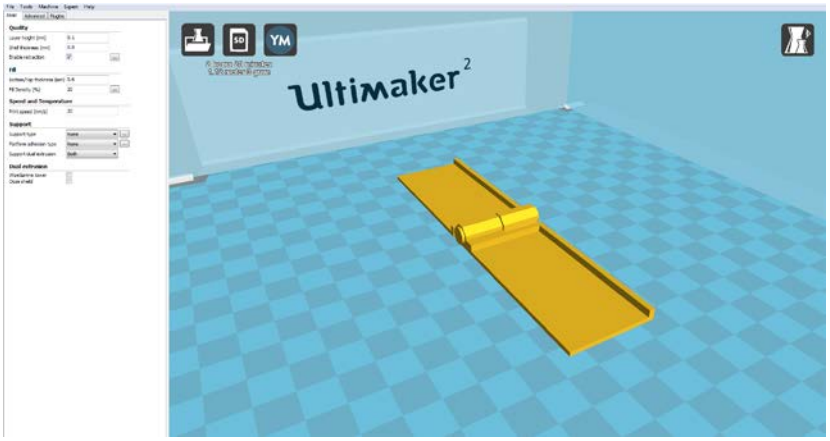

Figure 4.18 Print setting of FDM machine controlled via CURA software.

The CURA software was also used to control the print parameters of the paste extrusion printer. Figure 4.19 shows print parameter settings of the extrusion printer via the CURA software. For controlling the extrusion printer, the G-code was applied to increase the extruder step. In G-code, M codes are machine specific miscellaneous functions, for example the temperature control of the machine.

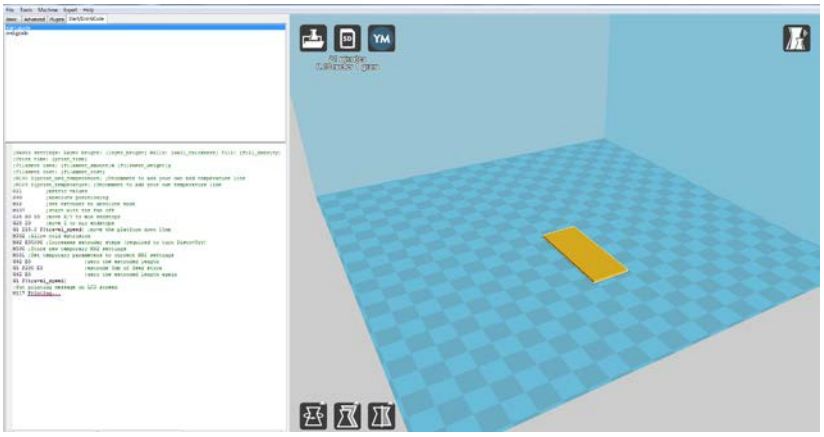

Figure 4.19 Print setting of paste extrusion printer controlled via CURA software.

Table 4.1 shows the list of G-code commands used to control the extruder printer. After all print settings were set, the software directly sent all print information to the extrusion printer to start printing.

Table 4.1 List of G-code commands

Command	**Description**
M 302	Allow cold extrusion
M 92 E 15000	Increase the extrusion step
M 107	Set the fan off

The ideal conductive current collector material is low cost, nontoxic, commonly available, and its viscosity and curing conditions should be compatible with the deposition system used. For these reasons, silver conductive paint was chosen as the current collector material in this test.

The activated carbon electrode was made from a slurry mixture of the carbon material with carboxy methyl cellulose (CMC) as a binder. The CMC binder was prepared by mixing a certain amount of CMC with water/ethanol (1:1) solvent at room temperature. It was stirred overnight with a magnetic stirrer. The concentration of CMC was fixed at 10wt% based on the total mass of AC and CMC. 0.5 g activated carbon was then added to the CMC binder solution. To obtain a uniform slurry, it was stirred for 8 hours.
The electrolyte applied in this experiment was a mixture of tetrabutylammonium tetrafluoroborate ($C_{16}H_{36}BF_4N$) with propylene carbonate ($C_4H_6O_3$). The concentration of the electrolyte used was fixed at 1 mol/L.

3) Frame – FDM printing process

The height of each layer was adjusted to 0.1 mm on the FDM machine and the printing speed was set at 50 mm/sec. The material used was PLA rod with a diameter of 2.89 mm. The 3D frame structure of the supercapacitor was fabricated using the main

extrusion head of the printer. The PLA material was heated and became semi-liquid. Then it was deposited layer by layer in ultra-fine beads along the extrusion path as shown in Figure 4.20. The temperature of the extruder was controlled at 220 ^{o}C, and 60 ^{o}C at the bed of the printer.

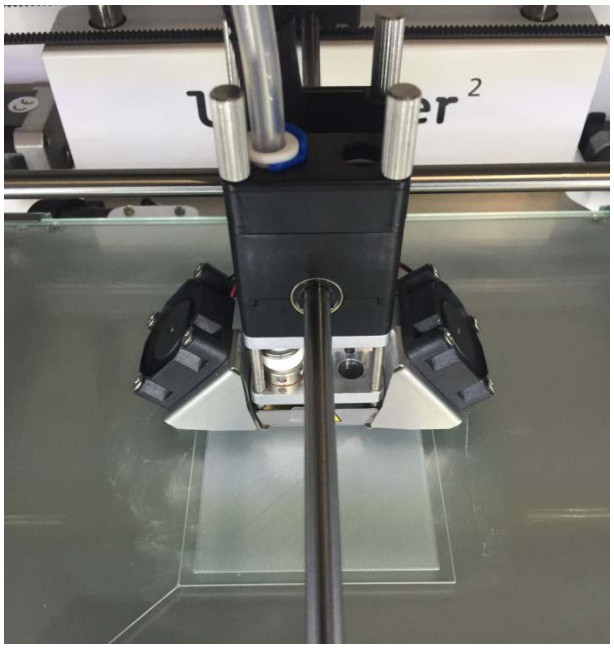

Figure 4.20 The frame of supercapacitor printed with FDM printer.

4) Current collector – paste extrusion process 1

Whereas the frame was printed using the FDM printer, other materials were printed using the paste extruder. In order to deposit the paste materials, the syringe was pressurised by the stepper motor to force the paste material to flow along the plastic tube to the nozzle. This function was automated and controlled by CURA software. CURA software is compatible with both FDM and paste extrusion system, able to set up all specifications for printing including transforming the STL file to g-code. G-code is one of many programming languages used in machine automation, which has also been used in this manufacturing process to control the speed of the stepper motor of the paste extrusion system in order for the appropriate amount of material to be printed.

To deposit the material, 0.6 tapered nozzle was connected to a 3.5 mm inner diameter of PVC rubber tube with length of 70 cm. A 30 ml BD luer-lock syringe was used to contain the materials. Layer height was set at 0.6 mm, 20% infill and printing speed of 50 mm/s.

The paste extrusion system was used to print two materials. First, the silver conductive paint was printed on to the frame. The conductive paint was printed three times with a size of 30 x 55 mm on each side of the 3D frame objects in order to build the conductive current collector layer. Then the sample was dried at room temperature around 30 minute after each of these layers was printed as shown in Figure 4.21.

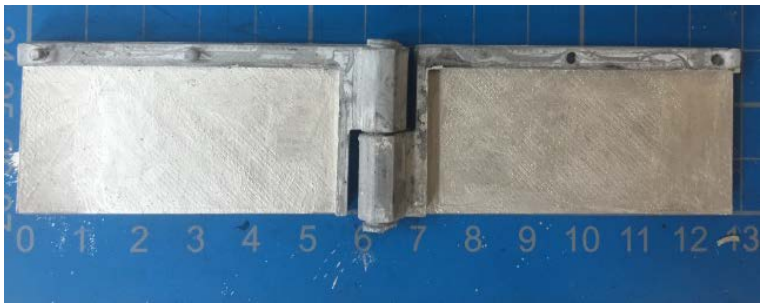

Figure 4.21 Paste Extrusion system prints the silver conductive paint on 3D packaging frame structure.

5) Electrodes – paste extrusion process 2

Carbon slurry was printed on top of the silver conductive paint with a size of 25 x 40 mm, to a thickness of 1.5 mm. It was printed five times to achieve the desired thickness and dried at room temperature as shown in Figure 4.22. The drying time used for each time of printed electrode was around 30 minutes and when the final layer of printed was completed due to the thickness 1.5 mm, the drying time used for the whole printed electrode was around 60 minutes. These slurry layers were applied as the material for the electrodes.

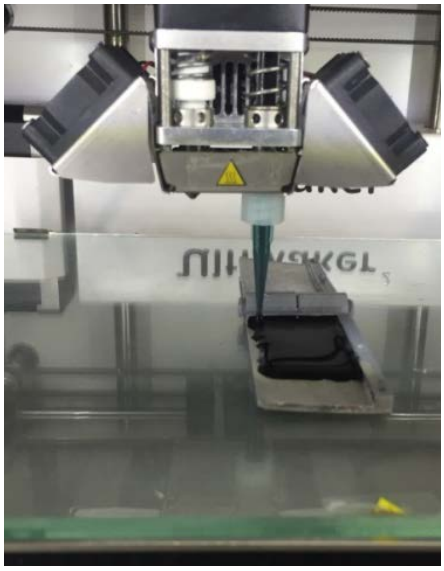

Figure 4.22 Printing slurry on the supercapacitor frame.

6) Separator – electrolyte preparation and assembly

The electrolyte was then dropped on the surface of the printed activated materials, and then these electrodes with absorbed electrolyte were held under vacuum for 30 minutes to allow the electrolyte to fully disperse within the carbon material. In the meantime, a filter paper was wetted with the electrolyte to be used as the separator. The two coated electrodes were finally folded over to sandwich the filter paper separator, and the assembled electrochemical supercapacitor was completed as shown in Figure 4.23 and Figure 4.24.

Figure 4.23 Showing the slurry printed on 3D object after printed the silver conductive ink.

Figure 4.24 Side view of 3D supercapacitor.

As shown in Figure 4.24, warpage occurs due to material shrinkage during the 3D-printing process, which causes the corners of the print to lift and detach from the build plate. When plastics are printed, they initially expand slightly, but then contract as they cool down. If the material contracts too much, this causes the print to bend up from the build plate. Some materials shrink more than others (e.g. PC has a higher shrinkage than PLA), which means there's a larger chance of warping when using it.

The best way to avoid warpage is by using a heated build plate. This keeps the material at a temperature just below the point where it solidifies (the glass transition temperature), ensuring it stays flat and connected to the build plate. When you use a heated build plate it is important to use the right temperature.

The warpage of the frame as shown in Figure 4.24 occurred at the edge of the frame. It did not appear to affect the performance of the EDLC sample because the both electrode materials built on those two sides of casing were still in good positions. The EDLC sample still operated as supercapacitor and the electrical performance were measured and presented in the following section.

4.3.2 Performance evaluation

The CV of the supercapacitor was assessed using the same VersaStat 3 electrochemical workstation. As shown in Figure 4.25, the electrochemical character of a 3D printed supercapacitor was measured according to the corresponding current response against the applied voltage. The CV curve shape shows that the device operated as a supercapacitor. From the Figure, the capacitance, C1, of the 3D printed EDLC can be calculated by the equation (3.1).

The capacitance calculated was 212 mF. The specific capacitance of the supercapacitor was about 205 mF/g. These results demonstrate that the manufacturing process for the supercapacitor printed by 3D printing illustrated above is a satisfactory fabrication method.

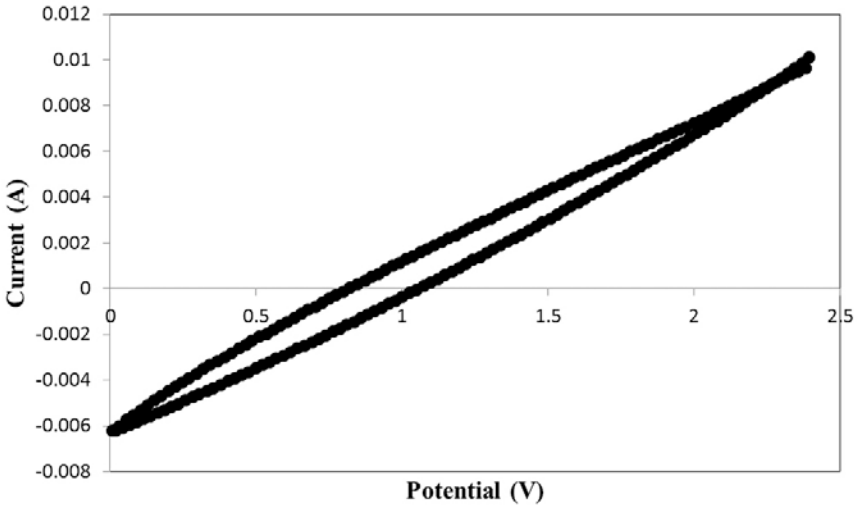

Figure 4.25 The cyclic voltammogram recorded of the 3D printed supercapacitors.

GCD is another method used to determine the capacitance of the ELDC. The charge and discharge processes are set at a specific current to evaluate the capacitance. The GCD curves of the EDLC samples are illustrated in Figure 4.26. The capacitance calculated was 258 mF. The specific capacitance of the supercapacitor was about 262 mF/g. Both the capacitance and specific capacitance were calculated using equation (3.3) and (3.4). The initial portion of a discharge curve exhibits the iR drop due to internal resistance. The high internal resistance was probably due to corrosion of the current collector.

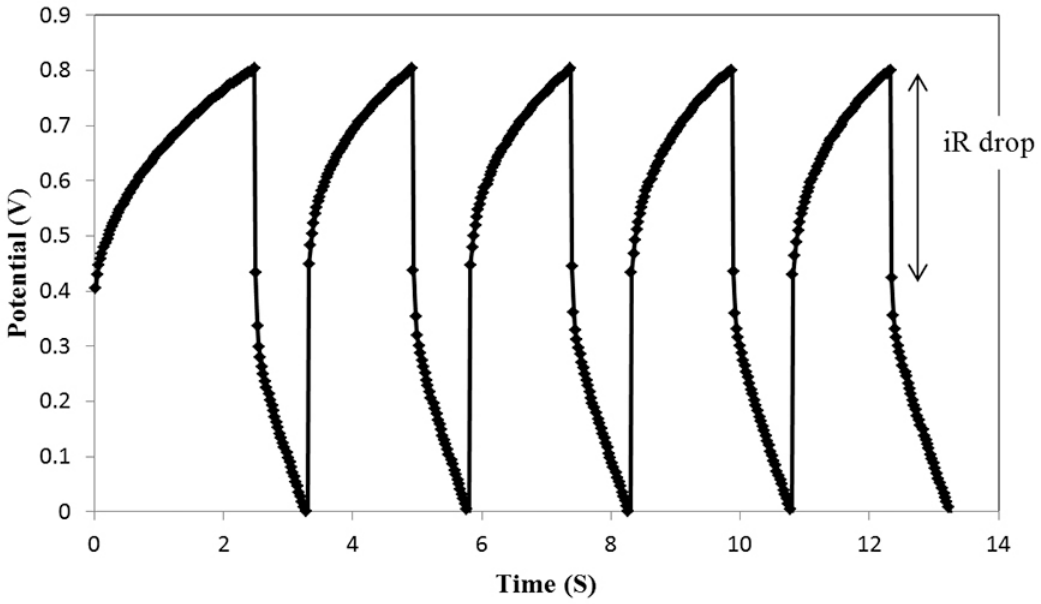

Figure 4.26 Galvanostatic charge/discharge curves recorded at a charging current of 0.015 A.

As mentioned above, integration of the two 3D printing methods created a fabrication process without any movement of sample, potentially giving a high dimensional accuracy of sample. However, the limitation of this method was the build platform required readjusting between printing the FDM and the paste materials. The print head modified required to be further modified in order to set both of the nozzle tips at the similar level at the beginning of the fabrication process without requiring an adjustment of the bed platform after the FDM printing was complete.

4.4 Conclusions

In this chapter, supercapacitors were manufactured using two fabrication methods. In the first method, a combination of inkjet printing and 3D printing process was applied. The FDM 3D printer offered freedom to create the frame of supercapacitor in different shapes, and the inkjet printing process provided the ability to print on an uneven surface with different designed patterns. This manufacturing method was successful in fabricating a functioning supercapacitor, however, building the current collector using inkjet printing required numerous iterations of printing in order to create an appropriately thick current collector. Furthermore, constructing electrode material using a coating method presented difficulty in the drying time process. Due to these reasons, it was decided to attempt to manufacture an alternative supercapacitor using the integration of two 3D printing technologies.

A combination of the two 3D printing processes was developed. An FDM system was employed to create the frame, and a paste extrusion system was used to deposit conductive current collectors and electrodes. A new frame design also used to simplify the supercapacitor and remove any assembly requirement. Moreover, this manufacturing method allows for a much wider range of component materials to be used than with inkjet printing, and more flexibility in terms of the design.

Table 4.2 Comparisons of capacitance and specific capacitance of the samples fabricated using the two different manufacturing methods

Manufacturing method	**Mass (g)**	**C1 (mF)**	**Cs1 (mF/g)**	**C2 (mF)**	**Cs2 (mF/g)**
FDM + Inkjet	0.386	6.29	53.83	6.51	59.23
FDM + Paste extrusion	0.727	212	205	258	262

It can be seen that the EDLC samples (Pilot sample 2) fabricated using the combination of the two 3D printing methods obtained higher values in both capacitance and specific

capacitance than the first fabrication method (Pilot sample 1). The difference in capacitance and specific capacitance can be accounted for several reasons:

1) A different electrolyte was applied. An organic electrolyte was used in the second manufacturing method which resulted in a higher energy density

2) Although both EDLC samples were fabricated with the same thickness of electrode, the length and width of electrodes were different. The EDLC sample fabricated using the second method had a larger surface area which resulted in improved performance.

3) During the fabrication process of the second method, drying time was considered carefully to avoid cracking of the carbon electrode. Cracks in the electrode of the first sample may have caused internal resistance and hence impaired the performance of the sample.

In conclusion, the FDM process integrated with the paste extrusion process appears to offer superior capabilities for fabricating supercapacitors, as compared with an integration of FDM and inkjet printing. However, the electrical performance and packaging frame of the supercapacitor would be improved by optimising the manufacturing process and component materials, which is explored in the next chapter. For example, it might be possible to increase the electrical performance when each printed layer is consistently and uniformly controlled.

Chapter 6 Design and fabrication of extendable supercapacitors

5.1 Introduction

This chapter describes the design and manufacturing process for an extendable 3D-printed electrochemical supercapacitor, and tests its performance properties. Based on the improvement shown in the pilot experiment by using a paste extruder to construct the current collectors and electrodes, this idea was taken forward.

The design of the supercapacitor was similar to that used for the pilot sample 2 in the previous chapter. An FDM printer was combined with a paste extrusion system, so that the device could be printed in a single process. The FDM printer first prints a plastic casing for the device consisting of two halves joined by a hinge. Once complete, the paste extruder is used to first print silver paint current collectors on each half, and then to print carbon electrodes on top.

A key advancement from the pilot sample 2 in the previous chapter is that the paste extruder now also prints the electrolyte separator. PVA electrolyte gel is used as the separator so the fabrication process is entirely 3D printed except for the closing of the casing (i.e. combining the two halves).

A further improvement attempted by the design is to make the devices extendable. The frame and current collectors of the devices are designed with slots and matching protrusions, such that multiple devices may be stacked end to end to form a larger supercapacitor. This chapter also seeks to assess the effectiveness of this design feature.

Four separate samples of these newly designed devices were tested using CV and GCD tests for their reproducibility, with moderately successful results. The design was also tested using 5 different thicknesses of electrodes, which determined 2.0mm to provide the optimal performance. Finally, the efficacy of the extendable design was successfully verified. These results are discussed in detail in the conclusion as well as possible improvements to the manufacturing process and durability.

5.2 Experimental methods

5.2.1 Material

The material used to build the supercapacitor frame in this experiment was polylactic acid (PLA) filament with a diameter of 2.89 mm. Silver conductive paint was used as the current collector material. The materials used for mixing electrode slurry and electrolyte include activated carbon (AC) (AR grade, 1375 μΩ.cm), Sodium carboxymethyl cellulose, CMC ($C_{28}H_{30}Na_8O_{27}$, MW: 250,000), ethanol (≥ 99.8%, ACS grade), phosphoric acid (H_3PO_4) and PVA (MW 146,000-186,000, > 99% hydrolysed). Preparation of the electrode slurry was achieved by mixing the activated carbon (AC) with CMC solution. The CMC binder solution was mixed with distilled water/ethanol (1:1) solvent at room temperature. The concentration of CMC was fixed at 5 wt% based on total mass of AC and CMC, in which 2 g activated carbon was added to the 50 ml of CMC binder solution. The slurry prepared was stirred for 8 hours before the experiment in order to make it homogeneous and suitable for printing. The conductivity of the slurry was about 10^2 Ω/sq.

The gel electrolyte was made by dissolving 0.8 mL H_3PO_4 and 1.0 g PVA in 10 mL deionized water. All the materials used in the experiment are low cost, nontoxic and easily available.

5.2.2 Printers and modification of the printer head

The printers used in this experiment were the same as in the previous chapter. The primary 3D printer used was the FDM printing machine (Ultimaker 2), which was integrated with the paste extrusion system. FDM technology offers a simple fabrication process, reliability, safe, low cost of material and accessibility to several different types of thermoplastics. In the FDM printer, thermoplastic filament material from feedstock

spool was driven using two rollers and forced out through a small temperature controlled extruder. Then the filament was transformed to the semi-molten polymer and deposited onto a platform in a layer by layer process. To build the sample, filament was deposited from the extruder that moved in the x-y plane. When each layer was complete, the base platform was lowered in order to deposit the next layer and so on. The temperature of the base platform was set at low temperature, so that the thermoplastic filament quickly hardens.

The printer head of the FDM machine was modified in order to match the height of the dual extrusion head. As shown in Figure 5.1, the Ultimaker printing head typically had two fans located on each side of the extrusion nozzle. The right-sided fan was removed and replaced by a clamp designed to fit the paste extruder tube and nozzle head. After the modification, the FDM extrusion head and paste extrusion head were set at the similar height as shown in Figure 5.2. This modification allowed for the nozzle tip of the paste extrusion system to be set at the beginning of the fabrication process without requiring an adjustment of the bed platform after the FDM printing was complete. This was done to simplify the manufacturing process and to simulate how a fully integrated printer might function.

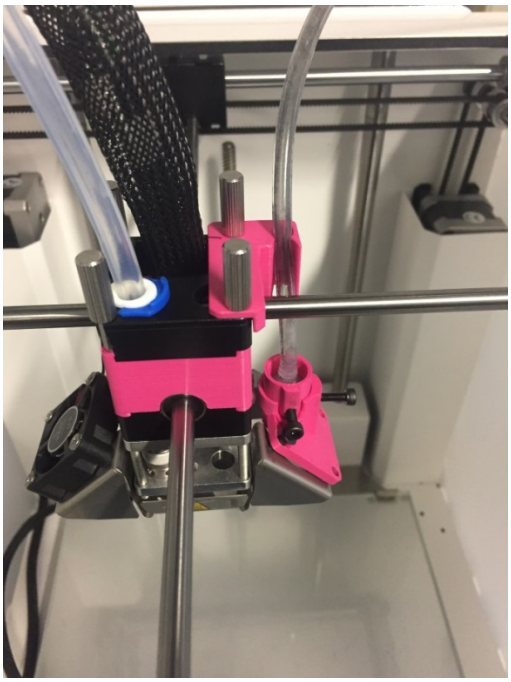

Figure 5.1 The modification of the Ultimaker printing head.

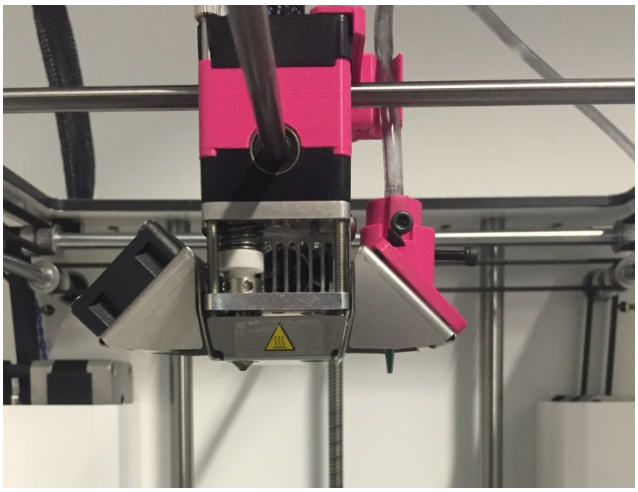

Figure 5.2 The position of the dual extrusion after modification.

The paste extrusion system was employed for building the current collector layer, electrode layer and separator with electrolyte layer. The system consists of a stepper motor, a syringe connected with a plastic tube and a nozzle. During the manufacturing process of supercapacitor, the frame was printed using the FDM printer, whereas, the other materials of the supercapacitor were printed by the paste extruder. In order to deposit the paste materials, the syringe was forced by the stepper motor and paste material flowed along the plastic tube to the nozzle. This function was automated and controlled by CURA software. CURA software was used to control the manufacturing process, which is compatible with both FDM and paste extrusion system, to set up all specifications of printing including transforming STL file to g-code. G-code is one of many programming languages used in machine automation, which has also been used in this manufacturing process to control the speed of the stepper motor of the paste extrusion system in order for the appropriate amount of the material to be printed. The most distinguished advantage of this manufacturing system is that it utilizes two printing systems at the same time, which can provides the following benefits: 1) different types of materials needed for manufacturing supercapacitors can be applied in the system, 2) the products designed can be fabricated in one continuous process to avoid being moved so a high dimensional accuracy can be achieved.

5.2.3 Manufacture of extendable supercapacitor

1) Design the extendable supercapacitor frame

The aim of this study was to develop one printing event to manufacture the supercapacitor and to design an easy assemblable and extendable supercapacitor. The structure of the extendable supercapacitors was designed based on the working mechanism of capacitor. Each individual supercapacitor consists of three layers (frame base, current collector layer and electrode layer) on each side with an electrolyte layer in the middle, as shown in Figure 5.3. The packaging frame of the supercapacitor was similar to a hinge with a size of 40 x 40 mm and technical drawing of designed sample was presented in an appendix A. There is a linking mechanism on the bottom of the supercapacitor, which offers the possibility for each frame to be directly connected, as shown in Figure 5.4. When these frames are connected, it will expand the storage area and also increase the energy storage performance. The design of the structure and all layers of the supercapacitor was created using Solidworks®.

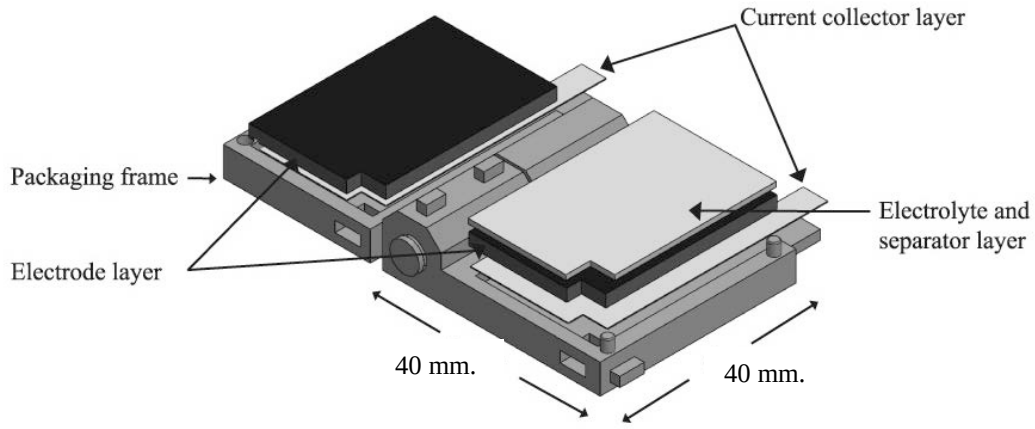

Figure 5.3 Schematic of the structure of the extendable supercapacitor.

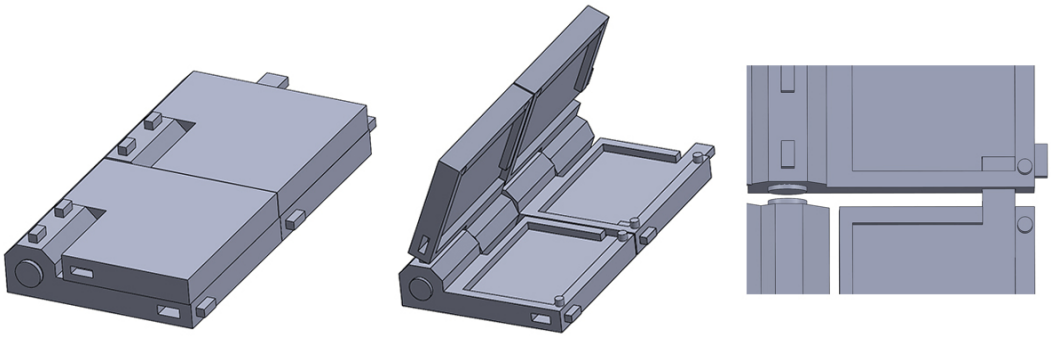

Figure 5.4 The frames of the supercapacitor and the extension functionality.

2) Manufacturing of the extendable supercapacitors

The FDM printing head was used for printing the frame. The speed of printing was adjusted to 50 mm/sec. PLA filament material was used in the printing process. In this process, PLA was heated and extruded through a nozzle with size of 0.4 mm that draws the cross sectional geometry of the part layer by layer. The temperature of the extruder was heated to 220 ^{o}C to melt the PLA filament and the platform was kept at 60 ^{o}C. After the packaging frame had been printed, the current collector layer was printed on the surface of the frames. The paste extrusion system being connected with FDM printer provided the possibility to print various materials which may not need to be heated, and it enabled the manufacturing process to be continuous without disruption. In this experiment, the extrusion head of the paste extrusion system was set next to the main extrusion without heating the materials. The distance between the extrusion head and substrate was adjusted to approximately 0.5 mm. This type of combined printing system was applied to print three different materials for manufacturing the supercapacitors. Silver conductive paint was printed over area of 32 x 32 mm on both sides of the frame. The silver paint was printed twice then dried at room temperature before the carbon slurry layer was printed on it in the next step. The drying time used for silver conductive paint was one hour for each layer of the printed silver current collectors. This silver material has been reported in manufacturing of EDLC devices previously [34, 47] and in their study, the silver material was used as current collector and presents a satisfactory performance. The electrode material layer (AC slurry) was deposited on top of the silver conductive paint over area of 30 x 30 mm on each side of the frame. The slurry of the electrode material was printed five times on the same position and dried at room temperature. The drying time used for each time of the printed electrode was around 30 minutes and when the final layer of printed was completed due to the thickness 2 mm as shown in Figure 5.5, the drying time used for the whole printed electrode was around 60 minutes. Finally, PVA gel electrolyte was printed on top of the AC material in order to build a separator for these supercapacitors, which was only on one side of the 3D frame.

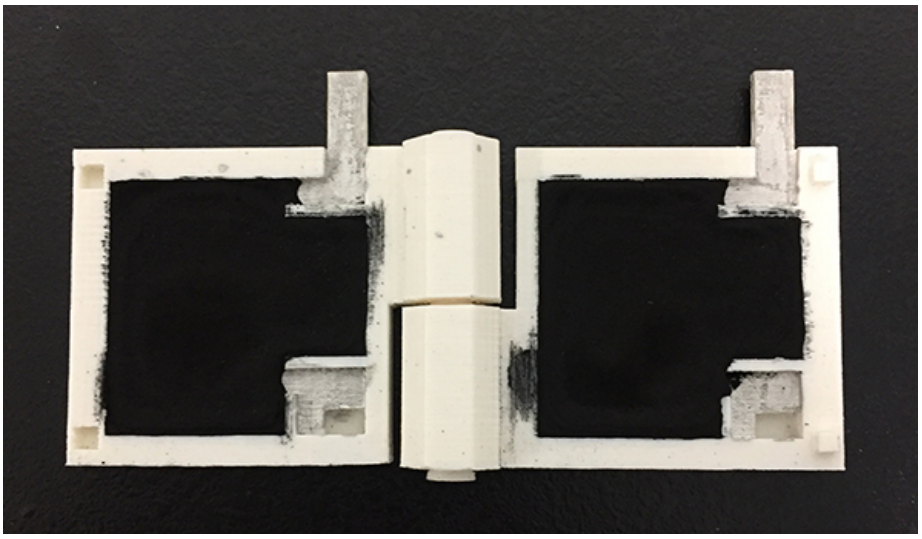

Figure 5.5 Electrode slurry material printed on top of the silver paint.

The frames were folded over to sandwich the separator, and an assembled electrochemical supercapacitor was completed, as shown in Figure 5.6. There was no pressure applied to the EDLC cell due to properties of the gel electrolyte used. This gel electrolyte had excellent film forming and adhesive properties because of the use of PVA. The PVA gel electrolyte not only performed as a separator for the EDLC devices but also behaved as a sealant for the devices. When the EDLC devices were assembled it was certain that both electrodes were in a good contact due to the properties of the gel.

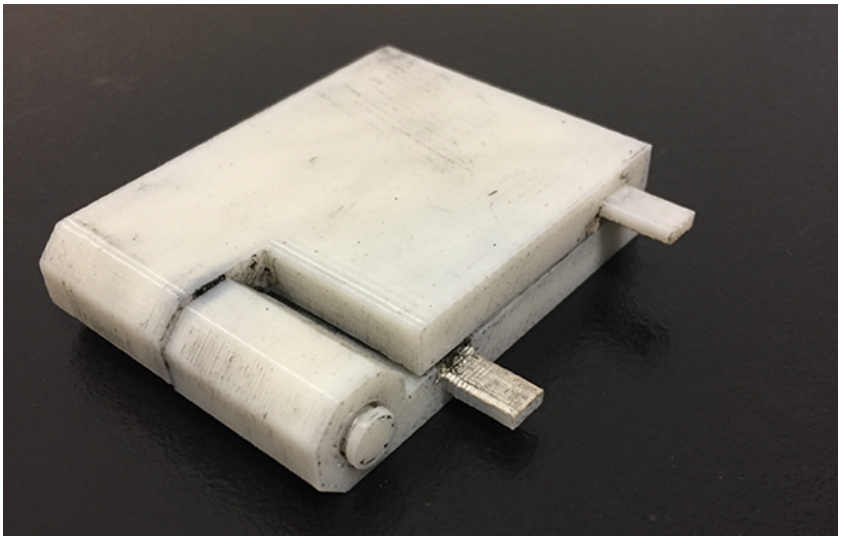

Figure 5.6 A complete extendable 3D printed supercapacitor.

5.3 Results and Discussions

5.3.1 Effect of scan rates on the capacitance of the 3D printed supercapacitor (Sample no: 1)

CV tests for Sample no: 1 were carried out and the CV curves were recorded using a potential window range of 0 ~ 0.8 V at different scan rates of 0.02 V/s, 0.06 V/s and 0.10 V/s as shown in Figure 5.7.

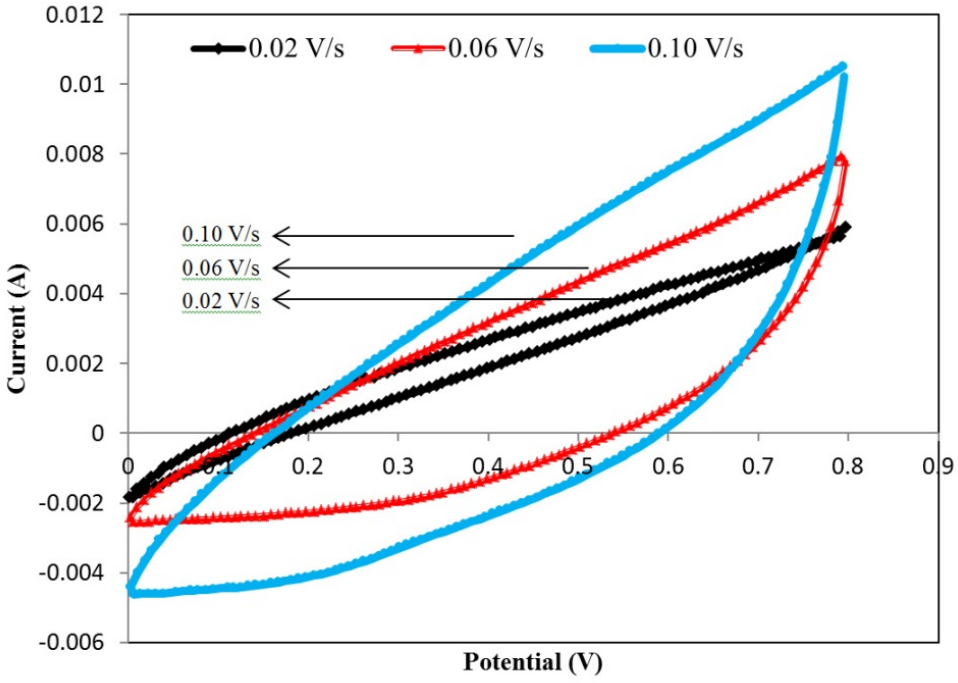

Figure 5.7 Cyclic voltammogram curves of the 3D printed supercapacitor sample at different scan rates.

The shape of the CV curve shows that the device operated as a typical supercapacitor, however, it is not completely rectangular as it would be expected for a perfect supercapacitor. This might be caused by high resistance of electrode material resulting in a deformed rectangular shape. The capacitance calculated using Equation (3.1) was 182 mF at the scan rate of 0.02 V/s, and decreased to 65 mF and 32 mF at the scan rates of 0.06 V/s and 0.10 V/s, respectively. It is implied that the change of scan rate affects the performance of the supercapacitor, e.g. the capacitance. The capacitance decreased with the increase of scan rate because the diffusion process of ions is less efficient at the higher scan rate. Generally, when lower scan rates are applied on the two electrodes of a

supercapacitor, the diffused ions from electrolyte have sufficient time to access into the inner porous of the electrode material, providing the supercapacitor with a high electricity capacitance. In contrast, when higher scan rates are employed, the efficiency of ions penetrating into the inner pores of the electrode material is gradually reduced, resulting in a lower electrical capacitance. Similar results of CV curves with different scan rate have been reported previously [139-140]. The highest capacitance of the EDLC Sample 1 printed by the 3D printing process was 182 mF at the scan rate of 0.02 V/s and it was not as high as expected. This is considered to be affected by the high resistance of the AC slurry electrode material due to PVA penetrating into the carbon pores leading to an increase of resistance. The specific capacitance was 193 mF/g calculated by Equation (3.2).

5.3.2 GCD measurement

The GCD curves recorded (five cycles at a charge current of 0.015 A) are shown in Figure 5.8.

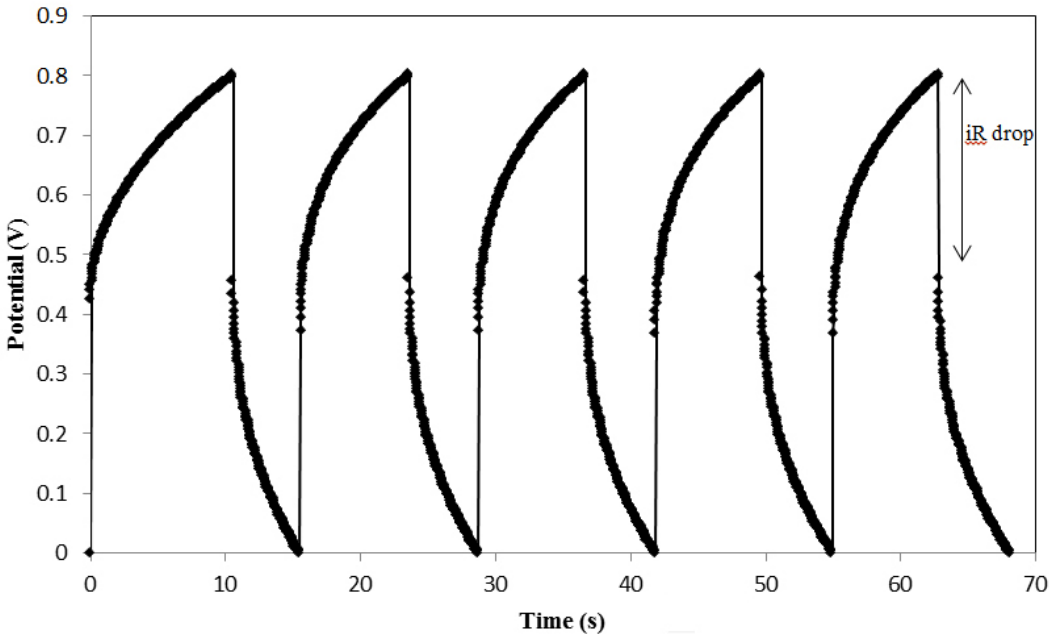

Figure 5.8 Galvanostatic charge/discharge curves recorded at a charging current of 0.015 A.

It can be seen from the charge/discharge curve shown in Figure 5.8 that the 3D printed supercapacitor (Sample no: 1) exhibits a stable performance as it can be seen from the

similar size of the iR drop for each charge/discharge curve. Five cycles of the charge and discharge curves show an ideal EDLC behaviour with a short charge/discharge period of less than 8 second. The capacitance calculated using Equation (3.3) from GCD was 224 mF, which is slightly different compared to total capacitance obtained from CV curve measured at 0.02 V/s. The different capacitance calculated from these two methods could be due to the time-scales applied in measurement. The time-scales in CV test can be defined using the scan rate and potential window. On the other hand, the GCD tests apply a specific charge/discharge current and a potential window. The total experiment time is a result of the calculated capacitance. The specific capacitance of the printed supercapacitor sample calculated using Equation (3.4) from GCD curve was 238 mF/g, which was based on the total mass of electrode materials.

5.3.3 Effect of charging/discharging on the capacitance of the 3D printed supercapacitor (Sample no: 1)

Figure 5.9 show the GCD curve of the 3D printed EDLC recorded at different charge current of 0.002, 0.004, 0.006, 0.008, 0.010, 0.012, and 0.014 A.

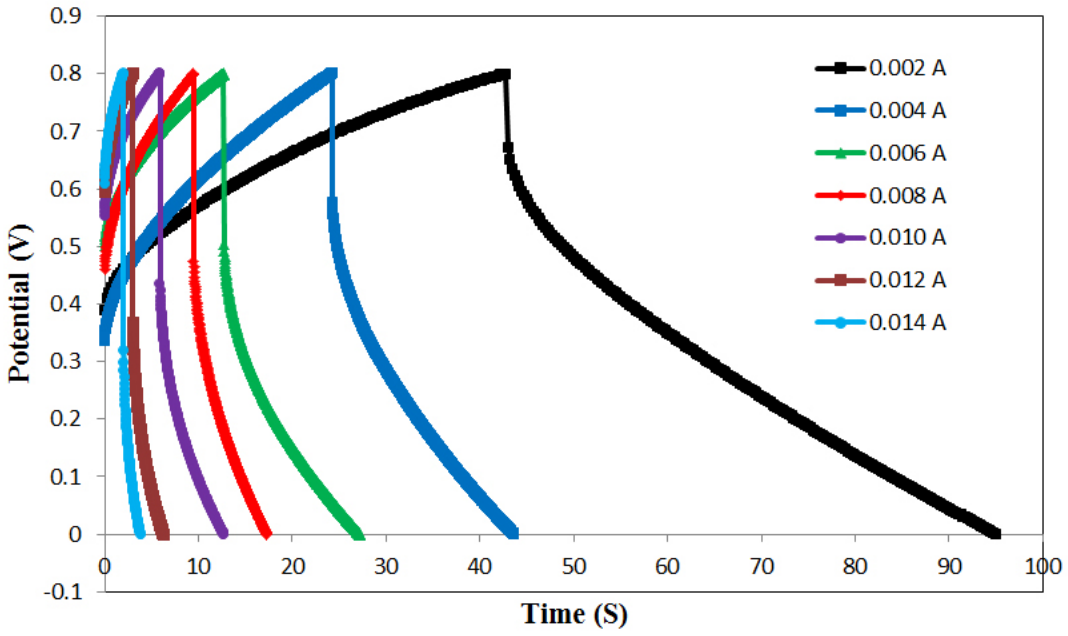

Figure 5.9 Galvanostatic charge/discharge curves recorded at different charging/ discharging current of 0.002, 0.004, 0.006, 0.008, 0.010, 0.012, and 0.014 A.

As shown in Figure 5.9 the GCD curve of a sample 1 recorded at different charge current of 0.002, 0.004, 0.006, 0.008, 0.010, 0.012, and 0.014 A. The iR drops of all GCD curves were presenting at an early stage. When the charging/discharging current was increased, the iR drop also increased. The increasing of the charge current significantly affected the charging/discharging time. (Figure 5.9 and Table 5.1) The capacitance of sample 1 decreased from 270 to 224 mF when the charging/discharging current increased from 0.002 to 0.014 A. The capacitance decreased at higher charge/discharge currents because the ions from electrolyte cannot transfer from the electrolyte to some of the available inner porous structure due to insufficient time. The capacitance at the charging current 0.014 A was still 84% of the measured at the charging current of 0.002 A. This can be implied that the AC used as electrode materials has an outstanding porous structure. The electrolyte can certainly access to this structure even under higher charge current.

Table 5.1 Capaciatance, iR drop and discharge time based on GCD curves for the 3D printed EDLC (Sample no:1) recorded at different charge/discharge currents.

Charging/discharging current (i), A	**iR drop (V)**	**Discharging time (S)**	**Capacitance (mF)**
0.002	0.128	17.29	270
0.004	0.224	14.89	265
0.006	0.296	12.78	259
0.008	0.325	10.12	249
0.010	0.364	8.98	246
0.012	0.433	8.74	242
0.014	0.485	7.78	224

5.3.4 EIS measurement

In addition, electrochemical impedance spectroscopy (EIS) is a method providing a further study insight of the electrical characteristics of a supercapacitor and can also be applied to the measure and calculation of the equivalent series resistance (ESR). The

ESR can be used to determine the resistance of cell components such as contact resistance between current collectors and electrodes and electrolyte resistance. In this method, an electrochemical supercapacitor sample is tested using a small alternating current (AC) over a different range of frequencies (0.01 Hz to 1 MHz). The result of measurement derives from changes in current caused by the impedance of the sample and is used to draw on a Nyquist plot which charts imaginary resistance (Z") against real resistance (Z). The ESR corresponds to the intersection of the impedance curve at the x-axis in the Nyquist plot [21-22]. Figure 5.10 shows a typical Nyquist plot of a 3D printed EDLC at high frequencies from 100 kHz down to 0.01 Hz and the ESR is about 38 Ω. In this study, there is no semicircle shape in the higher frequency range because contact resistance and the charge transfer resistance were low. At intermediate frequencies, some ion diffusion behaviour of the electrolyte inside the electrode was seen as the inclined line. At lower frequencies, the device with aqueous acid electrolyte exhibited characteristics of a high internal resistance.

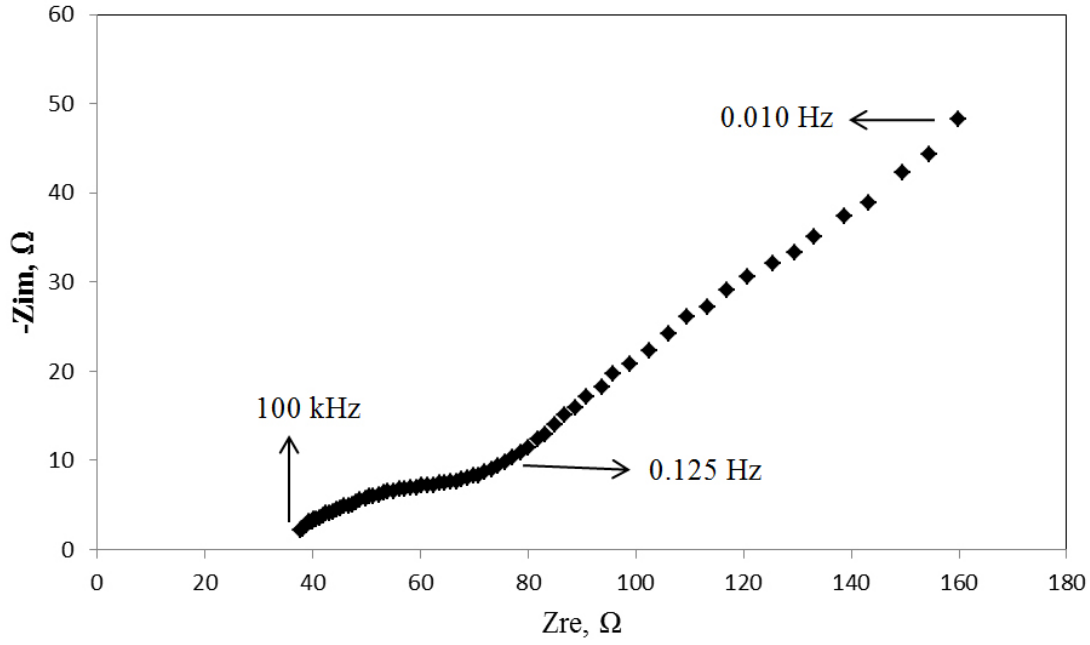

Figure 5.10 A typical Nyquist impedance plot of a 3D printed supercapacitor.

The energy density and power density of the supercapacitor were calculated as follow [141]:

$$E = \frac{C.\Delta v}{2} \tag{5.1}$$

$$P = \frac{E}{\Delta t} \tag{5.2}$$

Where C (F/cm^2) is the specific capacitance of the supercapacitor; ΔV (V) is the applied voltage; Δt (s) is the discharge time. E and P are the corresponding energy density and power density, respectively.

Table 5.2 shows electrical performance of the 3D printed EDLC. The single-electrode specific capacitance of the device calculated using Equation 3.5 was 953 mF/g. The energy density was 76.26 mWs g^{-1} with a corresponding power density of 95.36 mWg^{-1}.

Table 5.2 Electrical performance of the 3D printed EDLC (Sample no:1).

Sample	**Total Mass (g)**	**Mass loading (mg/cm^2)**	**C1 (mF)**	**Cs1 (mF/g)**	**C2 (mF)**	**Cs2 (mF/g)**	**Energy density (mWs/g)**	**Power density (mW/g)**
no:1	0.942	45.99	182	193	224	238	76.29	95.36

The 3D printed EDLC showed this limited electrical performance because of high internal resistance. The high internal resistance was probably due to the thickness of the electrode and poor penetration of PVA gel electrolyte and also corrosion of the current collector. The electrode material was prepared using AC and CMC without H_3PO_4 and fabricated with 2 mm thickness. This might have caused a low capacitance because not all pores of the thick carbon electrode were filled with the electrolyte solution. In addition, the PVA gel electrolyte (as separator of the device) that penetrated into the electrode and might obstruct the pores of the carbon electrode may have resulted in inactive areas of the electrode. As mentioned above, both electrode materials have been penetrated by the gel electrolyte. This might have destroyed some area of the silver current collector which would increase the resistance and decrease the capacitance.

These three factors significantly influenced the high internal resistance of the device and are reasoned to decrease the capacitance of the device.

Compared to other methods for manufacturing EDLC, 3D printing techniques provided a possible way to create a supercapacitor frame in different sizes and shapes, and the paste extrusion system offered a wide range of materials that can be applied to deposit through the system. As mentioned above, integration of the two 3D printing methods encouraged one continuous fabrication process without any movement of sample, potentially giving a high dimensional accuracy of sample. However, the limitation of this method was the lack of a uniform AC printed electrode. The electrode slurry had a low viscosity which resulted in an uneven surface. The properties of the slurry could be improved in the future. In addition, the fabrication technique needs to be carefully controlled to provide consistency.

5.3.5 Reproducibility of the manufacturing process

After the initial manufacturing and testing, another three new EDLCs (Samples no: 2, 3, and 4) were manufactured under the same conditions as Sample 1 and characterized by CV and GCD tests. The CV and GCD curves of the four samples are shown in Figure 5.11 and 5.12. It can be seen that the areas of the CV and GCD curves measured are all similar and the capacitances, and specific capacitances calculated from the CV and GCD curves are only slightly different, as shown in Table 5.3. The average capacitance and specific capacitance calculated from CV curves for the three new supercapacitors are about 174 mF, and 183 mF/g respectively. In addition, the average capacitance and specific capacitance calculated from GCD curves for the three new supercapacitors are about 215 mF, and 227 mF/g respectively. Both capacitance and specific capacitance calculated from CV and GCD curves are about 94% and 95% of Sample 1. Standard deviations of all experimental data results are also less than 0.01 %. These results demonstrate that the manufacturing process developed in this study for printing the EDLCs illustrated above has a good reproducibility.

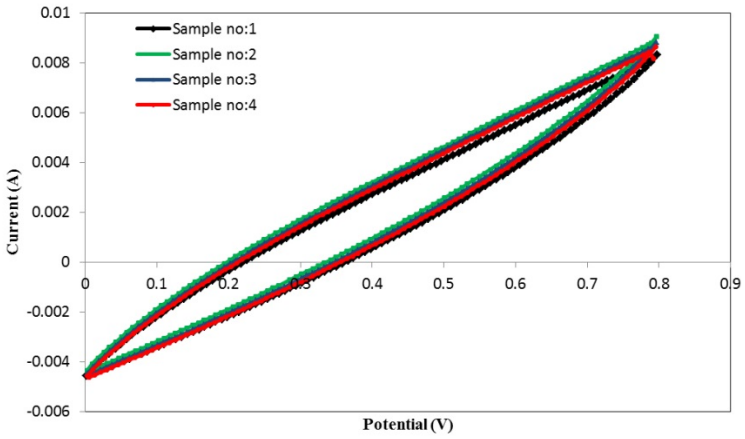

Figure 5.11 CV curves of the four EDLC samples at the scan rate of 0.02 V/s.

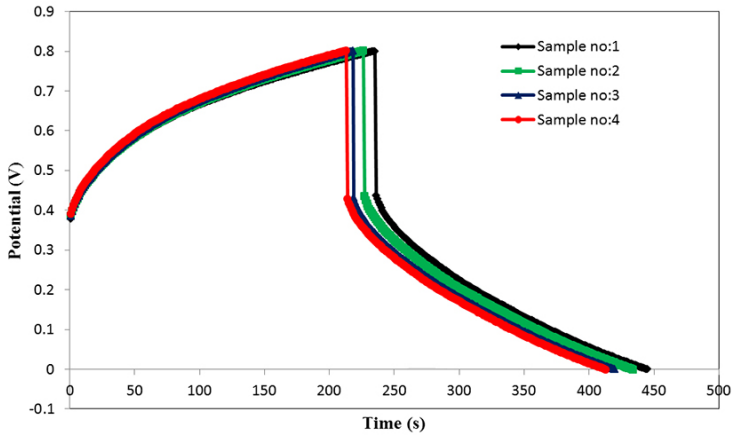

Figure 5.12 Galvanostatic charge/discharge curves recorded of the four EDLC samples at a charging current of 0.015 A.

Table 5.3 Capacitance and specific capacitance of four EDLC samples manufactured under the same condition.

	Calculated from CV		**Calculated from GCD**	
Sample	**C1, (mF)**	**Cs1, (mF/g)**	**C2, (mF)**	**Cs2, (mF/g)**
no:1	182	193	224	238
no:2	177	189	218	232
no:3	168	171	209	214
no:4	169	181	208	224
Average value	174	183	215	227
Standard deviation (%)	0.006	0.009	0.007	0.010

5.3.6 The effect of the thickness of electrode on capacitance

The frame of the supercapacitor was designed and fabricated with different depths, e.g. 0.5, 1.0, 1.5, 2.0 and 2.5 mm, in order to study the effect of electrode thickness on capacitance. All the EDLC samples were made under the same manufacturing process. The capacitances of the five samples with different thicknesses of electrode were determined using the CV and GCD curves. The CV curves were recorded using a potential window range of 0.8 V at the scan rate of 0.02 V/s, and the GCD curves were recorded at a charge current of 0.015 A, as shown in Figure. 5.13 and 5.14.

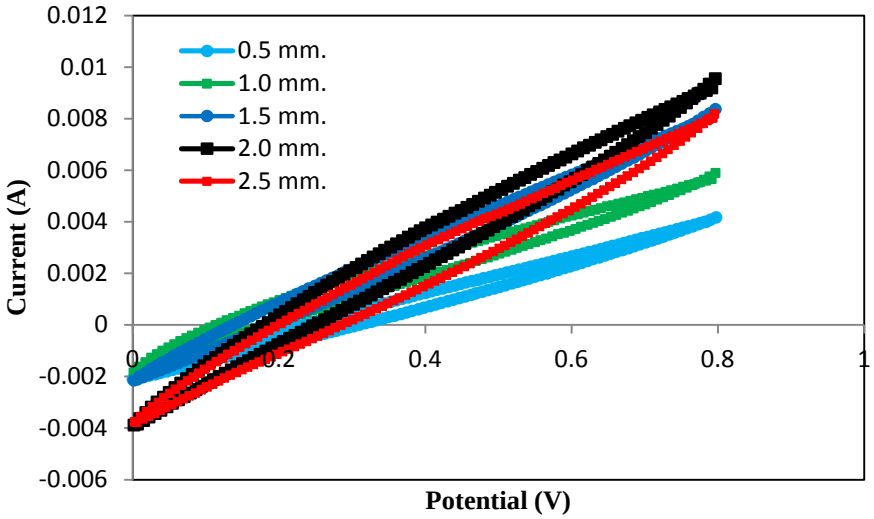

Figure 5.13 The cyclic voltammogram curves of the five EDLC samples with different electrode thicknesses.

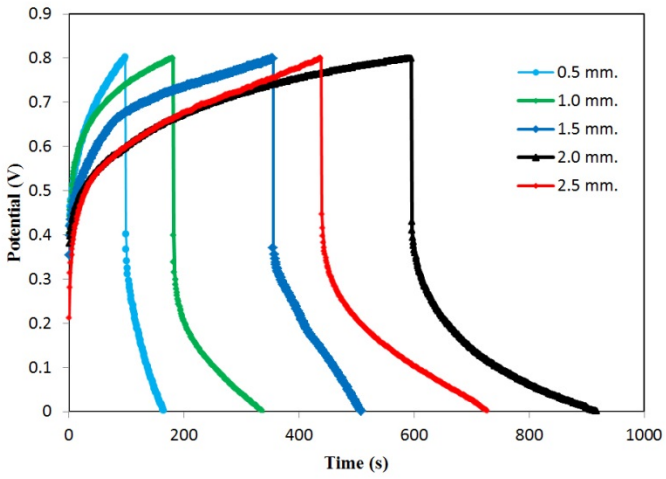

Figure 5.14 Galvanostatic charge/discharge curves of the five EDLC samples with different electrode thicknesses.

Table 5.4 shows the capacitance of C1 and C2 of the 5 samples calculated from the CV and GCD measurements and their corresponding specific capacitance Cs1 and Cs2. Figure 5.15 shows the mass of the two electrodes and the capacitance of the 5 samples as a function of the electrode thickness. It can be seen that increasing the AC electrode thickness directly affects the mass of AC electrode and also the capacitance of the samples. Below the thickness of 2 mm, the mass of the electrode and the capacitance of the EDLCs increase together as the thickness of the electrode increases, and they increase almost linearly and at the similar increasing rate. However, when the thickness of the electrode is more than 2 mm, the capacitance of the EDLC decreases although the mass of the electrode continuously increases. The decreased capacitance of the thicker electrode can be caused by the following reasons; 1) thicker electrode may increase the internal resistance of the supercapacitor, 2) the diffusion time of electrolyte was extended longer when the thickness of electrode increased.

Table 5.4 Capacitance and specific capacitance of the samples calculated from CV curve and GCD curves.

		Calculated from CV curve		**Calculated from GCD curve**	
AC electrode thickness (mm.)	**Mass of AC (g)**	**C1 (mF)**	**Cs1 (mF/g)**	**C2 (mF)**	**Cs2 (mF/g)**
0.5	0.212	125	589	166	785
1	0.455	155	340	195	463
1.5	0.698	172	240	212	313
2	0.945	194	205	234	248
2.5	1.195	182	152	222	198

Figure 5.16 shows that the specific capacitance of the EDLCs decreases at almost the same rate when the AC electrode thickness increases from 0.5 mm to 2.5 mm; and it decreases a faster speed when the thickness of the electrode is more than 2 mm. This is in agreement with the results shown in Figure 5.15.

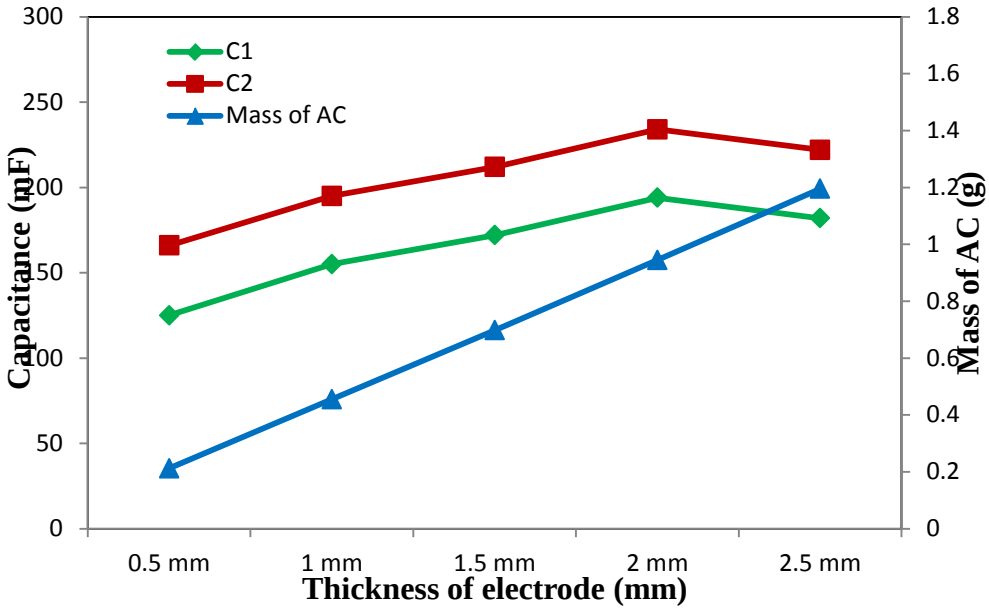

Figure 5.15 Capacitances calculated from CV and GCD for the five samples with different electrode thicknesses.

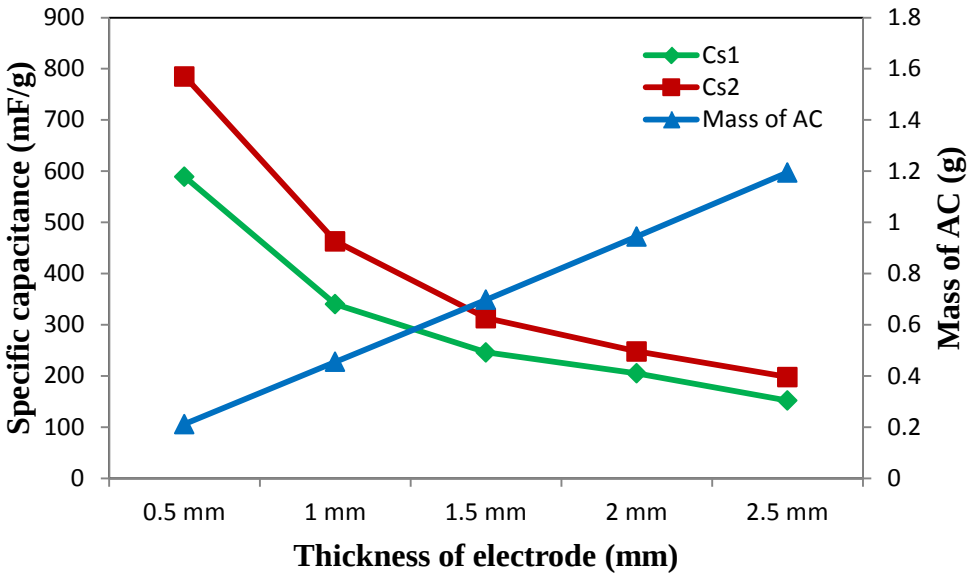

Figure 5.16 Specific capacitances calculated from CV and GCD for the five samples with different electrode thicknesses.

5.3.7 Testing the extendable supercapacitor

Supercapacitors can be applied in a wide range of applications when operated in different combination, e.g. to form series or parallel circuits, which can offer a desired operating voltage and energy. As mention above, the supercapacitor frames in this experiment were designed to be able to connect to each other. To verify the energy storage capability and operating potential, two extendable supercapacitors were examined in three combination circuits, which are series, parallel and direct connection (which is the same as the parallel circuit in theory). The sample with 2.0 mm thickness described above (sample a) and a new sample made with the same condition (sample b) were used in this test. Figure 5.17 shows the schematic structure of the two single extendable supercapacitors and their series, parallel and direct connection combination circuits. In order to examine these combination circuits, two different working potential were applied. The working potential (0.8 V) was applied for the individual single supercapacitors, two extendable samples in parallel circuit, and the two samples in direct connection. For the series combination circuit, the working potential was two times (1.6 V) the samples in parallel.

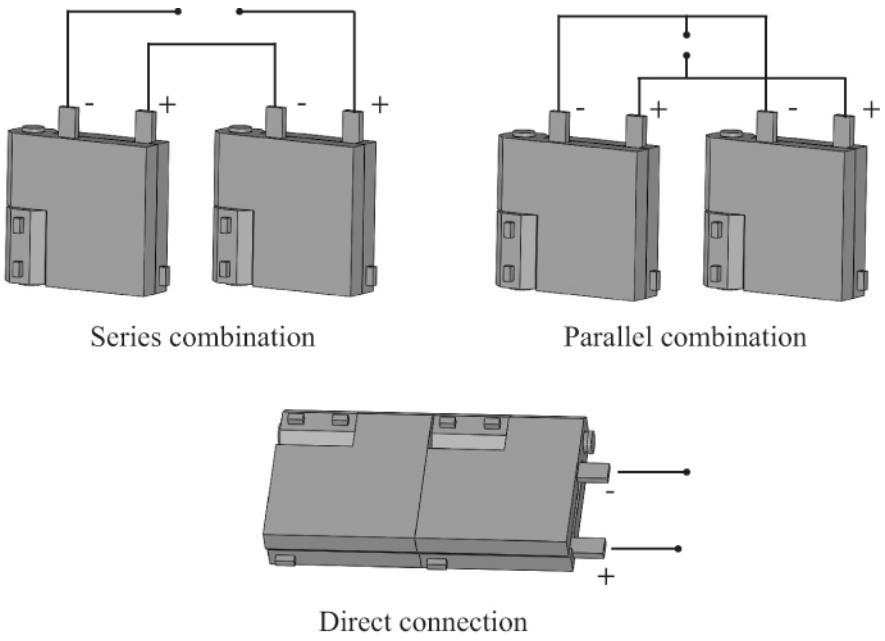

Figure 5.17 Schematic of two extendable supercapacitors combined in series, parallel and direct connection circuits.

The capacitances from CV curves of all samples and combination circuits were calculated by Equation 3.1 and 3.2 and shown in Table 5.5. Figure 5.18 presents the CV curves for the different combination circuits. The capacitance of the direct connection circuit and parallel circuits are similar to the sum of the capacitance of the two individual samples a and b; the capacitance of the series circuit is nearly half of the capacitance of the individual samples. The direct connection of two EDLCs samples show the results of slightly higher capacitance compared to the parallel circuit combination.

Table 5.5 The Capacitance of the samples calculated from CV curve and GCD curve.

	Capacitance (mF) (CV)		**Capacitance (mF)** (GCD)	
	experiment	Theory	experiment	Theory
Sample 1	194		221	
Sample 2	165		195	
Series	87	86	112	103
Parallel	342	359	405	416
Direct connection	355	359	411	416

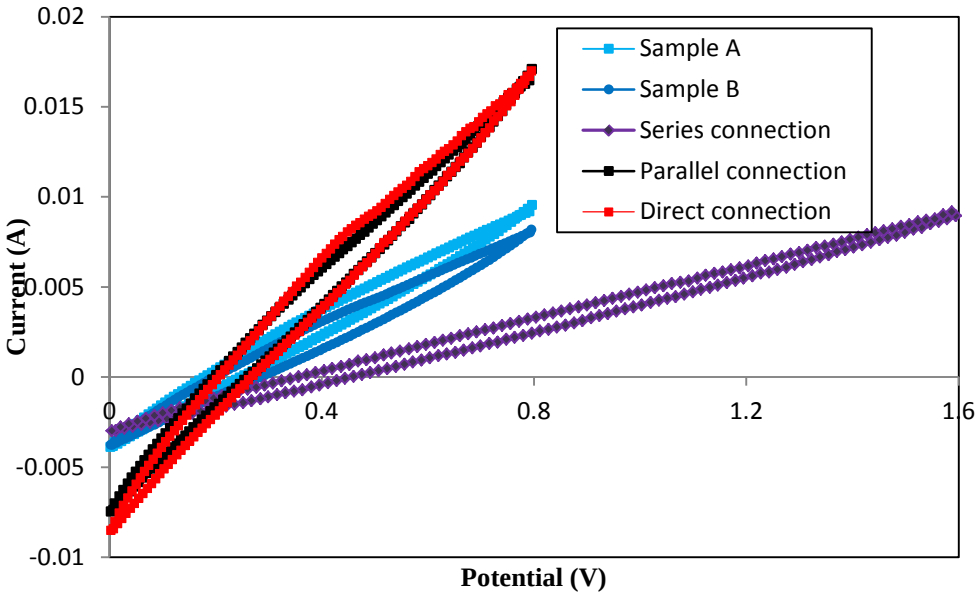

Figure 5.18 CV curves recorded at 0.02 Vs^{-1} for the two single extendable supercapacitors and their electrical combination in series, parallel and direct connection.

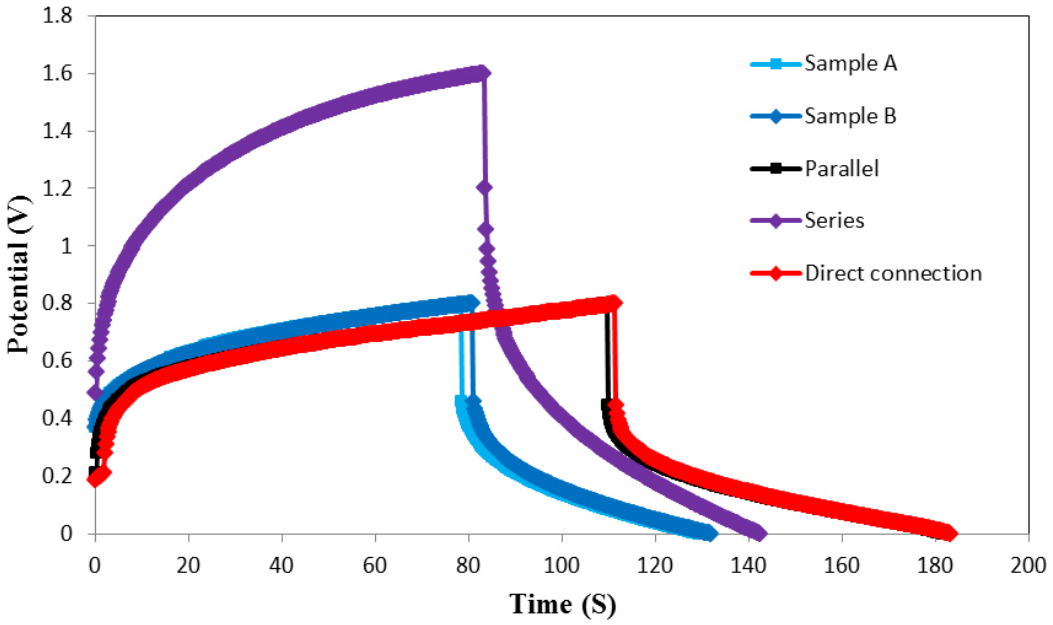

Figure 5.19 GCD curves recorded at 0.015 A for the two single extendable supercapacitors and their electrical combination in series, parallel and direct connection.

Figure 5.19 shows the GCD curve at charge currents of 0.015 A for the two individual samples and the series circuit and 0.030 A for the parallel and the direct connection circuit. The potential window of the parallel and the direct connection circuit was 0.8 V, similar to those of the two single EDLC samples, and half of the series circuit. The capacitances of different combination circuits calculated from the GCD curves exhibited similar results to those calculated from CV curves. This is believed to be because the direct connection between two EDLC samples without any wires provided a lower resistance compared to the parallel circuit connected by wires. Furthermore, it can be seen from the above results that the designed frame of these EDLCs can be operated to extend the storage capacity of supercapacitors. The most important observation is that all the experimental results obtained from the different combination circuits are very close to the theoretical results, as given in Table 5.5. This demonstrates that all the EDLCs have a good and stable electrical performance and can be used as a energy storage.

5.3.8 The electrochemical stability of the extendable supercapacitors

Another important property of supercapacitors is their cycle stability. Commercial supercapacitors are well recognised for possessing long life cycles in which they can operate at full capacity, even after half a million cycles. At lab-scale testing, 1000 to 10,000 cycles are generally conducted for investigating the cell's cycle durability. One cycle would equal to one charge/discharge cycle at a constant current density. Extensive cycling degrades the electrodes and induces corrosion in the cell's components, resulting in capacitance reduction and rise in ESR. Therefore, comparing the initial and the final performance from the cycle testing provides a foresight on how the material will perform in real applications where it may be utilised to through thousands of cycles.

The electrochemical stability of the 3D printed EDLC was examined through repeated use and reiterations of CV measurement up to the 500^{th} cycle. The time used in this experiment was about 4 hours. Figure 5.20 shows CV curves for different cycles recorded at the scan rate of 0.10 V/s. It can be seen that as the cycle iteration increased, the area of the CV curve reduced indicating a reduction in the capacitance of the sample.

The corresponding capacitances calculated from the CV curves are shown in Figure 5.21. If the capacitance calculated from the 5th curve is taken to be the initial capacitance (100%), by cycle iteration 100, the capacitance had decreased to 77.03% of the initial capacitance. Furthermore, by cycle iteration 300, the capacitance had dropped further to 57.19% of the initial capacitance. The capacitance continued to drop to 49.12% of the initial capacitance by the final measurement at iteration 500. The cause of this continuous loss of capacitance is assumed to be due to decreasing ion diffusion in the electrolyte through the evaporation of the electrolyte solvent.

500 cycles was considered enough to determine the rate of degradation such that future degradation may be extrapolated. Being one of many tests carried out, time constraints were inevitably a factor discouraging a longer life-cycle test. Commercial supercapacitors can remain effective after hundreds of thousands of cycles, so the samples are not comparable in this respect.

The EDLC samples were examined in cycle stability, however they could operate around 500 cycles. These EDLC sample could not operate more than 500 cycles

because of decreasing ion diffusion in the electrolyte through the evaporation of the electrolyte solvent. In addition, silver conductive paint could corrode resulted to decrease the cycle stability of the samples.

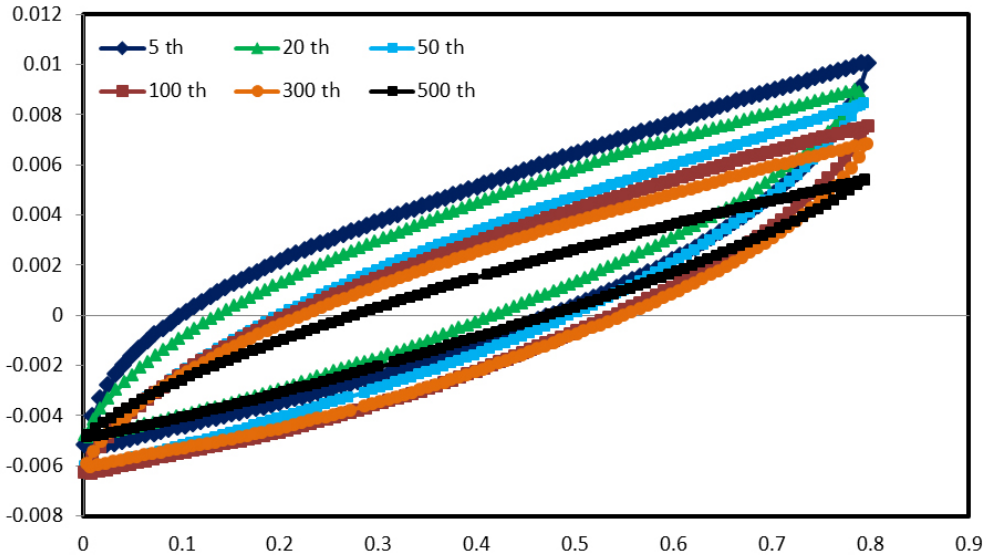

Figure 5.20 Stability of CV measurement for 3D printed supercapacitor.

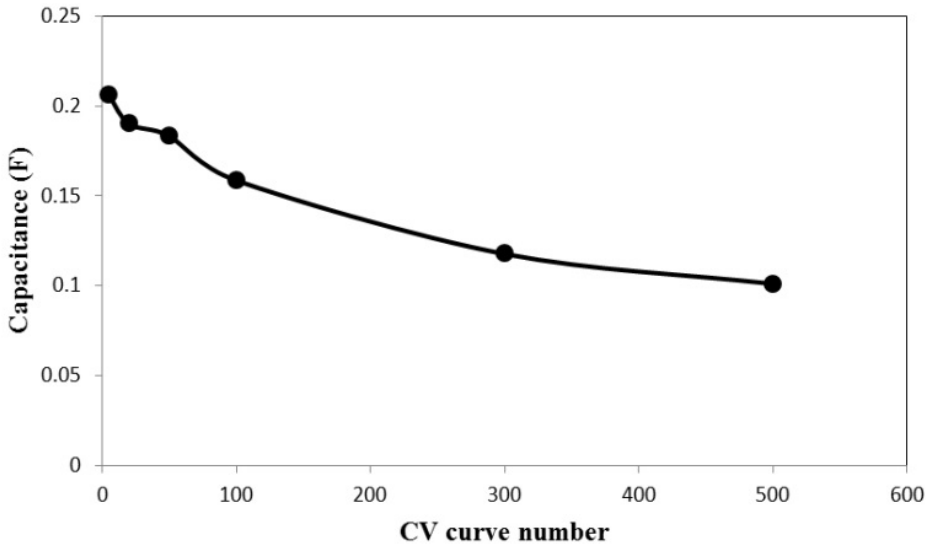

Figure 5.21 The relationship between the capacitance calculated from the CV curve and the number of CV cycles.

5.3.9 Demonstration of the practical usage of the extendable supercapacitors

As shown in Figure 5.22, the three extendable supercapacitors have been connected to a portable LED lamp in order to demonstrate their function in an example practical application. The electrolyte used in the extendable EDLC was phosphoric acid (H_3PO_4) which provided the EDLC with a working voltage of about 0.8 V. Since the LED possessed the working potential of about 2.0 V, the three EDLCs were required to power it. These three samples were directly connected to each other and can be fully charged within about 2 mins. Afterwards these three samples were connected in series combination to power the LED lamp. The fully charged samples were able to keep the LED properly lit for more than 3 mins. This demonstration shows that the extendable supercapacitor has the potential to be employed as a mobile energy supply.

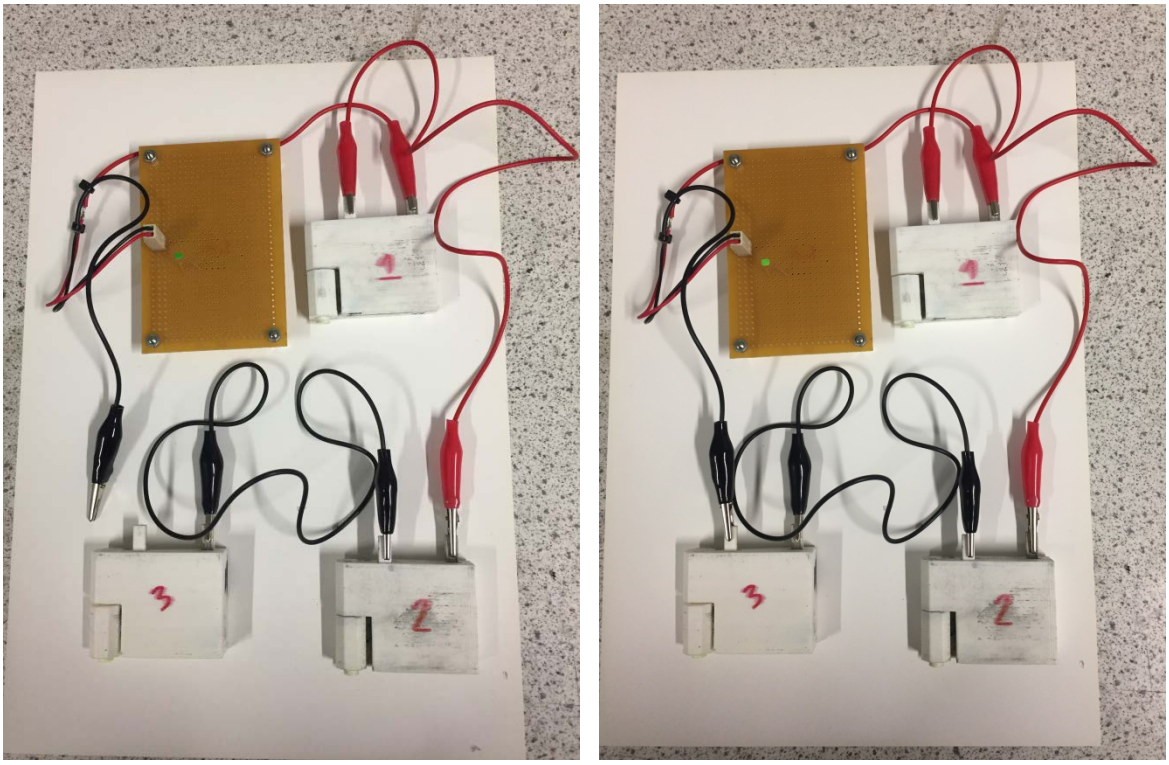

(a) **(b)**

Figure 5.22 (a) Photograph of a green LED and three charged extendable supercapacitors in an open circuit; (b) Photograph of a green LED turn on by three charged extendable supercapacitors connected in series.

5.4 Conclusions

In this chapter, the extendable supercapacitors were fabricated using the combination of two 3D printing technologies, an FDM system and a paste extrusion system. Based on the method used in the second pilot experiment, the printer head of the FDM machine was modified to match the height of the dual extrusion head. This modification allowed for the nozzle tip of the paste extrusion system to be set at the beginning of the fabrication process without requiring an adjustment of the bed platform after the FDM printing was complete. This was done to simplify the manufacturing process and to simulate how a fully integrated printer might function. In addition, the paste extruder was employed to deposit the PVA electrolyte as the separator so the fabrication process is entirely 3D printed except for the closing of the casing (i.e. combining the two halves).

The most significant advantage of this manufacturing system is that it utilises two printing systems at the same time, which provides the following benefits:

1) Different types of materials needed for manufacturing supercapacitors can be applied in the system.

2) The products designed can be fabricated in one continuous process to avoid being moved so a high dimensional accuracy can be achieved.

The frame was further improved in design to make the EDLC device extendable. This was done by adding slots and matching protrusions, so the devices could be connected end to end to form, in effect, a larger supercapacitor.

For the single device, the first electrical performance test was the effect of scan rates on the capacitance. The CV curves were recorded using a potential window range of 0 - 0.8 V at different scan rates of 0.02 V/s, 0.06 V/s and 0.10 V/s. The results showed that changing the scan rate affects the performance of the supercapacitor, e.g. the capacitance. The capacitance decreased with the increase of scan rate because the diffusion process of ions is less efficient at the higher scan rate. In addition, an examination of the effect of charging/discharging on the capacitance was carried out. The GCD curves of the device were recorded at different charge current of 0.002, 0.004, 0.006, 0.008, 0.010, 0.012, and 0.014 A. The results showed that the capacitance decreased at higher charge/discharge currents because the ions from electrolyte cannot

transfer from the electrolyte to some of the available inner porous structure due to insufficient time.

Certain properties of supercapacitors were assessed using Electrochemical Impedance Spectroscopy (EIS), which outputs the results in the format of Nyquist plots. The plot typically displays information about the capacitance, ion-diffusion, and resistance of the device. There was no semicircle shape exhibited in the higher frequency range indicating that contact resistance and the charge transfer resistance were low. At intermediate frequencies, some ion diffusion behaviour of the electrolyte inside the electrode was seen as the inclined line. At lower frequencies, the device with aqueous acid electrolyte exhibited characteristics of a high internal resistance. It is reasoned that the high internal resistance was due to the thickness of the electrode and poor penetration of PVA gel electrolyte and corrosion of the current collector. These three factors significantly influenced the high internal resistance of the device and are believed to have decreased the capacitance of the device.

After the initial manufacturing and testing, another three new EDLCs (Samples no: 2, 3, and 4) were manufactured under the same conditions and characterised by CV and GCD tests. The manufacturing process showed a good reproducibility.

Different electrode thicknesses of EDLC samples delivered different capacitances. The electrode with 2.0 mm thickness showed the highest capacitance. The capacitance did not increase after it reached the maximum even though there was a further increase in the electrode thickness. In addition, increasing the electrode thickness resulted in decreasing the specific capacitance.

Cycle stability is one of the most important properties of supercapacitors. The electrochemical stability of the 3D printed EDLC was examined through repeated use and reiterations of CV measurement up to the 500^{th} cycle. The results showed that as the cycle iteration increased, the area of the CV curve reduced, indicating a reduction in the capacitance of the sample. The cause of this continuous loss of capacitance is assumed to be due to decreasing ion diffusion in the electrolyte through the evaporation of the electrolyte solvent.

To characterise their electrical properties as a power supply, two EDLCs samples were connected in three different combinations. All three combinations showed a good correspondence with the theoretical circuit models of series and parallel circuit

combinations, which implies that the extendable supercapacitors can be joined in different combination circuits to provide energy/power as desired. The designed frame offered possibility of two or more EDLCs to be simply connected to each other without wires and also provided a good performance for storing energy as a parallel connection.

For the practical usage of the extendable supercapacitors, the three extendable supercapacitors have been connected to a portable LED lamp in order to demonstrate their function in an example practical application. These three samples were directly connected to each other and can be fully charged within about 2 mins. Afterwards these three samples were connected in series combination to power the LED lamp. The fully charged samples were able to keep the LED properly lit for more than 3 mins. This demonstration shows that the extendable supercapacitor has the potential to be employed as a mobile energy supply.

In comparison to the sample 2 of the pilot test from the previous chapter, the extendable supercapacitors obtained a better electrical performance. The difference in capacitance and specific capacitance can be accounted for several reasons:

1) A different electrolyte was applied. EDLC devices with an aqueous acid electrolyte normally present lower energy densities than devices with an organic electrolyte. In this experiment, the extendable supercapacitors with an aqueous acid electrolyte and an electrode thickness of 1.5 mm obtained a capacitance and specific capacitance similar to sample 2 of the pilot test. The electrode areas of the extendable devices were smaller. This result represented an improvement of manufacturing method in terms of uniform control of different pastes in the process. Moreover, the PVA gel electrolyte performed well and can be used to replace the filter paper separator.

2) As mentioned above, the modification of the printer head and usage of PVA gel electrolyte provided possibility to fabricate the EDLC devices in one continuous process to avoid being moved, so a high dimensional accuracy could be achieved.

For further development of 3D printed supercapacitors, improving the electrical performance of the EDLCs can be performed by applying different electrode materials and also controlling consistency of the manufacturing process in order to obtain a uniform AC electrode. These issues will be discussed in the next chapter.

Chapter 7 Development of metal-free supercapacitor and optimization of electrode material

6.1 Introduction

The purpose of this chapter is to investigate, experimentally, the performance of the designed 3D-printed supercapacitor when altering the materials used to construct the current collectors and electrodes. Beyond improving performance, there may be other reasons for wishing to change the fabrication materials. Depending on the designed purpose; durability, cost, manufacturing simplicity, or ecological impact, for example, may be a priority over optimum performance of the EDLC. To this end, this chapter also investigates the effectiveness of a metal-free supercapacitor, which may have the potential to improve durability, and reduce dependence on increasingly scarce metals.

As detailed in the literature review (2.4.1 and 2.4.2), general performance of electrode and current collector materials has been previously studied. Although this existing research acts as a strong guide for the expected performance of materials, the performance may differ in this study's design due to the different manufacturing process. In particular, although materials such as activated carbon and silver have been previously examined, they have not been intensively studied when deposited in paint or slurry form, as is required for 3D printing. For this reason, it was considered necessary to investigate the materials used within this design experimentally.

Activated carbon conductive paint was previously identified as a suitable candidate electrode material, and is used in all but one of the material combinations tested. The raw product used, Bare Conductive® Electric Paint, was too viscous for 3D printing, so it was necessary to dilute it in water. The first part of this chapter experiments to find the optimal ratio of carbon paint to water within a metal-free design, using carbon paint as the current collector and electrode. Results suggest the highest usable concentration

of carbon paint produces highest capacitance. Concentrations above 13 wt% were found to be unusable in this case because it was too viscous so that the mixture of slurry could not be deposited through the nozzle of the printing head.

As metals are finite global resources and can also deteriorate through corrosion, there is a special interest in metal-free designs. There are several existing studies of metal-free supercapacitors, most of which fabricate current collectors from graphite foil or carbon nanotubes with a coating method. 3D printing offers new possibilities for metal-free supercapacitors in terms of geometries and materials which may result in improved performance or lower production costs. The metal-free supercapacitor sample developed in the first part of this chapter was further tested for reproducibility and optimal electrode thickness. The design was found to be highly reproducible and optimised with a 2 mm electrode thickness.

Finally, this chapter compares the performance of sample EDLCs constructed to the same design used in the previous chapter, but varying the form of carbon used as the electrode material. Different electrode materials based on activated carbon (AC), carbon conductive paint, and a mixture of the two were prepared as three different slurries and deposited to form the electrodes of the respective EDLC samples. These samples were also compared with the metal-free design developed in the first part of the chapter. Results show that both carbon and silver paint functioned well as current collectors, but silver paint slightly more so. Carbon conductive paint mixed with AC appears most effective as the electrode material.

6.2 Development of metal-free supercapacitors using 3D printing

Metal-free supercapacitors were designed and fabricated using a 3D printing process. An attempt was made to use carbon conductive paint to create both current collectors and electrodes. The method described in this part of the chapter shows a new approach for manufacturing metal-free supercapacitors. The effectiveness of different thickness of electrodes has been assessed and the reproducibility of the manufacturing process for the supercapacitors has been investigated in this work.

6.2.1 Materials

The frames of supercapacitors were built using polylactic acid (PLA) filaments with a diameter of 2.89 mm. The current collectors and electrodes in this experiment were

made from carbon conductive paint (Bare Conductive Electric Paint). This carbon conductive paint offers the possibility of creating electrically conductive areas onto objects using 3D printing. The carbon conductive paint is a water-based material which is non-toxic and organic solvent free, and is used for making low-current circuits and sensors. The electrolyte in this study consists of phosphoric acid and PVA. The gel electrolyte was made by dissolving 0.8 mL H_3PO_4 and 1.0 g PVA in 10 mL deionized water.

6.2.2 Preparation of the AC slurry for current collectors and electrodes

Table 6.1 shows different types of AC slurry made from carbon conductive paint mixed with distilled water. Five different AC slurries were prepared for the use as current collector and electrode. The carbon conductive paint is solvent free and water soluble which can be used in stencil and screen printing processes. In this study, the distilled water was fixed at 20 g and mixed with carbon conductive paint of 1, 1.5, 2.0, 2.5, and 3.0 g individually. The slurry was stirred for 2 hours to make a homogenous mixture. This slurry does not separate during the processing. When making the AC slurry for depositing using 3D printing, it must not be too sticky to flow along a tube of the deposition system. The slurry made with 3.0 g of the carbon conductive paint was tested and found to be too viscous so that the mixture of slurry could not be deposited through the nozzle of the printing head.

Table 6.1 List of AC-carbon paint mixtures tested

AC slurry	Carbon conductive paint	Distilled water	Concentration of AC slurry
AC no: 1	1.0 g	20 g	4.76 wt%
AC no: 2	1.5 g	20 g	6.97 wt%
AC no: 3	2.0 g	20 g	9.09 wt%
AC no: 4	2.5 g	20 g	11.11 wt%
AC no: 5	3.0 g	20 g	13.04 wt%

*Note that as the concentration of carbon in the carbon conductive paint is unknown, the concentration of AC slurry represents the paint/water ratio, not the carbon/water ratio.

6.2.3 The effect of the concentration of carbon conductive paint

To define the suitable concentration of AC slurries, carbon conductive paint was prepared in five different concentrations as shown in Table 6.1. Four different AC slurries (no: 1-4) were selected as the material to build current collectors and electrodes as they had viscosities that enabled deposition by the paste extrusion system. AC slurry no: 5 was too sticky and could not be deposited. Four metal-free supercapacitors were fabricated with a laydown thickness of 0.5 mm using AC slurries containing different concentrations of carbon conductive paint. The CV curves were recorded using a potential window range of 0.8 V at the scan rate of 0.02 V/s, and the GCD curves were recorded at a charge current of 0.015 A, as shown in Figure 6.1 and 6.2

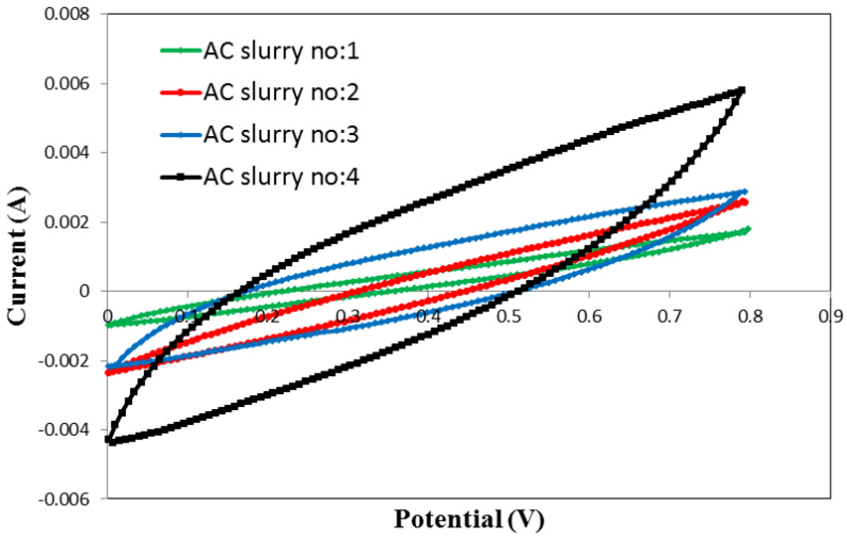

Figure 6.1 The cyclic voltammogram curves of the four EDLC samples with different concentrations of AC slurry.

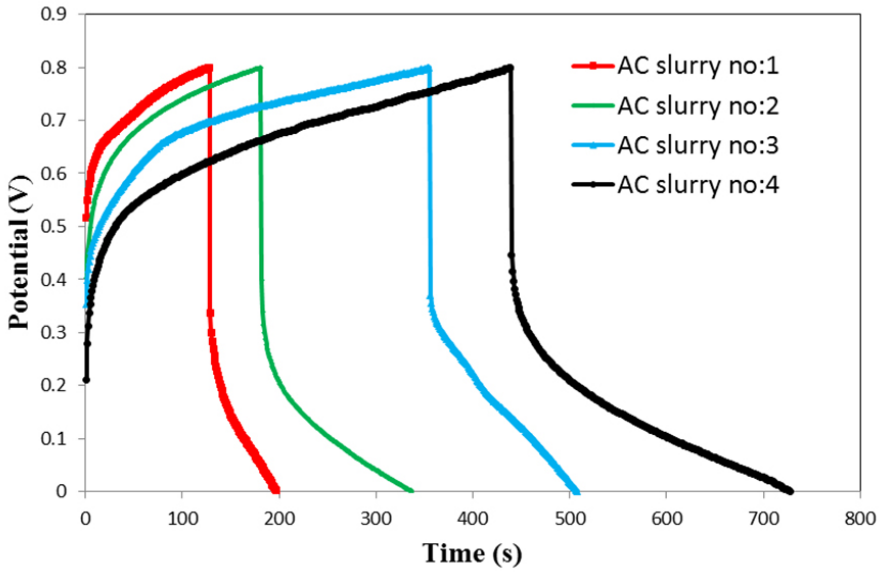

Figure 6.2 Galvanostatic charge/discharge curves of the four EDLC samples with different concentrations of AC slurries.

Table 6.2 shows the capacitance of C1 and C2 of the four samples calculated from the CV and GCD measurements and their corresponding specific capacitance Cs1 and Cs2. The shape of the CV curve shown in Figure 6.1 demonstrates that the device worked as a typical supercapacitor, which implied that the carbon conductive paint is an appropriate material for both current collector and electrode. The maximum capacitance achieved was 133 mF at the scan rate of 0.02 V/s. As the results shown in Table 6.2, the metal-free supercapacitor made from AC slurry no:4 (carbon conductive paint 2.5 g mixed with 20 g distilled water) produced a higher capacitance compared to the other AC slurries under the same manufacturing and testing conditions. Figure 6.3 shows the relationship between the concentration of carbon conductive paint and the capacitance of metal-free supercapacitor. It can be seen that the capacitances of the samples increased with increasing concentration of carbon conductive paint in the AC slurries. The concentration of AC in the slurries in this experiment increased by adding more carbon conductive paint into distilled water, which suggests an increase amount of carbon in the slurries. When the amount of activated carbon was increased, the conductivity of AC slurries increased and the capacitance of the metal-free supercapacitor increased consequently. However, increasing the amount of carbon conductive paint further for making AC slurry has to be a concern because the excessive viscosity of the AC slurry will not be suitable for 3D printing.

Table 6.2 Capacitance and specific capacitance of the four samples calculated from CV curve and GCD curves

		Calculated from CV curve		Calculated from GCD curve	
AC slurry	**Concentration of the paint**	**C1 (mF)**	**Cs1 (mF/g)**	**C2 (mF)**	**Cs2 (mF/g)**
no: 1	4.76 wt%	34	69	76	151
no: 2	6.97 wt%	61	120	103	201
no: 3	9.09 wt%	91	182	132	264
no: 4	11.11 wt%	133	259	174	339

In addition, the capacitance in this experiment can be affected by the different printing times required to build the electrode in order to complete the 0.5 mm thickness. Due to different concentrations of these slurries, less concentrated AC slurries had to be deposited around five times to achieve the thickness of 0.5 mm. On the other hand, the high concentration AC slurry was deposited two times to achieve at the same thickness as shown in Table 6.3. Although the thicknesses of these EDLC samples were similar, they were created with different layers. Printing more layers will have generated more bonding layers which could increase the internal resistance. This is considered a possible reason for the lower capacitance of lower paint concentration samples.

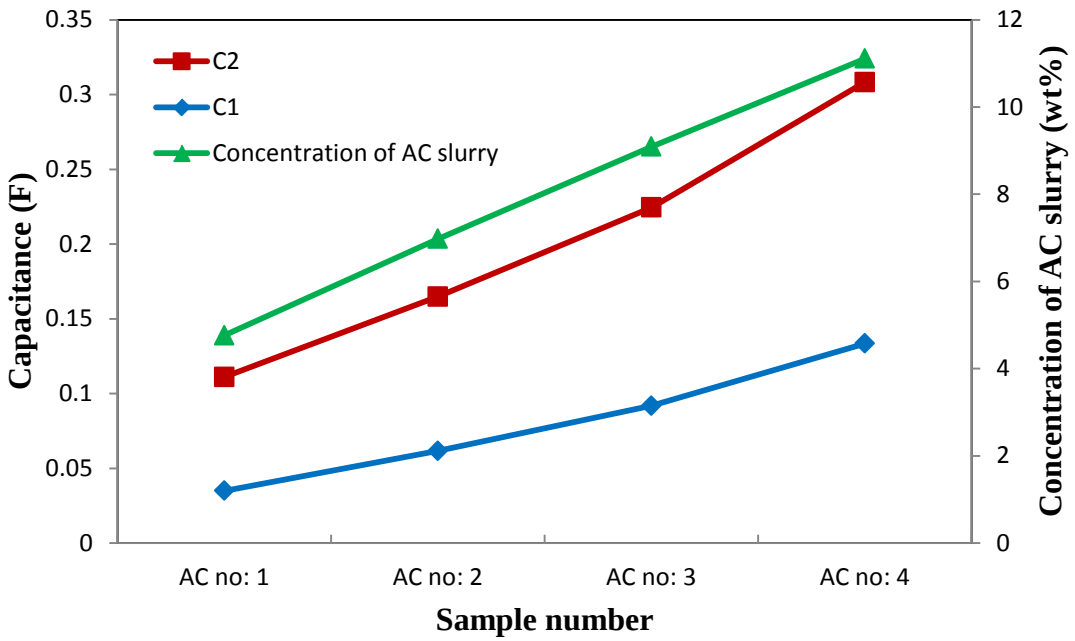

Figure 6.3 The capacitances of the four EDLC samples with different concentrations of the AC slurries.

Table 6.3 Deposition time and mass of electrode of different concentrations of the AC slurries

AC Slurry	Number of deposit (time)	Mass of each electrode layer (g)	Mass of Electrode (g)
No: 1	5	0.101	0.511
No: 2	4	0.127	0.516
No: 3	3	0.173	0.513
No: 4	2	0.259	0.515

6.2.4 Reproducibility of the manufacturing process

After a suitable concentration of AC slurry for manufacturing metal-free supercapacitor was verified and tested, the reproducibility of the manufacturing process was investigated. Having identified the sample with AC slurry no: 4 to have the best performance, another three metal-free EDLCs were fabricated under the same

conditions using the AC slurry no: 4, and designated as sample A, B, and C. The thickness of electrode was set at 0.5 mm. All the new EDLCs were characterized by CV and GCD tests. Figures 6.4 and 6.5 show the CV curve and GCD curve of the three new samples. The areas of the CV curves and GCD curves measured are almost the same. The average capacitance and specific capacitance calculated for the three new supercapacitors are about 0.131 F, and 0.250 F/g respectively, which is about 98% and 97% as the sample with AC slurry no: 4 described above. Standard deviations of all experimental data results are less than 0.01 %. Table 6.4 demonstrates that the results of the capacitance and specific capacitance of all samples calculated from CV measurement using equation (3.1) and (3.2) and from GCD measurement using equation (3.3) and (3.4) are only slightly different. These results illustrate that the manufacturing process for the metal-free supercapacitors in this study has very good reproducibility.

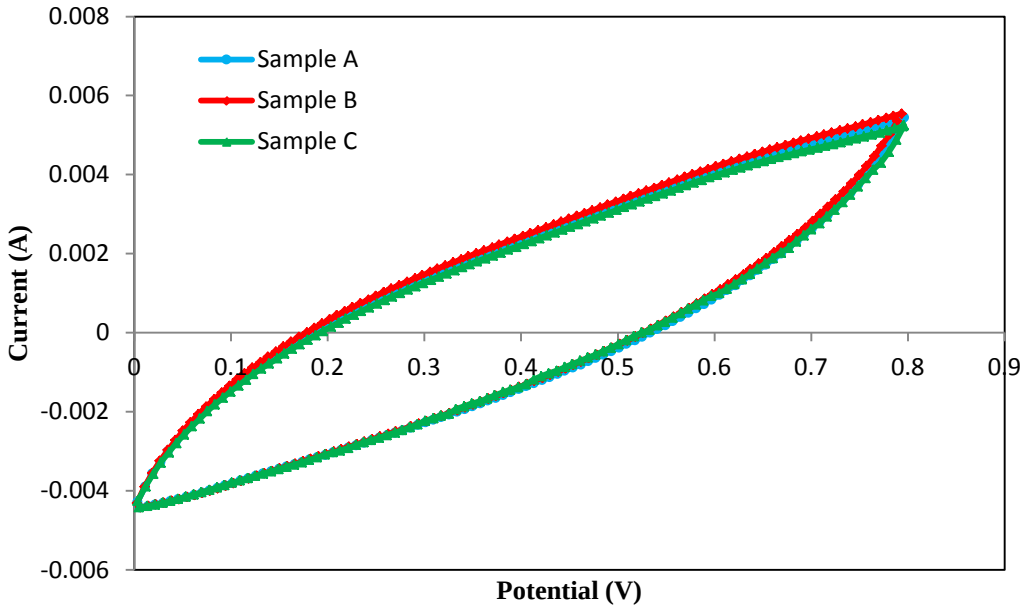

Figure 6.4 The cyclic voltammogram curves of the three new EDLC samples at the scan rate of 0.02 V/s.

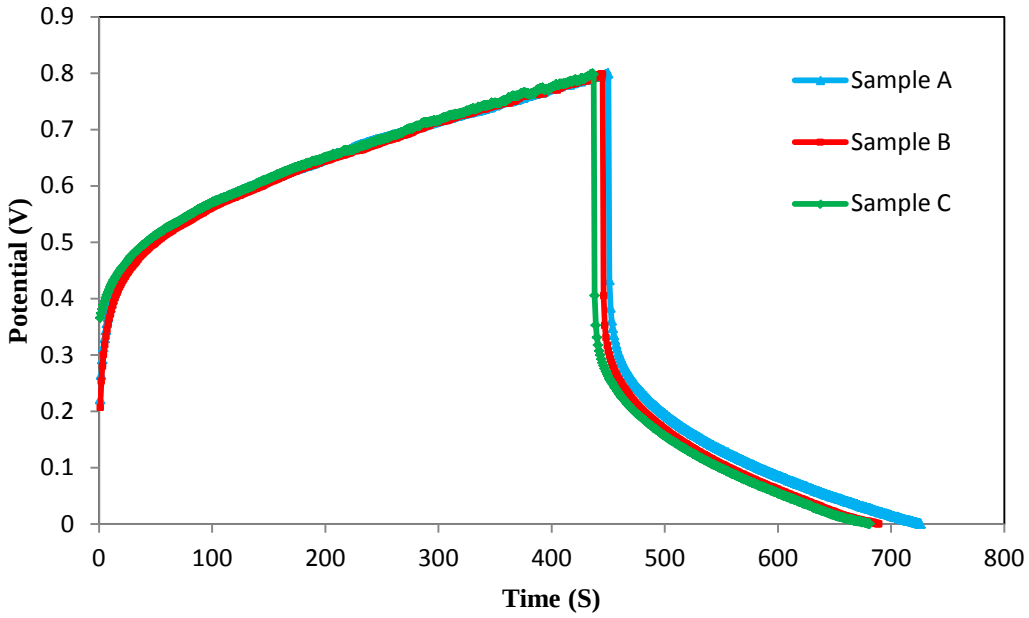

Figure 6.5 Galvanostatic charge/discharge curves of the three EDLC samples at a charge current of 0.015 A.

Table 6.4 Capacitance and specific capacitance of the three samples calculated from CV curve and GCD curves

	Calculated from CV curve		**Calculated from GCD curve**	
Sample	C1, (mF)	Cs1, (mF/g)	C2, (mF)	Cs2, (mF/g)
Sample A	131	250	171	327
Sample B	131	255	171	334
Sample C	130	252	169	328
Average value	131	253	171	330
Standard deviation (%)	0.0002	0.002	0.0008	0.002

6.2.5 The effect of the thickness of electrode on capacitance

The metal-free supercapacitors were fabricated under the same conditions with different electrode thicknesses, which were 0.5 mm, 1.0 mm, 1.5 mm, 2.0 mm and 2.5 mm. The capacitances, C1 and C2, and their corresponding specific capacitances, Cs1 and Cs2, of the five samples were calculated from the CV and GCD measurements as shown in Table 6.5 and Figures 6.6 and 6.7. Figure 6.8 shows the mass of the two electrodes of the five metal-free EDLCs samples and their capacitances as a function of the electrodes thickness. The mass of electrodes was measured before and after the AC slurry was deposited and dried. The mass of electrode in this experiment also included the mass of the current collector since this slurry was used for both current collector and electrode. It was believed that the current collector would function as part of the electrode attached with it. For this reason, when charging the supercapacitor samples, the current collector not only transported the electric charge to the electrode but also stored energy in the same time.

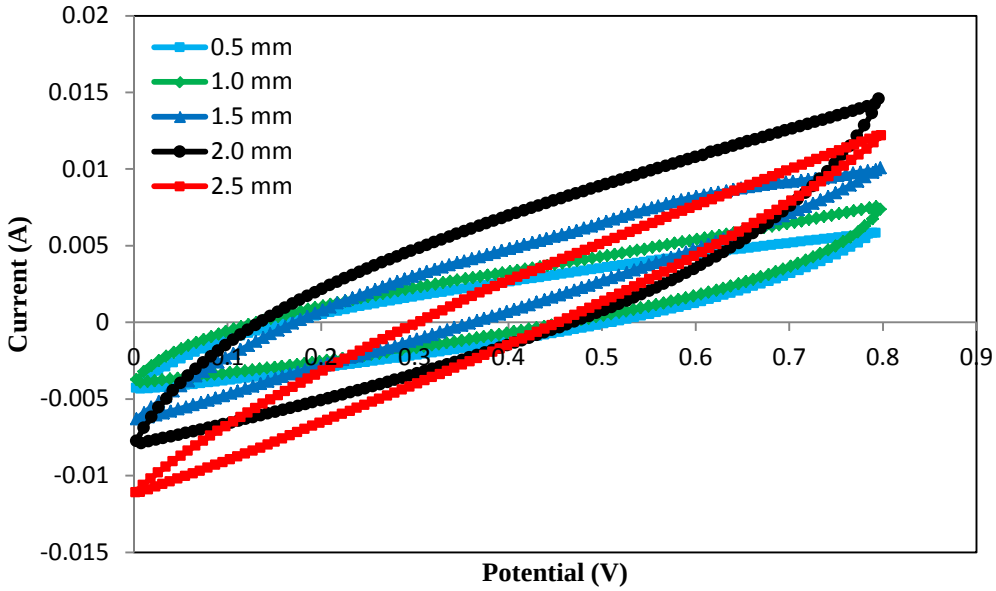

Figure 6.6 The cyclic voltammogram curves of the five EDLC samples with different electrode thicknesses.

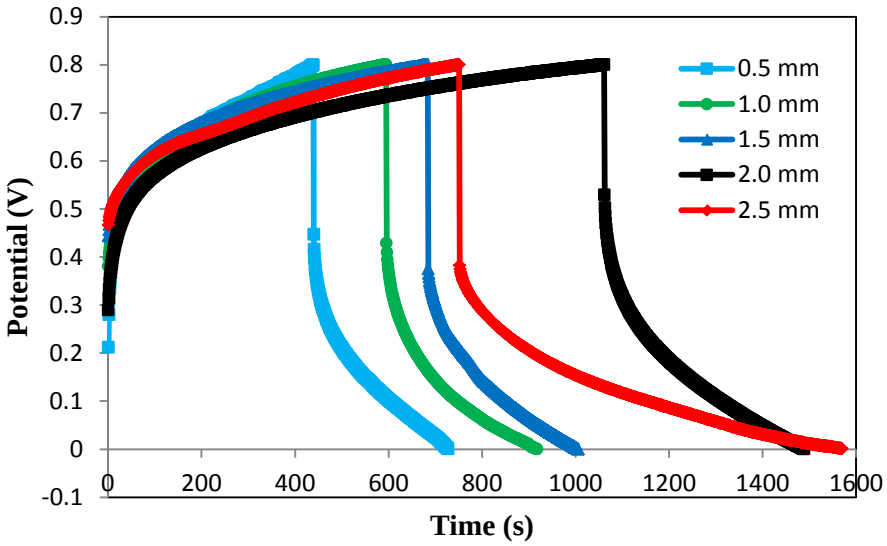

Figure 6.7 Galvanostatic charge/discharge curves of the five EDLC samples with different electrode thicknesses.

Table 6.5 Capacitance and specific capacitance of the samples calculated from CV curve and GCD curves

		Calculated from CV curve		Calculated from GCD curve	
AC electrode thickness (mm.)	**Mass of AC (g)**	**C1 (mF)**	**Cs1 (mF/g)**	**C2 (mF)**	**Cs2 (mF/g)**
0.5	0.514	133	259	173	338
1	0.848	178	209	217	256
1.5	1.174	228	194	263	229
2	1.498	297	198	338	225
2.5	1.828	250	136	290	159

The results shown in Figure 6.8 demonstrate that the thickness of the electrodes significantly affected the capacitance of samples as expected. Below the thickness of 2 mm, both capacitance and the mass of the electrodes increased linearly with the increase of the thickness of the electrode. When the thickness of the electrode was increased

above 2 mm, i.e.2.5 mm, the capacitance of the EDLC sample decreased. The decrease of the capacitance obtained with the thicker electrode might be caused by the rate of electrolyte diffusion which will be extended when the thickness of electrode is increased. In addition, the thicker electrode needed more printing times, which increased the internal resistance and thus resulted in a decrease of capacitance. Figure 6.9 shows the specific capacitances of the samples (Cs1 and Cs2) continuously decreased when the thickness of electrode increased. This is in good agreement with the literature review obtained by Wang [42], who suggested that the thin film electrode can produce a high specific capacitance because its low internal resistance and ease of electrolyte ion diffusion. On the other hand the specific capacitance of the electrode material could decrease when the electrode material was constructed of a thick layer because the transport of the electrolyte ions into/from active layers becomes more difficult. In addition, similar results of different electrode thickness have been reported previously [181-182].

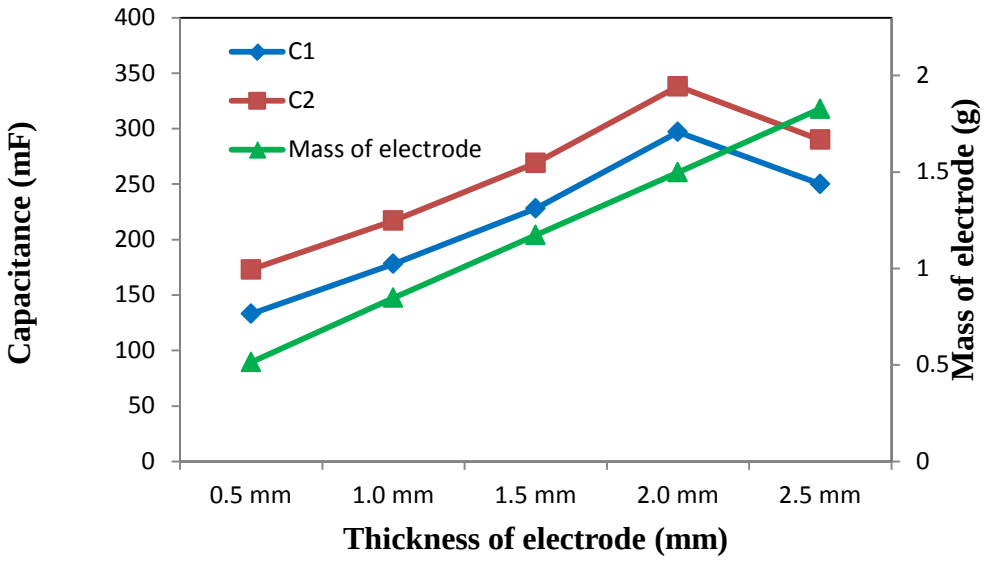

Figure 6.8 Capacitances calculated from CV and GCD for the five samples with different electrode thicknesses.

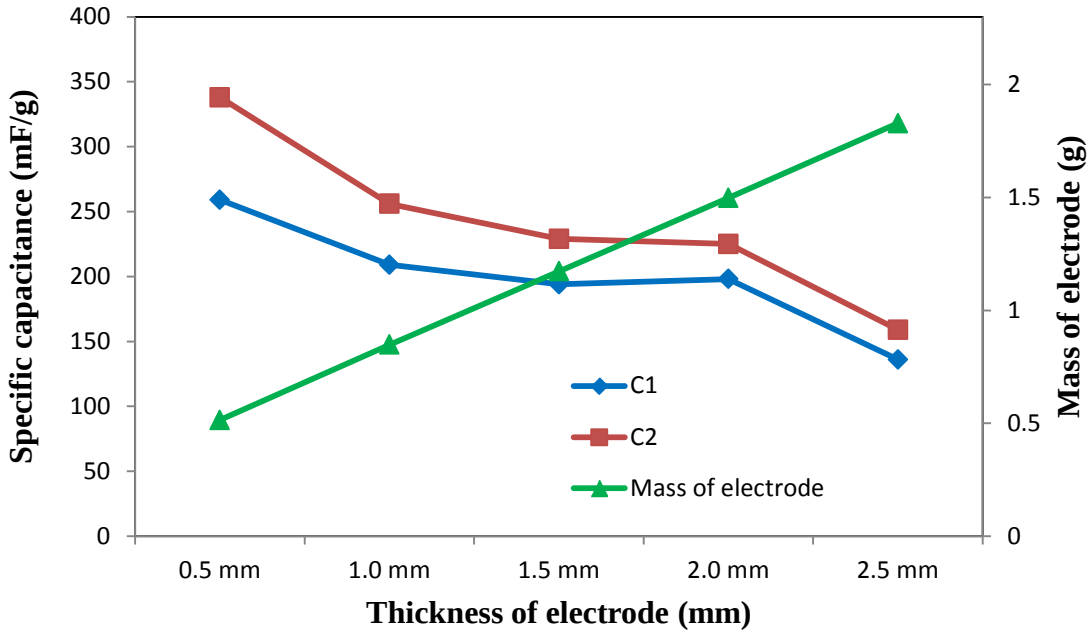

Figure 6.9 Specific capacitances calculated from CV and GCD for the five samples with different electrode thicknesses.

6.3 A comparison study of electrical performance of 3D printed supercapacitors fabricated with different materials

6.3.1 Materials used

The frame of the supercapacitors was made of polylactic acid (PLA) filament with a diameter of 2.89 mm. Silver conductive paint and carbon conductive paint (Bare Conductive Electric Paint) was used to build current collector. The carbon conductive paint was selected for this experiment because it is a water-based non-toxic and organic solvent free material, which is widely used to create low-current circuits and sensors including electrically conductive areas. Carbon conductive paint, activated carbon (AC), and their mixture were prepared as the electrode materials. CMC (sodium carboxymethyl cellulose), ethanol and distilled water were used as a binder. Phosphoric acid and polyvinyl alcohol (PVA) were used as the electrolyte solution. All the above materials used in the experiment are low cost, nontoxic and readily available.

6.3.2 Preparation of electrode materials and gel electrolyte

Three different slurries were prepared as an electrode material to examine the electrical performance of supercapacitors made from different materials. The composition of the three slurries is shown in Table 6.6. The main materials used to prepare for the slurries were activated carbon and carbon conductive paint. These two materials with different formulas were mixed with distilled water and stirred for 8 hours at room temperature to produce uniform slurries.

The gel electrolyte consists of phosphoric acid (H_3PO_4) and polyvinyl alcohol (PVA). 1 g of PVA powder was mixed with 10 ml distilled water and stirred in a magnetic stirrer at 50 ºC for 1 hour until fully dissolved. 0.8 ml of H_3PO_4 was then mixed with the PVA solution in the magnetic stirrer overnight until uniform.

Table 6.6 List of slurries and material composition for electrodes

Slurries	**Composition**				
	AC (g)	carbon conductive paint (g)	CMC 5 wt% (g)	Ethanol (ml)	Distilled water (ml)
no:1	2	N/A	2	20	20
no:2	N/A	2.5	N/A	N/A	20
no:3	0.5	2.5	N/A	N/A	20

6.3.3 Fabrication of EDLCs

The design of the EDLCs was identical except for the electrode and current collector materials. Silver conductive paint or carbon conductive paint was used to print the current collector layers, and the three slurries detailed above were used as electrode materials. In total, four samples were produced and tested to compare their electrical performance. The four material combinations tested are shown in Table 6.7.

Table 6.7 EDLC material combinations tested

Sample	Material for current collector	Material for electrode
A	Silver conductive paint	Slurry no:1 (AC)
B	Silver conductive paint	Slurry no:2 (carbon conductive paint)
C	Silver conductive paint	Slurry no:3 (mixture of AC and carbon conductive paint)
D	Carbon conductive paint	Slurry no:2 (carbon conductive paint)

Solidworks® was used to design all parts of the supercapacitor and this was exported for printing using the combination of the two 3D printing processes. The frame of supercapacitor was created using the FDM printer. PLA filament was fed into the heated controlled temperature nozzle so that the filament was melted and extruded to build the part's cross-sectional geometry layer by layer. The printing parameters were set as follows: printing speed at 50 mm/sec, fill density at 20 %, 0.6 mm for wall line width, and the temperatures of the nozzle and the build platform at 220 °C and 60 °C, respectively. After the printing of frame was accomplished, the current collector, the electrodes and the separator with electrolyte were printed using the paste extrusion system. After the electrode layer of each sample was totally deposited, the samples were dried at room temperature (approximately 22-24 °C). Then the separator of PVA gel electrolyte was printed on top of the electrodes. The two sides of the frame were then manually folded over to complete assembly.

6.3.4 Performance evaluation

1) CV and GCD testing results

Table 6.8 gives the CV and GCD testing results for all four EDLC samples manufactured with different materials, including their capacitance and specific capacitance.

Table 6.8 Capacitance and specific capacitance of the four samples calculated from CV curve and GCD curves

		Calculated from CV curve		**Calculated from GCD curve**	
Sample	***m* (g)**	**C1, (mF)**	**Cs1, (mF/g)**	**C2, (mF)**	**Cs2, (mF/g)**
A	0.945	194	205	234	248
B	0.948	342	360	382	403
C	0.946	391	413	431	456
D	1.498	297	198	338	225

Figure 6.10 shows the CV curves of the four EDLC samples. The sample C exhibits the largest enclosed area and the sample A shows the smallest enclosed area. Theoretically, the CV curve that has a rectangular shape indicates the capacitor to be functionally ideal. However, in this study the electrode materials fabricated in EDLC did not show an ideal performance which is considered to be due to the high resistance of the 2 mm thick electrode material. The CV curves of the samples B and C are slightly more rectangular shape than the samples A and D, implying B and C have a better electrical capacitance.

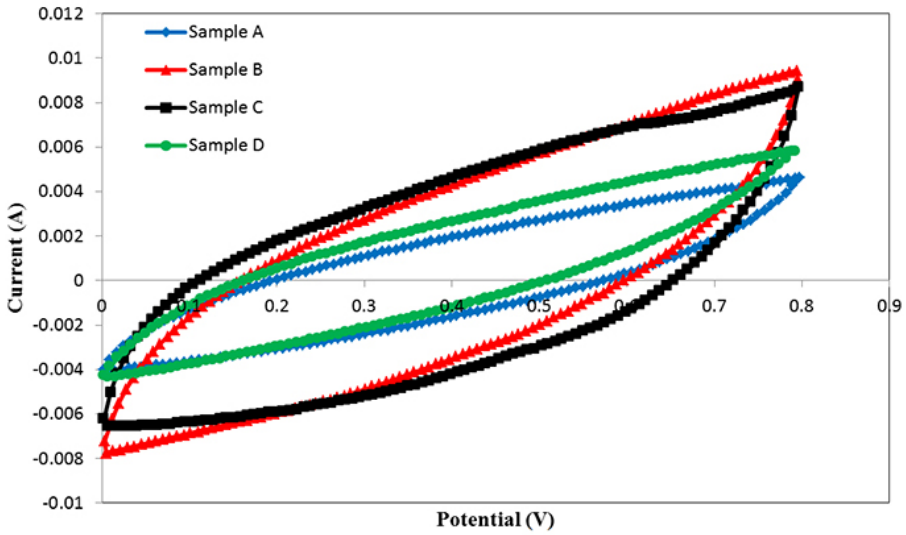

Figure 6.10 CV measurements of the four samples with different materials recorded at the scan rate of 0.02 V/s.

GCD is another method used to determine the capacitance of the ELDC. The charge and discharge processes are set at a specific current to evaluate the capacitance. The GCD curves of the four EDLC samples are illustrated in Figure 6.2. The capacitances of the four samples calculated from the GCD tests are similar to the CV tests, and show the same order of the capacitance values from highest to lowest, as shown in Table 6.3. The GCD curves of the sample B and C are quite similar, but the GCD curve of sample A is very different from other samples. This will be explained a in later section.

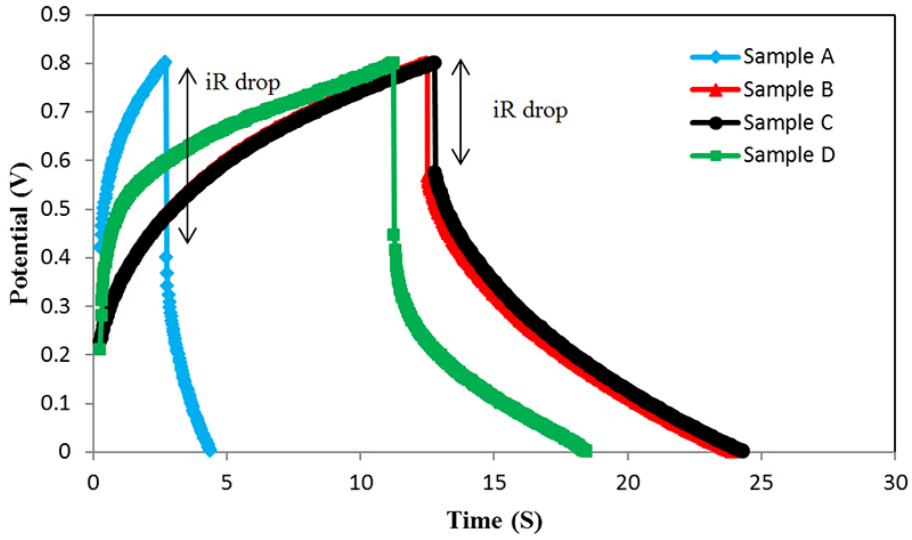

Figure 6.11 GCD measurements for the four EDLC samples with different materials recorded at the charge current of 0.015 A.

In summary, the results from the CV curves and GCD curves are broadly similar, but the highest capacitance was obtained from sample C, while the lowest capacitance was obtained from sample A.

2) The effect of different materials used for current collectors

The samples B and D have the same electrode material (carbon conductive paint) but different materials as current collectors (silver conductive paint for B and carbon conductive paint for D). It can be seen from Figure 6.10 that the area of the sample B is larger than the area of the sample D indicating the capacitances of the sample B is larger than the sample D. This result can be explained by the evidence of GCD curves shown in Figure 6.11. The GCD curves of both samples show a difference in the voltage drop (iR drop) at the beginning of discharge curve, i.e. sample D has a larger iR drop compared with sample B which directly resulted in a decreased ΔV compared with sample B. The initial portion of a discharge curve exhibits the iR drop due to internal resistance including the resistance from the current collector material. In previous experiments [149-150], the resistance of carbon conductive paint has been found to be much higher than that of silver conductive paint. In this study, the measured resistances of the current collector of the sample B and D were 0.52 Ω and 18.2 Ω respectively. These results suggest that high resistance of the current collector material significantly affected the capacitance. This would explain why sample B, with the lower resistance current collector material, had a higher capacitance than sample D.

From this result, it can be suggested that although carbon conductive paint can be used as the current collector material for supercapacitors and it shows the ability to collect/transport electron from/to the electrode material during the charge-discharge process, silver conductive material is more effective, because of its lower volume resistivity compared to the carbon conductive material.

3) The effect of changing electrode material on capacitance

The samples A, B, and C are used to compare the effect of different materials for electrodes as they were manufactured with the same current collector material (silver conductive paint) but with different electrode materials, as shown in Table 6.3. There is only AC material used as the electrode material for the sample A, only the carbon conductive paint for the sample B, and the mixture of AC and carbon conductive paint for the sample C. The capacitance measured for sample C was higher than that for

sample B, which was higher than that for sample A. The carbon paint performed the function of a binder in the mixture with AC, used in sample C, so no other binder was deemed necessary.

A scanning electron microscopy (SEM) was applied to study the surface morphology of the three different electrodes as shown in Figure 6.12. This SEM measurement was operated at an acceleration voltage of 5 kV using a Zeiss SUPRA 35 VP. Figure 6.3 (a), (b) and (c) show the SEM image of the surface of electrodes and magnified particle surface of AC, carbon conductive paint and carbon conductive paint mixed with AC respectively. SEM images indicated that the surface of three samples were completely different. The surface of AC material reveals its complex porous structure, comprised of various particle sizes. The surface area of carbon conductive paint was smoother than other the samples due to component in the carbon conductive material. According to the information provided by the manufacturer [149], the binder used in the carbon conductive paint is comprised of “natural resin” (precise substance is a trade secret). This likely causes the surface to be quite smooth. Figure 6.12 (b) also shows a magnification at 1 µm of carbon conductive material which reveals the small particles of the material. On the other hand, the surface of the mixture of AC and carbon conductive paint was quite rough which in theory should provide a more accessible for the electrolyte resulting in higher capacitance.

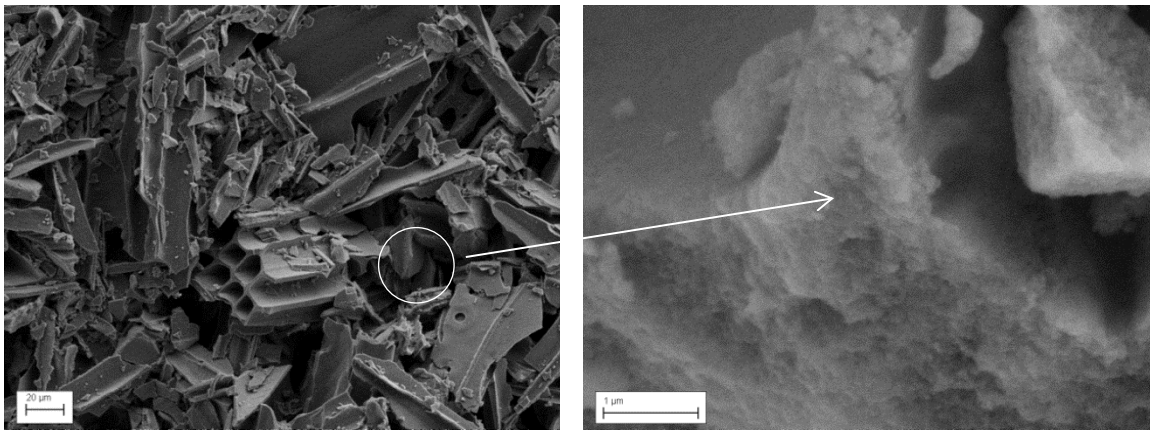

(a)

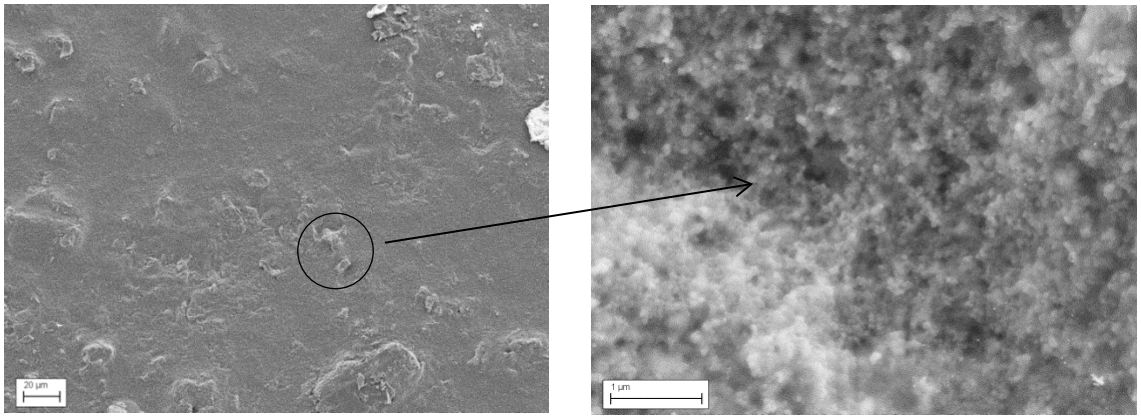

(b)

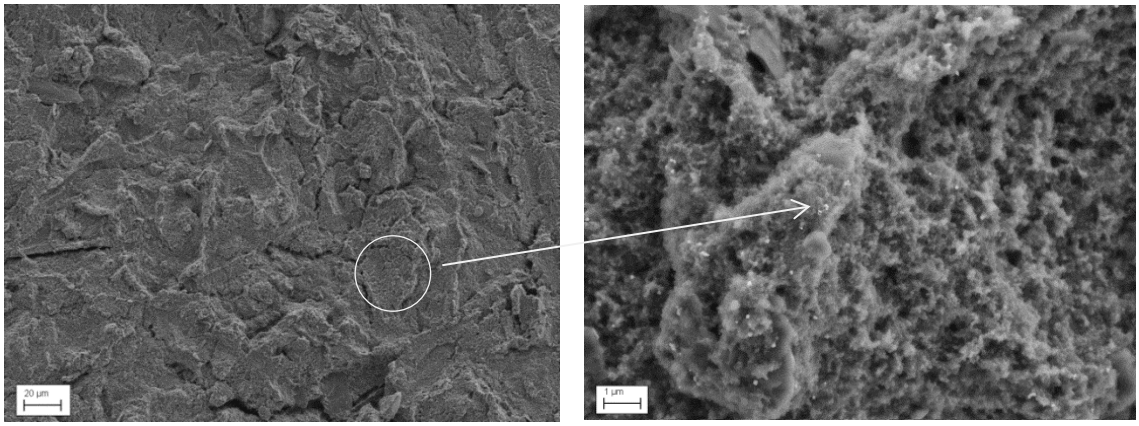

(c)

Figure 6.12 SEM images of three different electrodes (a) activated carbon, (b) carbon conductive paint, (c) carbon conductive paint mixed with activated carbon.

According to the information provided by the manufacturer, the carbon conductive paint used in this study consists of activated carbon and graphite. Graphite, an allotrope of carbon, is considered to be the most stable form of carbon and can be used as an electrode material in its own right. It has been widely demonstrated that graphite electrodes possess high specific surface area and good electrical conductivity [151-153]. Therefore, it can be deduced that the carbon conductive paint not only increased the specific surface area, but also enhanced the electrical conductivity of activated carbon (AC) material. This supports results obtained by Conway [7], who suggested that the electrode for EDLC must possess high specific surface area and good electrical conductivity. This study's results demonstrate that the carbon conductive paint has good electrical conductivity as it is suitable to be used as current collector, although it is not as effective as the silver conductive paint. The binder material (CMC) used in the electrode material of sample A deteriorated the electrical conductivity of AC material. Thus, the capacitance of the sample C is better than B and better than A. This is also the reason that the GCD curve of sample A is very different from the sample B and C, exhibiting a much larger iR drop.

Electrochemical Impedance Spectroscopy (EIS) is an effective tool that is applied to estimate the capacitive and resistive properties of a supercapacitor, which outputs the results in the format of Nyquist plots. The plot typically displays information about the capacitance, ion-diffusion, and resistance of the device. Information about the resistance is contained within the high-frequency region; information about the ion-diffusion properties in the mid-frequency region; and information about the capacitance in the low frequency region. A perfect supercapacitor would be represented by a straight line parallel to the imaginary axis (the Y-axis) of the Nyquist plot.

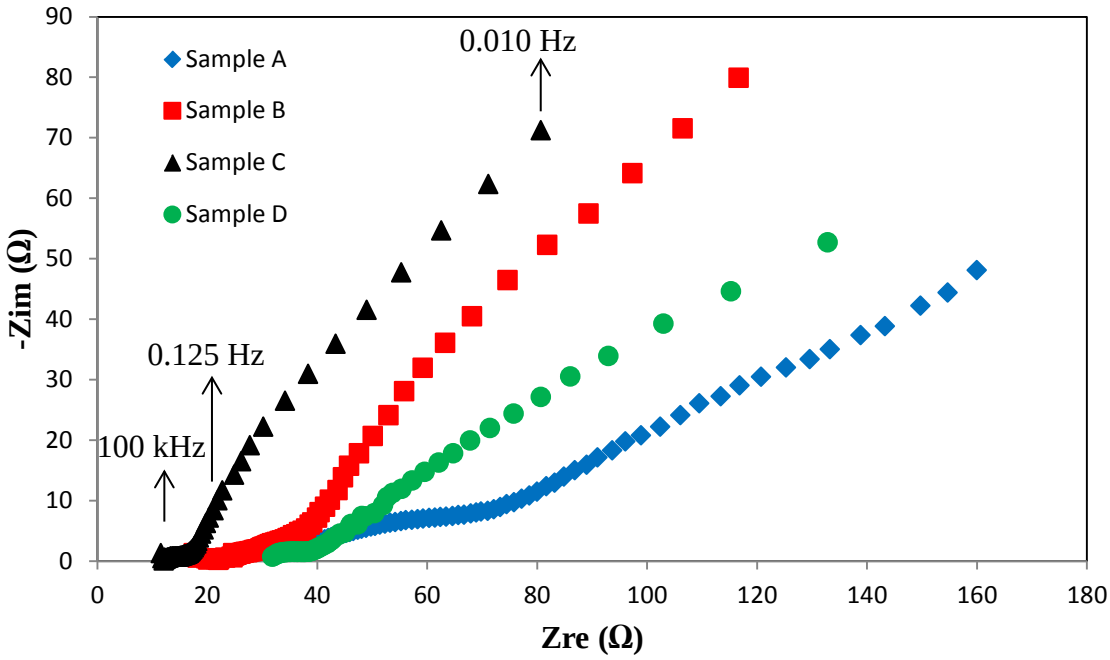

Figure 6.13 Nyquist plot of the 3D printed EDLC with different material for a frequency range between 100 kHz to 0.01 Hz.

Figure 6.13 shows a typical Nyquist plot of the four samples at high frequencies from 100 kHz down to 0.01 Hz. The equivalent series resistance (ESR) is about 38, 17, 11 and 29 Ω for sample A, B, C and D respectively. There is no semicircle shape in the higher frequency range because contact resistance and the charge transfer resistance were low. At intermediate frequencies, some ion diffusion of the electrolyte inside the electrode was seen as the inclined line. At lower frequencies, sample A, C, and D exhibited high internal resistance, especially sample D. These results correspond with the results of the CV curve and GCD measurements.

Table 6.8 also gives the values of the specific capacitances of these three EDLC samples A, B and C. The order of the values of the specific capacitance are corresponding to their capacitance values, i.e. C is higher than B and higher than A, which implies that the high capacitance and high specific capacitance are both directly proportional to the high specific surface area of the materials. This result is also in a good agreement with the literature [42, 152] which suggest that the specific capacitance of the electrode material can be effectively improved by using the material with high specific surface area. In addition, the capacitance and the specific capacitance also depends on the electrode layer structure and transfer capability of the electrons and ions

within the layer. It has been demonstrated above that the mixture of carbon conductive paint and AC has better conductivity than the carbon conductive paint and better than AC with CMC binder, thus sample C has a higher capacitance and specific capacitance than sample B, which in turn had higher than had sample A. From these results, the mixture of the carbon conductive paint and the activated carbon is determined to be the most effective material, of those tested, for fabricating the electrodes in this design.

6.4 Conclusion

6.4.1 Metal-free Design: Carbon Paint Concentration, Reproducibility and Electrode Thickness

Of the 5 carbon paint slurries produced, the slurry with concentration 11.1 wt% produced the sample with highest capacitance, although the slurry with concentration 13.0 wt% could not be tested as it was too sticky and it cannot flow along a tube of the deposition system. The samples tested consistently increased their capacitance as the carbon paint content was increased. The cause of this result was not investigated, but it was assumed to be due to the increased printing iterations required for lower concentrations reducing connectivity, and thus causing increased internal resistance.

The metal-free supercapacitor was found to be extremely reproducible, more so even than the design tested in chapter 5. Capacitances of the 3 samples had a standard deviation of less than 0.1% on both measures (CV and GCD). If we extend the sample to include the two other samples produced to the same design in parts 6.2.3 and 6.2.5 the standard deviations rise to around 0.1% on CV measurements, and 0.2% on the GCD measurements. This still compares favourably to the standard deviations of around 0.7% in the chapter 5 design reproducibility test. This improvement was to be expected since producing the current collector and electrodes from the same material simplifies the process.

Changing from a silver to a carbon current collector appeared to make little difference to the effects of changing the thickness of the electrodes. As with the chapter 5 design, capacitance consistently increased as the thickness of the electrode increased up to a thickness of 2.0 mm, while increasing the thickness further to 2.5 mm decreased capacitance to a similar level as the sample with 1.5 mm electrode thickness. The electrode thickness was only examined a 0.5 mm intervals, so the optimum thickness

may lie anywhere between 1.5 mm and 2.5 mm. The symmetry of the capacitance corresponding to electrode thickness 1.5 mm and 2.5 mm suggests though that the optimum is likely to be very close to 2.0 mm.

These results again show the samples operating consistently. To a certain point, increasing the thickness of the electrodes allows more charge to be stored, however, beyond that point the rate of electrolyte diffusion may reduce overall capacitance, and the increased printing iterations increase the internal resistance.

As in chapter 5, specific capacitance was maximised with the thinnest electrode sample (0.5mm electrode). As specific capacitance is measured in proportion to the active materials, this was to be expected; however, this result does show that the sample still functioned efficiently with this ultra-thin electrode. The feasibility of ultra-thin electrodes may be of interest for more complex structural designs.

6.4.2 Electrode and Current Collector Material Comparison

Of the three forms of carbon electrode tested, the slurry mixture of carbon conductive paint with activated carbon (AC) performed best, measuring a capacitance of 431 mF by GCD curve. Scanning electron microscopy (SEM) appeared to show this mixture to have a rougher surface texture than either the carbon paint or AC in isolation. This is one probable cause for it being the most effective, since an increased active surface area is associated with greater capacitance. In addition, the Electrochemical Impedance Spectroscopy (EIS) low-frequency Nyquist plot revealed this hybrid material sample to exhibit the least internal resistance, which is another probable reason for its superiority.

That mixing the carbon paint with additional AC was more effective than carbon paint alone also tallies with the findings on the effect of changing the concentration of the carbon paint earlier on - that a higher concentration of carbon paint produces better electrodes. This mixture enabled the creation of a slurry with a higher concentration of carbon without rendering the slurry too sticky for paste extrusion. This opens a promising avenue for future research into whether performance can be improved by further increasing the carbon content of the slurry.

Though not a failure, the AC with sodium carboxymethyl cellulose, ethanol, and distilled water performed least well, its sample measuring roughly half the capacitance of the AC combined with carbon paint electrode sample. As mentioned in chapter 5,

electrical performances of these samples were limited because of high internal resistance. The high internal resistance was probably due to the thickness of the electrode and poor penetration of PVA gel electrolyte and also corrosion of the current collector.

The silver paint appeared a bit more effective than the carbon paint as a current collector. Sample B (silver current collector, carbon paint electrode) had approximately 14% higher capacitance compared with Sample D (carbon paint current collector and electrodes). The effect was much more pronounced when considering the specific capacitance, as the carbon paint current collector was considerably heavier. Sample B had approximately 80% higher specific capacitance than Sample D. This was as expected because silver is known to have better electrical conductivity than carbon. In fact, the relatively small difference in performance makes a good case for the cost effectiveness of carbon paint, which is much cheaper. Furthermore, it would be of interest to find out whether the capacitance of the metal-free design could be improved further by using the AC/carbon paint mixture that was successful as an electrode material.

Chapter 8 Conclusions and suggestions for further work

7.1 Addressal of Objectives

The introduction to this thesis set six objectives for this research as listed below:

1) To design a functional shape and structure for 3D printed supercapacitors using computer aided design.
2) To fabricate the supercapacitors using low cost and environmentally friendly materials.
3) To characterise the electrical performance of the supercapacitors.
4) To develop metal-free supercapacitors.
5) To investigate factors that affect the performance of supercapacitors.
6) To improve the electrical performance and the manufacturing process of supercapacitors.

By way of conclusion, it seems logical to now consider to what extent this research has addressed those objectives.

1) Computer aided design (CAD) was successfully used to develop a few different versions of a small cuboidal supercapacitor to be printed in two halves and then manually pressed together. CAD was also configured to operate two separate 3D printing systems in a single integrated process. The final design included intricate features: conductive slots and protrusions for connecting devices together, and a built-in hinge to simplify assembly. More than 20 samples were fabricated using 3D printing, all of which were functional as a supercapacitor.

2) The materials used were environmentally friendly and non-toxic. The silver conductive paint requires some attention with regards to its disposal, so the metal-free samples produced represent the most environmentally friendly design. The carbon conductive paint is described by the manufacturer as water based and biodegradable, and comes without any significant hazard warnings. PLA, which is used for the casing,

is derived from renewable plant-based resources, and is bio-compatible and biodegradable.

3) All samples produced were tested for their capacitance using a CV test and GCD test. The best performing sample in terms of capacitance and specific capacitance was Sample C detailed in Chapter 6, with a capacitance of 0.4 F and a specific capacitance of 0.4 F/g. This sample had a current collector formed from silver conductive paint, and 2mm thick electrodes produced from a mixture of carbon conductive paint and activated carbon.

Furthermore, in Chapter 5, samples underwent a series of other tests:

- Samples were tested for their performance at different scan rates using CV tests. The capacitance was found to decrease with the increase of scan rate.
- Galvanostatic charge/discharge curves were used to assess stability of performance with repeated use, and assess functionality at various charging currents. Performance was stable over 5 usage cycles, and although increasing the charging current reduced capacitance, performance was much improved in comparison to the pilot sample.
- Electrochemical impedance spectroscopy (EIS) was used to determine the resistance of components, presented in the form of a Nyquist plot.
- The “extendable” feature of the samples was tested for effectiveness by connecting in series, parallel and via a direct connection, running CV and GCD tests for each setup. This feature was found to operate perfectly.

4) Metal-free supercapacitors were developed in chapter 6 using carbon conductive paint as the current collector as well as the electrode material. These did not have quite the same level of capacitance as samples produced with silver paint current collectors, but they were not unsatisfactory by comparison. The metal-free sample measured a capacitance of 320 mF (average of CV and GCD tests), compared to a capacitance of 360 mF measure in the equivalent sample with a silver current collector. The finding that adding AC to carbon paint enhanced the capacitance in a sample with a silver current collector suggests that the performance of the metal-free design could be enhanced also; though this requires further research.

5) A range of factors that affect the performance of the samples produced was investigated. Electrode material, current collector material, electrode thickness, carbon

paint concentration, scan rates, and long-term repeated use were all considered. The respective findings were as follows:

- Increasing the scan rate reduced capacitance.
- Capacitance was maximised with an electrode thickness of 2.0 mm. Specific capacitance was maximised with an electrode thickness of 0.5 mm.
- Although carbon conductive paint was effective as a current collector, silver conductive paint was superior.
- Long-term, the samples were less stable. After 500 iterations of CV measurements, capacitance had fallen to half of its initial level.
- Capacitance improved as the concentration ratio of carbon paint to distilled water was increased. Capacitance was maximised at 11.1 wt%, but a higher concentration was found to be too sticky to be deposited by the paste extruder.
- Diluted carbon conductive paint with added AC was more effective than other forms of carbon material for constructing electrodes.

Furthermore, it was assumed from the pilot experiments that appropriate drying times between 3D printed layers, and the electrolyte used, significantly affected the performance of samples.

6) The 3D printing process and performance of samples was dramatically improved over the course of this research as shown in Table 7.1; eventually to a standard comparable to low-cost commercial equivalents. The first pilot sample produced measured a specific capacitance of only 6 mF/g, but by the end of this research a sample with specific capacitance of 430 mF/g (CV/GDC average) was achieved. Regardless of its comparison with standard commercial production techniques, 3D printing seems a promising option for the production of bespoke, experimental, and prototype supercapacitors. For these purposes it may well be an improvement on alternative methods.

Table 7.1 All EDLCs samples and their electrical performance

					CV measurement		GCD measurement	
	Sample	**thickness (mm)**	**Mass (g)**	**Electrode/electrolyte**	**C1 (mF)**	**Cs1 (mF/g)**	**C2 (mF)**	**Cs2 (mF/g)**
Chapter 4	Pilot sample 1	1.5	0.386	AC+CMC/H3PO4 + distilled water	6.29	53.83	6.51	59.23
	Pilot sample 2	1.5	0.727	AC+CMC/C16H36BF4N+C4H6O3	212	205	528	262
Chapter 5	Sample no : 1	2	0.942	AC+CMC/H3PO4 + PVA + distilled water	182	193	224	238
	Sample no : 2	2	0.942	AC+CMC/H3PO4 + PVA + distilled water	177	189	218	232
	Sample no : 3	2	0.941	AC+CMC/H3PO4 + PVA + distilled water	168	171	209	214
	Sample no : 4	2	0.945	AC+CMC/H3PO4 + PVA + distilled water	169	181	208	224
	Sample with 0.5 mm thickness	0.5	0.212	AC+CMC/H3PO4 + PVA + distilled water	125	598	166	785
	Sample with 1.0 mm thickness	1	0.455	AC+CMC/H3PO4 + PVA + distilled water	155	340	195	463
	Sample with 1.5 mm thickness	1.5	0.698	AC+CMC/H3PO4 + PVA + distilled water	172	240	212	313
	Sample with 2.0 mm thickness	2	0.945	AC+CMC/H3PO4 + PVA + distilled water	194	205	234	248
	Sample with 2.5 mm thickness	2.5	1.195	AC+CMC/H3PO4 + PVA + distilled water	182	152	222	198
Chapter 6	Sample with AC slurry no : 1	0.5	0.511	CCP+distilled water/H3PO4 + PVA + distilled water	34	69	76	151
	Sample with AC slurry no : 2	0.5	0.516	CCP+distilled water/H3PO4 + PVA + distilled water	61	120	103	201
	Sample with AC slurry no : 3	0.5	0.513	CCP+distilled water/H3PO4 + PVA + distilled water	91	182	132	264
	Sample with AC slurry no : 4	0.5	0.515	CCP+distilled water/H3PO4 + PVA + distilled water	133	259	174	339
	Sample A	0.5	0.514	CCP+distilled water/H3PO4 + PVA + distilled water	131	250	171	327
	Sample B	0.5	0.513	CCP+distilled water/H3PO4 + PVA + distilled water	131	255	171	334
	Sample with 0.5 mm thickness	0.5	0.515	CCP+distilled water/H3PO4 + PVA + distilled water	130	252	169	328
	Sample with 1.0 mm thickness	1	0.848	CCP+distilled water/H3PO4 + PVA + distilled water	178	209	217	256
	Sample with 1.5 mm thickness	1.5	1.174	CCP+distilled water/H3PO4 + PVA + distilled water	228	194	263	229
	Sample with 2.0 mm thickness	2	1.498	CCP+distilled water/H3PO4 + PVA + distilled water	297	198	338	225
	Sample with 2.5 mm thickness	2.5	1.828	CCP+distilled water/H3PO4 + PVA + distilled water	250	136	290	159
	Sample A	2	0.945	AC+CMC/H3PO4 + PVA + distilled water	194	205	234	248
	Sample B	2	0.948	CCP+distilled water/H3PO4 + PVA + distilled water	342	360	382	403
	Sample C	2	0.946	CCP+ AC+ distilled water/H3PO4 + PVA + distilled water	391	413	431	456
	Sample D	2	1.498	CCP+distilled water/H3PO4 + PVA + distilled water	297	198	338	225

7.2 The main contributions

From this work, the following points summarise the main contributions to knowledge made in this thesis:

First of all, 3D printing has been demonstrated as a viable means for the production of basic small supercapacitors. Fused deposition modelling (FDM) and a paste extrusion system were successfully employed to produce numerous varying versions of the design without functional failure. In total, more than 20 different samples were produced using 3D printing methods, and while some performed far better than others, none failed to function as a supercapacitor altogether.

Furthermore, the process proved to be very consistent in reproducibility tests. The capacitance of samples produced to the same designs differed in capacitance by as little as 1-5%. This reflects the accuracy and simplicity of the production process.

The manner in which the FDM machine was combined with the paste extruder and modified so that samples could be printed in a single operation was an innovative approach. In addition to simplifying the process, it also allowed for more precision and less chance of human error, because the sample did not need to be moved from one machine to another. Although there are other examples of these two methods being integrated, it is not common. This contribution has significance not only for the 3D-printing of supercapacitors, but for 3D-printing in general.

The hinges that were part of the design used in this study were successful in assisting the final assembly of samples. They were a good example of how 3D-printing can be used to produce support mechanism to ensure the precision of final assembly. This also has significance for the wider field of 3D-printing.

Finally, the connection jacks that were also part of the final design proved very successful. Despite their small size, they were produced without fault and operated extremely effectively. Again this demonstrated the precision of the 3D-printing process, while also exemplifying a means of extending the capacitance as required through connecting multiple devices. This also showed how the supercapacitors may be designed to connect to other electronic devices without the need for wires, as may be required within compact electronic devices.

7.3 Suggestions for further work

This part of chapter briefly presents a number of ideas of how future research in this area can build on what has been explored in this work, and on what has been studied previously in this field.

1) Testing Larger Designs

The samples produced in this thesis were all very small. This was to limit production costs, test the 3D system's ability to produce minute details, and to consider a design suitable for use in compact devices. Other purposes may require a larger supercapacitor, so one potential for further work would be to test the efficacy of 3D printing for larger designs with more capacitance.

2) Testing More Complex Designs

Similarly, this thesis only focused on producing a slim cuboidal geometry. Future work could consider exploring new shapes, such as a thicker cuboid, or cylinder which is commonly used for modern supercapacitors. The design used in this thesis only required the conductive materials to be repeatedly printed along a single flat plane. Thicker supercapacitors require the electrode planes to meander or spiral in order to maximise electrode surface area within the volume of the design. 3D printing these more complex designs would present a more robust test of the CAD and the system's precision.

3) Fabrication of Other Devices Using the Integrated FDM-Paste Extrusion System

Within this research, an innovative dual-headed 3D printer was fashioned by fixing a paste extruder to the mechanism of the FDM printer. This made the process easier, as well as improving the level of precision. This was one of the most successful elements of this research, proving to provide excellent reproducibility. This manufacturing process could be of interest for further study on different designs or even different components.

4) Pneumatic Paste Extrusion System

In this thesis, the paste extrusion system consisted of a stepper motor, a syringe connected to a plastic tube, and a nozzle at the end of the plastic tube. To extrude the paste material, the stepper motor is driven to rotate the screw underneath the syringe plunger. After the plunger is pushed, the paste material flows through the plastic tube

into the nozzle, and the material is then deposited in the desired position. This system functioned fairly well, however a paste extrusion machine with a pneumatic control may be able to provide more accuracy for the volumetric control, repeatability of dispensing, the accuracy of the start-stop deposition process, and the speed of deposition. Whether such a machine could be combined with an FDM printer as was achieved in this study, and whether it does indeed produce more reliable samples, could be a focus for future research.

5) Further Study of Carbon Paint with AC Additives

The carbon conductive paint used in this thesis (Bare Conductive® Electric Paint) was stable and presented good electrochemical performance. However, the performance was found to be improved with the addition of granular AC, which produced the best performing sample evaluated in this thesis. This finding requires much further study though. Since only one sample was produced using this form of slurry, the reproducibility, cycle life stability, and optimal AC concentration remains unexamined. Furthermore, the performance of this slurry as the current collector/electrode material within a metal-free design would be of great interest.

Reference

1. BOICEA, V.A., 2014. Energy Storage Technologies: The Past and the Present. *Proceedings of the IEEE,* **102**(11), pp. 1777-1794.

2. BURKE, A., 2000. Ultracapacitors: why, how, and where is the technology. *Journal of Power Sources,* **91**(1), pp. 37-50.

3. HALPER, M.S. and ELLENBOGEN, J.C., 2006. Supercapacitors: A brief overview. *MITRE Nanosystems Group,* .

4. KIEBELE, A., KAEMPGEN, M. and GRUNER, G., 2008. Printed Energy and Power Storage: Batteries and Supercapacitors. *Nanotech.L.& Bus.,* **5**, pp. 7.

5. KIM, B.K., SY, S., YU, A. and ZHANG, J., 2015. Electrochemical supercapacitors for energy storage and conversion. *Handbook of Clean Energy Systems,* .

6. KÖTZ, R. and CARLEN, M., 2000. Principles and applications of electrochemical capacitors. *Electrochimica Acta,* **45**(15), pp. 2483-2498.

7. CONWAY, B. and PELL, W., 2003. Double-layer and pseudocapacitance types of electrochemical capacitors and their applications to the development of hybrid devices. *Journal of Solid State Electrochemistry,* **7**(9), pp. 637-644.

8. CONWAY, B., Electrochemical supercapacitor: scientific principles and technological application, Plenum, New York, 1999

9. YU, A., CHABOT, V. and ZHANG, J., Electrochemical supercapacitors for energy storage and delivery: Fundamentals and Applications, CRC Press, New York, 2017

10. VANGARI, M., PRYOR, T. and JIANG, L., 2012. Supercapacitors: Review of materials and fabrication methods. *Journal of Energy Engineering,* **139**(2), pp. 72-79.

11. TIAN, X., JIN, J., YUAN, S., CHUA, C.K., TOR, S.B. and ZHOU, K., 2017. Emerging 3D-Printed Electrochemical Energy Storage Devices: A Critical Review. *Advanced Energy Materials,* .

12. ZHAKEYEV, A., WANG, P., ZHANG, L., SHU, W., WANG, H. and XUAN, J., 2017. Additive manufacturing: unlocking the evolution of energy materials. *Advanced Science,* .

13. ZHANG, F., WEI, M., VISWANATHAN, V.V., SWART, B., SHAO, Y., WU, G. and ZHOU, C., 2017. 3D Printing Technologies for Electrochemical Energy Storage. *Nano Energy,* .

14. ZHU, C., LIU, T., QIAN, F., CHEN, W., CHANDRASEKARAN, S., YAO, B., SONG, Y., DUOSS, E.B., KUNTZ, J.D. and SPADACCINI, C.M., 2017. 3D printed functional nanomaterials for electrochemical energy storage. *Nano Today,* .

15. BAK, D., 2003. Rapid prototyping or rapid production? 3D printing processes move industry towards the latter. *Assembly Automation,* **23**(4), pp. 340-345.

16. BERMAN, B., 2012. 3-D printing: The new industrial revolution. *Business horizons,* **55**(2), pp. 155-162.

17. BIKAS, H., STAVROPOULOS, P. and CHRYSSOLOURIS, G., 2016. Additive manufacturing methods and modelling approaches: a critical review. *The International Journal of Advanced Manufacturing Technology,* **83**(1-4), pp. 389-405.

18. VAEZI, M., SEITZ, H. and YANG, S., 2013. A review on 3D micro-additive manufacturing technologies. *The International Journal of Advanced Manufacturing Technology,* **67**(5-8), pp. 1721-1754.

19. WONG, K.V. and HERNANDEZ, A., 2012. A review of additive manufacturing. *ISRN Mechanical Engineering,* **2012**.

20. YAN, X. and GU, P., 1996. A review of rapid prototyping technologies and systems. *Computer-Aided Design,* **28**(4), pp. 307-318.

21. YAN, Y., LI, S., ZHANG, R., LIN, F., WU, R., LU, Q., XIONG, Z. and WANG, X., 2009. Rapid Prototyping and Manufacturing Technology: Principle, Representative Technics,

22. CAMPBELL, T.A. and IVANOVA, O.S., 2013. 3D printing of multifunctional nanocomposites. *Nano Today,* **8**(2), pp. 119-120.

23. GAO, W., ZHANG, Y., RAMANUJAN, D., RAMANI, K., CHEN, Y., WILLIAMS, C.B., WANG, C.C., SHIN, Y.C., ZHANG, S. and ZAVATTIERI, P.D., 2015. The status, challenges, and future of additive manufacturing in engineering. *Computer-Aided Design,* **69**, pp. 65-89.

24. KRUTH, J., LEU, M. and NAKAGAWA, T., 1998. Progress in additive manufacturing and rapid prototyping. *CIRP Annals-Manufacturing Technology,* **47**(2), pp. 525-540.

25. LEVY, G.N., SCHINDEL, R. and KRUTH, J.P., 2003. RAPID MANUFACTURING AND RAPID TOOLING WITH LAYER MANUFACTURING (LM) TECHNOLOGIES,

STATE OF THE ART AND FUTURE PERSPECTIVES. *CIRP Annals - Manufacturing Technology,* **52**(2), pp. 589-609.

26. PHAM, D. and GAULT, R., 1998. A comparison of rapid prototyping technologies. *International Journal of Machine Tools and Manufacture,* **38**(10-11), pp. 1257-1287.

27. SACHS, E., CIMA, M. and CORNIE, J., 1990. Three-Dimensional Printing: Rapid Tooling and Prototypes Directly from a CAD Model. *CIRP Annals - Manufacturing Technology,* **39**(1), pp. 201-204.

28. SACHS, E., CIMA, M., CORNIE, J., BRANCAZIO, D., BREDT, J., CURODEAU, A., FAN, T., KHANUJA, S., LAUDER, A., LEE, J. and MICHAELS, S., 1993. Three-Dimensional Printing: The Physics and Implications of Additive Manufacturing. *CIRP Annals - Manufacturing Technology,* **42**(1), pp. 257-260.

29. UTELA, B., STORTI, D., ANDERSON, R. and GANTER, M., 2008. A review of process development steps for new material systems in three dimensional printing (3DP). *Journal of Manufacturing Processes,* **10**(2), pp. 96-104.

30. YEONG, W., CHUA, C., LEONG, K. and CHANDRASEKARAN, M., 2004. Rapid prototyping in tissue engineering: challenges and potential. *Trends in biotechnology,* **22**(12), pp. 643-652.

31. SUN, K., WEI, T., AHN, B.Y., SEO, J.Y., DILLON, S.J. and LEWIS, J.A., 2013. 3D Printing of Interdigitated Li-Ion Microbattery Architectures. *Advanced Materials,* **25**(33), pp. 4539-4543.

32. MACDONALD, E., SALAS, R., ESPALIN, D., PEREZ, M., AGUILERA, E., MUSE, D. and WICKER, R., 2014. 3d printing for the rapid prototyping of structural electronics.

33. ZHANG, R., XU, Y., HARRISON, D., FYSON, J., QIU, F. and SOUTHEE, D., 2015. Flexible strip supercapacitors for future energy storage. *International Journal of Automation and Computing,* **12**(1), pp. 43-49.

34. ZHANG, R., XU, Y., HARRISON, D., FYSON, J., SOUTHEE, D. and TANWILAISIRI, A., 2014. Fabrication and characterisation of energy storage fibres, *Automation and Computing (ICAC), 2014 20th International Conference on* 2014, IEEE, pp. 228-230.

35. LEWANDOWSKI, A., OLEJNICZAK, A., GALINSKI, M. and STEPNIAK, I., 2010. Performance of carbon–carbon supercapacitors based on organic, aqueous and ionic liquid electrolytes. *Journal of Power Sources,* **195**(17), pp. 5814-5819.

36. JOST, K., STENGER, D., PEREZ, C.R., MCDONOUGH, J.K., LIAN, K., GOGOTSI, Y. and DION, G., 2013. Knitted and screen printed carbon-fiber supercapacitors for applications in wearable electronics. *Energy & Environmental Science*, **6**(9), pp. 2698-2705.

37. CONÉDÉRA, V., MESNILGRENTE, F., BRUNET, M. and FABRE, N., 2009. Fabrication of activated carbon electrodes by inkjet deposition, *Quantum, Nano and Micro Technologies, 2009. ICQNM'09. Third International Conference on* 2009, IEEE, pp. 157-161.

38. ERVIN, M.H., LE, L.T. and LEE, W.Y., 2011. Inkjet-Printed Flexible Graphene Based Supercapacitors. *Chemical Engineering*, **89**, pp. 1342-1356.

39. FRACKOWIAK, E. and BEGUIN, F., 2001. Carbon materials for the electrochemical storage of energy in capacitors. *Carbon*, **39**(6), pp. 937-950.

40. PANDOLFO, A. and HOLLENKAMP, A., 2006. Carbon properties and their role in supercapacitors. *Journal of Power Sources*, **157**(1), pp. 11-27.

41. QU, D. and SHI, H., 1998. Studies of activated carbons used in double-layer capacitors. *Journal of Power Sources*, **74**(1), pp. 99-107.

42. WANG, G., ZHANG, L. and ZHANG, J., 2012. A review of electrode materials for electrochemical supercapacitors. *Chemical Society Reviews*, **41**(2), pp. 797-828.

43. HARTMAN, A., O'HARA, L., TONKIN, C., DARBY, D., GUSTAFSON, J., RAY, W. and LOCKETT, V., Printing carbon nanotube based supercapacitors.

44. KOSSYREV, P., 2012. *Carbon black supercapacitors employing thin electrodes.*

45. ZHANG, L.L. and ZHAO, X., 2009. Carbon-based materials as supercapacitor electrodes. *Chemical Society Reviews*, **38**(9), pp. 2520-2531.

46. MOORE, J.J.E., 2011. Fabrication of single-walled carbon nanotube electrodes for ultracapacitors.

47. STOLLER, M.D. and RUOFF, R.S., 2010. Best practice methods for determining an electrode material's performance for ultracapacitors. *Energy & Environmental Science*, **3**(9), pp. 1294-1301.

48. BLOMQUIST, N., WELLS, T., ANDRES, B., BACKSTROM, J., FORSBERG, S. and OLIN, H., 2017. Metal-free supercapacitor with aqueous electrolyte and low-cost carbon materials. *Scientific reports*, **7**, pp. 39836.

49. BO, Z., ZHU, W., MA, W., WEN, Z., SHUAI, X., CHEN, J., YAN, J., WANG, Z., CEN, K. and FENG, X., 2013. Vertically Oriented Graphene Bridging Active-Layer/Current-Collector Interface for Ultrahigh Rate Supercapacitors. *Advanced Materials*, **25**(40), pp. 5799-5806.

50. DYATKIN, B., PRESSER, V., HEON, M., LUKATSKAYA, M.R., BEIDAGHI, M. and GOGOTSI, Y., 2013. Development of a green supercapacitor composed entirely of environmentally friendly materials. *ChemSusChem*, **6**(12), pp. 2269-2280.

51. LIU, J., MIRRI, F., NOTARIANNI, M., PASQUALI, M. and MOTTA, N., 2015. High performance all-carbon thin film supercapacitors. *Journal of Power Sources*, **274**, pp. 823-830.

52. XU, B., WU, F., CHEN, R., CAO, G., CHEN, S., ZHOU, Z. and YANG, Y., 2008. Highly mesoporous and high surface area carbon: a high capacitance electrode material for EDLCs with various electrolytes. *Electrochemistry Communications*, **10**(5), pp. 795-797.

53. ZHONG, C., DENG, Y., HU, W., QIAO, J., ZHANG, L. and ZHANG, J., 2015. A review of electrolyte materials and compositions for electrochemical supercapacitors. *Chemical Society Reviews*, **44**(21), pp. 7484-7539.

54. YEO, J., KIM, G., HONG, S., KIM, M.S., KIM, D., LEE, J., LEE, H.B., KWON, J., SUH, Y.D. and KANG, H.W., 2014. Flexible supercapacitor fabrication by room temperature rapid laser processing of roll-to-roll printed metal nanoparticle ink for wearable electronics application. *Journal of Power Sources*, **246**, pp. 562-568.

55. AGUILERA, E., RAMOS, J., ESPALIN, D., CEDILLOS, F., MUSE, D., WICKER, R. and MACDONALD, E., 3D Printing of Electro Mechanical Systems.

56. ESPALIN, D., MUSE, D.W., MACDONALD, E. and WICKER, R.B., 2014. 3D Printing multifunctionality: structures with electronics. *The International Journal of Advanced Manufacturing Technology*, **72**(5-8), pp. 963-978.

57. LEIGH, S.J., BRADLEY, R.J., PURSSELL, C.P., BILLSON, D.R. and HUTCHINS, D.A., 2012. A simple, low-cost conductive composite material for 3D printing of electronic sensors. *PloS one*, **7**(11), pp. e49365.

58. PALMER, J., YANG, P., DAVIS, D., CHAVEZ, B., GALLEGOS, P., WICKER, R. and MEDINA, F., 2004. Rapid prototyping of high density circuitry, *Proc. Rapid Prototyping & Manufacturing 2004 Conference Proceedings* 2004, pp. 10

59. READY, S., ENDICOTT, F., WHITING, G.L., NG, T.N., CHOW, E.M. and LU, J., 2013. 3D Printed Electronics, *NIP & Digital Fabrication Conference* 2013, Society for Imaging Science and Technology, pp. 9-12.

60. SAENGCHAIRAT, N., TRAN, T. and CHUA, C., 2017. A review: Additive manufacturing for active electronic components. *Virtual and Physical Prototyping*, **12**(1), pp. 31-46.

61. SARIK, J., BUTLER, A., SCOTT, J., HODGES, S. and VILLAR, N., Combining 3D printing and printable electronics.

62. GIBSON, I., ROSEN, D. and STUCKER, B., Additive Manufacturing Technologies: 3D printing, Rapid Prototyping and Direct Digital Manufacturing, Springer, New York, 2015

63. AHN, D., KWEON, J., KWON, S., SONG, J. and LEE, S., 2009. Representation of surface roughness in fused deposition modeling. *Journal of Materials Processing Technology*, **209**(15–16), pp. 5593-5600.

64. ANITHA, R., ARUNACHALAM, S. and RADHAKRISHNAN, P., 2001. Critical parameters influencing the quality of prototypes in fused deposition modelling. *Journal of Materials Processing Technology*, **118**(1–3), pp. 385-388.

65. CHAKRABORTY, D., ANEESH REDDY, B. and ROY CHOUDHURY, A., 2008. Extruder path generation for Curved Layer Fused Deposition Modeling. *Computer-Aided Design*, **40**(2), pp. 235-243.

66. CHOI, J., MEDINA, F., KIM, C., ESPALIN, D., RODRIGUEZ, D., STUCKER, B. and WICKER, R., 2011. Development of a mobile fused deposition modeling system with enhanced manufacturing flexibility. *Journal of Materials Processing Technology*, **211**(3), pp. 424-432.

67. PANDEY, P.M., REDDY, N.V. and DHANDE, S.G., 2003. Real time adaptive slicing for fused deposition modelling. *International Journal of Machine Tools and Manufacture*, **43**(1), pp. 61-71.

68. PANDEY, P.M., VENKATA REDDY, N. and DHANDE, S.G., 2003. Improvement of surface finish by staircase machining in fused deposition modeling. *Journal of Materials Processing Technology*, **132**(1–3), pp. 323-331.

69. LANZOTTI, A., GRASSO, M., STAIANO, G. and MARTORELLI, M., 2015. The impact of process parameters on mechanical properties of parts fabricated in PLA with an open-source 3-D printer. *Rapid Prototyping Journal*, **21**(5), pp. 604-617.

70. LEE, B.H., ABDULLAH, J. and KHAN, Z.A., 2005. Optimization of rapid prototyping parameters for production of flexible ABS object. *Journal of Materials Processing Technology*, **169**(1), pp. 54-61.

71. MASOOD, S.H. and SONG, W.Q., 2004. Development of new metal/polymer materials for rapid tooling using Fused deposition modelling. *Materials & Design,* **25**(7), pp. 587-594.

72. NIKZAD, M., MASOOD, S.H. and SBARSKI, I., 2011. Thermo-mechanical properties of a highly filled polymeric composites for Fused Deposition Modeling. *Materials & Design,* **32**(6), pp. 3448-3456.

73. TORRES, J., COTELO, J., KARL, J. and GORDON, A.P., 2015. Mechanical property optimization of FDM PLA in shear with multiple objectives. *JOM,* **67**(5), pp. 1183-1193.

74. WITTBRODT, B. and PEARCE, J.M., 2015. The effects of PLA color on material properties of 3-D printed components. *Additive Manufacturing,* **8**, pp. 110-116.

75. XINHUA, L., SHENGPENG, L., ZHOU, L., XIANHUA, Z., XIAOHU, C. and ZHONGBIN, W., 2015. An investigation on distortion of PLA thin-plate part in the FDM process. *International Journal of Advanced Manufacturing Technology,* **79**.

76. AZHARI, A., MARZBANRAD, E., YILMAN, D., TOYSERKANI, E. and POPE, M.A., 2017. Binder-jet powder-bed additive manufacturing (3D printing) of thick graphene-based electrodes. *Carbon,* **119**, pp. 257-266.

77. CZYŻEWSKI, J., BURZYŃSKI, P., GAWEŁ, K. and MEISNER, J., 2009. Rapid prototyping of electrically conductive components using 3D printing technology. *Journal of Materials Processing Technology,* **209**(12–13), pp. 5281-5285.

78. DEINER, L.J. and REITZ, T.L., 2017. Inkjet and Aerosol Jet Printing of Electrochemical Devices for Energy Conversion and Storage. *Advanced Engineering Materials,* .

79. FU, K., YAO, Y., DAI, J. and HU, L., 2017. Progress in 3D Printing of Carbon Materials for Energy-Related Applications. *Advanced Materials,* **29**(9),.

80. GOTH, C., PUTZO, S. and FRANKE, J., 2011. Aerosol Jet printing on rapid prototyping materials for fine pitch electronic applications, *Electronic Components and Technology Conference (ECTC), 2011 IEEE 61st* 2011, IEEE, pp. 1211-1216.

81. NAVARRETE, M., LOPES, A., ACUNA, J., ESTRADA, R., MACDONALD, E., PALMER, J. and WICKER, R., 2007. *Integrated layered manufacturing of a novel wireless motion sensor system with GPS,* .

82. PAULSEN, J.A., RENN, M., CHRISTENSON, K. and PLOURDE, R., 2012. Printing conformal electronics on 3D structures with Aerosol Jet technology, *Future of Instrumentation International Workshop (FIIW), 2012* 2012, IEEE, pp. 1-4.

83. SUBRAMANIAN, V., CHANG, J.B., DE LA FUENTE VORNBROCK, ALEJANDRO, HUANG, D.C., JAGANNATHAN, L., LIAO, F., MATTIS, B., MOLESA, S., REDINGER, D.R. and SOLTMAN, D., 2008. Printed electronics for low-cost electronic systems: Technology status and application development, *Solid-State Circuits Conference, 2008. ESSCIRC 2008. 34th European* 2008, IEEE, pp. 17-24.

84. WILLIS, K., BROCKMEYER, E., HUDSON, S. and POUPYREV, I., 2012. Printed optics: 3d printing of embedded optical elements for interactive devices, *Proceedings of the 25th annual ACM symposium on User interface software and technology* 2012, ACM, pp. 589-598.

85. YANG, B. and LEU, M.C., 1999. Integration of Rapid Prototyping and Electroforming for Tooling Application. *CIRP Annals - Manufacturing Technology,* **48**(1), pp. 119-122.

86. ZHANG, Q., ZHANG, F., MEDARAMETLA, S.P., LI, H., ZHOU, C. and LIN, D., 2016. 3D printing of graphene aerogels. *Small,* **12**(13), pp. 1702-1708.

87. MEDINA, F., LOPES, A., INAMDAR, A., HENNESSEY, R., PALMER, J., CHAVEZ, B., DAVIS, D., GALLEGOS, P. and WICKER, R., 2005. Hybrid manufacturing: integrating direct-write and stereolithography. *Proceedings of the 2005 Solid Freeform Fabrication.Journal of Manufacturing Science and Engineering,* .

88. LOPES, A.J., MACDONALD, E. and WICKER, R.B., 2012. Integrating stereolithography and direct print technologies for 3D structural electronics fabrication. *Rapid Prototyping Journal,* **18**(2), pp. 129-143.

89. HO, C.C., EVANS, J.W. and WRIGHT, P.K., 2010. Direct write dispenser printing of a zinc microbattery with an ionic liquid gel electrolyte. *Journal of Micromechanics and Microengineering,* **20**(10), pp. 104009.

90. WANG, Z., CHEN, A., WINSLOW, R., MADAN, D., JUANG, R., NILL, M., EVANS, J. and WRIGHT, P., 2012. Integration of dispenser-printed ultra-low-voltage thermoelectric and energy storage devices. *Journal of Micromechanics and Microengineering,* **22**(9), pp. 094001.

91. ZHAO, C., WANG, C., GORKIN III, R., BEIRNE, S., SHU, K. and WALLACE, G.G., 2014. Three dimensional (3D) printed electrodes for interdigitated supercapacitors. *Electrochemistry Communications,* **41**, pp. 20-23.

92. AMBROSI, A., MOO, J.G.S. and PUMERA, M., 2016. Helical 3D-Printed Metal Electrodes as Custom-Shaped 3D Platform for Electrochemical Devices. *Advanced Functional Materials,* **26**(5), pp. 698-703.

93. LIU, X., JERVIS, R., MAHER, R.C., VILLAR-GARCIA, I.J., NAYLOR-MARLOW, M., SHEARING, P.R., OUYANG, M., COHEN, L., BRANDON, N.P. and WU, B., 2016. 3D-Printed Structural Pseudocapacitors. *Advanced Materials Technologies,* **1**(9),.

94. V. KHOMENKO, E. FRACKOWIAK, F. BÉGUIN, Determination of the specific capacitance of conducting polymer/nanotubes composite electrodes using different cell configurations, Electrochim. Acta. 50 (2005) 2499–2506.

95. CALVERT, P., 2001. Inkjet printing for materials and devices. *Chemistry of Materials,* **13**(10), pp. 3299-3305.

96. CUMMINS, G. and DESMULLIEZ, M.P., 2012. Inkjet printing of conductive materials: a review. *Circuit World,* **38**(4), pp. 193-213.

97. DERBY, B., 2010. Inkjet printing of functional and structural materials: fluid property requirements, feature stability, and resolution. *Annual Review of Materials Research,* **40**, pp. 395-414.

98. JUNG, H.C., CHO, S., JOUNG, J.W. and OH, Y., 2007. Studies on inkjet-printed conducting lines for electronic devices. *Journal of Electronic Materials,* **36**(9), pp. 1211-1218.

99. KAMYSHNY, A., BEN-MOSHE, M., AVIEZER, S. and MAGDASSI, S., 2005. Ink-Jet Printing of Metallic Nanoparticles and Microemulsions. *Macromolecular Rapid Communications,* **26**(4), pp. 281-288.

100. KAMYSHNY, A., STEINKE, J. and MAGDASSI, S., 2011. Metal-based inkjet inks for printed electronics. *Open Applied Physics Journal,* **4**, pp. 19-36.

101. KANG, J.S., KIM, H.S., RYU, J., HAHN, H.T., JANG, S. and JOUNG, J.W., 2010. Inkjet printed electronics using copper nanoparticle ink. *Journal of Materials Science: Materials in Electronics,* **21**(11), pp. 1213-1220.

102. MORRIN, A., 2012. Inkjet Printed Electrochemical Sensors. *Inkjet-Based Micromanufacturing, ,* pp. 295-311.

103. NIE, X., WANG, H. and ZOU, J., 2012. Inkjet printing of silver citrate conductive ink on PET substrate. *Applied Surface Science,* **261**(0), pp. 554-560.

104. SINGH, M., HAVERINEN, H.M., DHAGAT, P. and JABBOUR, G.E., 2010. Inkjet printing—process and its applications. *Advanced Materials,* **22**(6), pp. 673-685.

105. SIRRINGHAUS, H. and SHIMODA, T., 2003. Inkjet printing of functional materials. *MRS Bulletin,* **28**(11), pp. 802-806.

106. YIN, Z., HUANG, Y., BU, N., WANG, X. and XIONG, Y., 2010. Inkjet printing for flexible electronics: Materials, processes and equipments. *Chinese Science Bulletin,* **55**(30), pp. 3383-3407.

107. VARELA, F., ARMENDÁRIZ, E. and WOLLUSCHEK, C., 2011. Inkjet printed electronics: The wet on wet approach. *Chemical Engineering and Processing: Process Intensification,* **50**(5), pp. 589-591.

108. LOTA, G., CENTENO, T.A., FRACKOWIAK, E. and STOECKLI, F., 2008. Improvement of the structural and chemical properties of a commercial activated carbon for its application in electrochemical capacitors. *Electrochimica Acta,* **53**(5), pp. 2210-2216.

109. GRYGLEWICZ, G., MACHNIKOWSKI, J., LORENC-GRABOWSKA, E., LOTA, G. and FRACKOWIAK, E., 2005. Effect of pore size distribution of coal-based activated carbons on double layer capacitance. *Electrochimica Acta,* **50**(5), pp. 1197-1206.

110. SONG, H., JUNG, Y., LEE, K. and DAO, L.H., 1999. Electrochemical impedance spectroscopy of porous electrodes: the effect of pore size distribution. *Electrochimica Acta,* **44**(20), pp. 3513-3519.

111. DEINER, L.J. and REITZ, T.L., 2017. Inkjet and Aerosol Jet Printing of Electrochemical Devices for Energy Conversion and Storage. *Advanced Engineering Materials,* .

112. KIPPHAN, H. Handbook of Print Media: Technologies and Production Methods, Springer, Heidelberg, 2001

113. CHEN, C., 2011. Inkjet printing of microcomponents: theory, design, characteristics and applications. *Features of Liquid Crystal Display Materials and Processes.* InTech, .

114. ZHU, C., LIU, T., QIAN, F., HAN, T.Y., DUOSS, E.B., KUNTZ, J.D., SPADACCINI, C.M., WORSLEY, M.A. and LI, Y., 2016. Supercapacitors based on three-dimensional hierarchical graphene aerogels with periodic macropores. *Nano letters,* **16**(6), pp. 3448-3456.

115. H.S. Technologies, M. Heights, Dip coating, Met. Finish. 108 (2010) 130-132.

116. HARRISON, D., QIU, F., FYSON, J., XU, Y., EVANS, P., & SOUTHEE, D. (2013). A coaxial single fibre supercapacitor for energy storage. *Physical Chemistry Chemical Physics*, 15 12215-12219.

117. YANG, Z., DENG, J., CHEN, X., REN, J. and PENG, H., 2013. A Highly Stretchable, Fiber-Shaped Supercapacitor. *Angewandte Chemie International Edition*, **52**(50), pp. 13453-13457.

118. XU, Y., SCHWAB, M.G., STRUDWICK, A.J., HENNIG, I., FENG, X., WU, Z. and MÜLLEN, K., 2013. Screen-Printable Thin Film Supercapacitor Device Utilizing Graphene/Polyaniline Inks. *Advanced Energy Materials*, **3**(8), pp. 1035-1040.

119. TEHRANI, Z., THOMAS, D., KOROCHKINA, T., PHILLIPS, C., LUPO, D., LEHTIMÄKI, S., O'MAHONY, J. and GETHIN, D., 2017. Large-area printed supercapacitor technology for low-cost domestic green energy storage. *Energy*, **118**, pp. 1313-1321.

120. CUI, Z., Printed electronics, material, technologies and applications, Wiley, Singapore, 2016

121. TIRUYE, G.A., MUÑOZ-TORRERO, D., PALMA, J., ANDERSON, M. and MARCILLA, R., 2016. Performance of solid state supercapacitors based on polymer electrolytes containing different ionic liquids. *Journal of Power Sources*, **326**, pp. 560-568.

122. INAGAKI, M., KONNO, H. and TANAIKE, O., 2010. Carbon materials for electrochemical capacitors. *Journal of Power Sources*, **195**(24), pp. 7880-7903.

123. CHEN, J., LI, W., WANG, D., YANG, S., WEN, J. and REN, Z., 2002. Electrochemical characterization of carbon nanotubes as electrode in electrochemical double-layer capacitors. *Carbon*, **40**(8), pp. 1193-1197.

124. WONG, H.P. and AKINWANDE, D., 2011. *Carbon nanotube and graphene device physics.* Cambridge ; New York: Cambridge University Press.

125. SLOMA, M., JANCZAK, D., WROBLEWSKI, G., MLOZNIAK, A. and JAKUBOWSKA, M., 2013. Graphene applications with printed electronics technology, *Microelectronics Packaging Conference (EMPC), 2013 European* 2013, IEEE, pp. 1-3.

126. SOLDANO, C., MAHMOOD, A. and DUJARDIN, E., 2010. Production, properties and potential of graphene. *Carbon,* **48**(8), pp. 2127-2150.

127. TAN, Y.B. and LEE, J., 2013. Graphene for supercapacitor applications. *Journal of Materials Chemistry A,* **1**(47), pp. 14814-14843.

128. TUNG, V.C., ALLEN, M.J., YANG, Y. and KANER, R.B., 2008. High-throughput solution processing of large-scale graphene. *Nature nanotechnology,* **4**(1), pp. nnano. 2008.329.

129. EMTSEV, K.V., BOSTWICK, A., HORN, K., JOBST, J., KELLOGG, G.L., LEY, L., MCCHESNEY, J.L., OHTA, T., RESHANOV, S.A. and RÖHRL, J., 2009. Towards wafer-size graphene layers by atmospheric pressure graphitization of silicon carbide. *Nature materials,* **8**(3), pp. 203-207.

130. NOVOSELOV, K.S., GEIM, A.K., MOROZOV, S.V., JIANG, D., ZHANG, Y., DUBONOS, S.V., GRIGORIEVA, I.V. and FIRSOV, A.A., 2004. Electric field effect in atomically thin carbon films. *Science (New York, N.Y.),* **306**(5696), pp. 666-669.

131. KOSYNKIN, D.V., HIGGINBOTHAM, A.L., SINITSKII, A., LOMEDA, J.R., DIMIEV, A., PRICE, B.K. and TOUR, J.M., 2009. Longitudinal unzipping of carbon nanotubes to form graphene nanoribbons. *Nature,* **458**(7240), pp. 872-876.

132. KIM, M., CHU, W., KIM, Y., AVILA, A.P.G. and AHN, S., 2009. Direct metal printing of 3D electrical circuit using rapid prototyping. *International Journal of Precision Engineering and Manufacturing,* **10**(5), pp. 147-150.

133. WANG, Y., WU, Y., HUANG, Y., ZHANG, F., YANG, X., MA, Y. and CHEN, Y., 2011. Preventing graphene sheets from restacking for high-capacitance performance. *The Journal of Physical Chemistry C,* **115**(46), pp. 23192-23197.

134. ZHU, Y., MURALI, S., STOLLER, M.D., GANESH, K.J., CAI, W., FERREIRA, P.J., PIRKLE, A., WALLACE, R.M., CYCHOSZ, K.A., THOMMES, M., SU, D., STACH, E.A. and RUOFF, R.S., 2011. Carbon-based supercapacitors produced by activation of graphene. *Science (New York, N.Y.),* **332**(6037), pp. 1537-1541.

135. HASSAN, F.M., CHABOT, V., LI, J., KIM, B.K., RICARDEZ-SANDOVAL, L. and YU, A., 2013. Pyrrolic-structure enriched nitrogen doped graphene for highly

efficient next generation supercapacitors. *Journal of Materials Chemistry A*, **1**(8), pp. 2904-2912.

136. ZHANG, L.L., ZHOU, R. and ZHAO, X., 2010. Graphene-based materials as supercapacitor electrodes. *Journal of Materials Chemistry*, **20**(29), pp. 5983-5992.

137. LOTA, G., CENTENO, T.A., FRACKOWIAK, E. and STOECKLI, F., 2008. Improvement of the structural and chemical properties of a commercial activated carbon for its application in electrochemical capacitors. *Electrochimica Acta*, *53*(5), pp.2210-2216.

138. YANG, C., JANG, Y.S. and JEONG, H.K., 2014. Bamboo-based activated carbon for supercapacitor applications. *Current Applied Physics*, **14**(12), pp. 1616-1620.

139. OBEIDAT, A.M., GHARAIBEH, M.A. and OBAIDAT, M., 2017. Solid-state supercapacitors with ionic liquid gel polymer electrolyte and polypyrrole electrodes for electrical energy storage. *Journal of Energy Storage*, **13**, pp. 123-128.

140. WANG, G., ZHANG, Y., ZHOU, F., SUN, Z., HUANG, F., YU, Y., CHEN, L. and PAN, M., 2016. Simple and fast synthesis of polyaniline nanofibers/carbon paper composites as supercapacitor electrodes. *Journal of Energy Storage*, **7**, pp. 99-103.

141. LI, M., ZHOU, M., WEN, Z.Q. and ZHANG, Y.X., 2017. *Flower-like NiFe layered double hydroxides coated MnO2 for high-performance flexible supercapacitors.*

142. YU, J., WU, J., WANG, H., ZHOU, A., HUANG, C., BAI, H. and LI, L., 2016. Metallic fabrics as the current collector for high-performance graphene-based flexible solid-State supercapacitor. *ACS applied materials & interfaces*, **8**(7), pp. 4724-4729.

143. MEHRABI-MATIN, B., SHAHROKHIAN, S. and IRAJI-ZAD, A., 2017. Silver Fiber Fabric as the Current Collector for Preparation of Graphene-Based Supercapacitors. *Electrochimica Acta*, **227**, pp. 246-254.

144. PORTET, C., TABERNA, P., SIMON, P. and LABERTY-ROBERT, C., 2004. Modification of Al current collector surface by sol–gel deposit for carbon–carbon supercapacitor applications. *Electrochimica Acta*, **49**(6), pp. 905-912.

145. BO, Z., ZHU, W., MA, W., WEN, Z., SHUAI, X., CHEN, J., YAN, J., WANG, Z., CEN, K. and FENG, X., 2013. Vertically Oriented Graphene Bridging Active-

Layer/Current-Collector Interface for Ultrahigh Rate Supercapacitors. *Advanced Materials,* **25**(40), pp. 5799-5806.

146. ZHOU, R., MENG, C., ZHU, F., LI, Q., LIU, C., FAN, S. and JIANG, K., 2010. High-performance supercapacitors using a nanoporous current collector made from super-aligned carbon nanotubes. *Nanotechnology,* **21**(34), pp. 345701.

147. DYATKIN, B., PRESSER, V., HEON, M., LUKATSKAYA, M.R., BEIDAGHI, M. and GOGOTSI, Y., 2013. Development of a green supercapacitor composed entirely of environmentally friendly materials. *ChemSusChem,* **6**(12), pp. 2269-2280.

148. XU, Y., TAO, Y., ZHENG, X., MA, H., LUO, J., KANG, F. and YANG, Q., 2015. A Metal-Free Supercapacitor Electrode Material with a Record High Volumetric Capacitance over 800 F cm− 3. *Advanced Materials,* **27**(48), pp. 8082-8087

149. Bare conductive paint, Electric paint®, Technical data sheet, [online] Available at https://www.bareconductive.com/wp-content/uploads/2016/05/ElectricPaint_ApplicationNotes.pdf

150. RS Pro Bottle of Silver Conductive Adhesive Paint - Electrocomponents, Data sheet, [online] Available at http://docs-europe.electrocomponents.com/webdocs/1513/0900766b815139bd.pdf

151. SHORNIKOVA, O., KOGAN, E., SOROKINA, N. and AVDEEV, V., 2009. The specific surface area and porous structure of graphite materials. *Russian Journal of Physical Chemistry A,* **83**(6), pp. 1022-1025.

152. CHMIOLA, J., YUSHIN, G., DASH, R. and GOGOTSI, Y., 2006. Effect of pore size and surface area of carbide derived carbons on specific capacitance. *Journal of Power Sources,* **158**(1), pp. 765-772.

153. LI, H., WANG, Y., WANG, C. and XIA, Y., 2008. A competitive candidate material for aqueous supercapacitors: High surface-area graphite. *Journal of Power Sources,* **185**(2), pp. 1557-1562.

154. FU, K., WANG, Y., YAN, C., YAO, Y., CHEN, Y., DAI, J., LACEY, S., WANG, Y., WAN, J. and LI, T., 2016. Graphene Oxide-Based Electrode Inks for 3D-Printed Lithium-Ion Batteries. *Advanced Materials,* **28**(13), pp. 2587-2594.

155. HILLER, J. and LIPSON, H., 2009. Design and analysis of digital materials for physical 3D voxel printing. *Rapid Prototyping Journal*, **15**(2), pp. 137-149.

156. SAENGCHAIRAT, N., CHUA, C.K. and TRAN, T., 2016. Additive Manufacturing for Active Electronic Components: A Review.

157. ROMÁN-MANSO, B., FIGUEIREDO, F.M., ACHIAGA, B., BAREA, R., PÉREZ-COLL, D., MORELOS-GÓMEZ, A., TERRONES, M., OSENDI, M.I., BELMONTE, M. and MIRANZO, P., 2016. Electrically functional 3D-architectured graphene/SiC composites. *Carbon*, **100**, pp. 318-328.

158. CHIU, W. and YU, K., 2008. Direct digital manufacturing of three-dimensional functionally graded material objects. *Computer-Aided Design*, **40**(12), pp. 1080-1093.

159. CHOI, J., KIM, H. and WICKER, R., 2011. Multi-material stereolithography. *Journal of Materials Processing Technology*, **211**(3), pp. 318-328.

160. CHOI, S.H. and SAMAVEDAM, S., 2002. Modelling and optimisation of Rapid Prototyping. *Computers in Industry*, **47**(1), pp. 39-53.

161. DING, Y., LAN, H., HONG, J. and WU, D., 2004. An integrated manufacturing system for rapid tooling based on rapid prototyping. *Robotics and Computer-Integrated Manufacturing*, **20**(4), pp. 281-288.

162. HU, D. and KOVACEVIC, R., 2003. Sensing, modeling and control for laser-based additive manufacturing. *International Journal of Machine Tools and Manufacture*, **43**(1), pp. 51-60.

163. HUANG, S.H., LIU, P., MOKASDAR, A. and HOU, L., 2013. Additive manufacturing and its societal impact: a literature review. *The International Journal of Advanced Manufacturing Technology*, **67**(5-8), pp. 1191-1203.

164. JOSHI, P.C., DEHOFF, R.R., DUTY, C.E., PETER, W.H., OTT, R.D., LOVE, L.J. and BLUE, C.A., 2012. Direct digital additive manufacturing technologies: Path towards hybrid integration, *Future of Instrumentation International Workshop (FIIW), 2012* 2012, IEEE, pp. 1-4.

165. KUMAR, S. and KRUTH, J.-., 2010. Composites by rapid prototyping technology. *Materials & Design*, **31**(2), pp. 850-856.

166. LAM, C.X.F., MO, X.M., TEOH, S.H. and HUTMACHER, D.W., 2002. Scaffold development using 3D printing with a starch-based polymer. *Materials Science and Engineering: C,* **20**(1–2), pp. 49-56.

167. LANZETTA, M. and SACHS, E., 2003. Improved surface finish in 3D printing using bimodal powder distribution. *Rapid Prototyping Journal,* **9**(3), pp. 157-166.

168. LU, K., HISER, M. and WU, W., 2009. Effect of particle size on three dimensional printed mesh structures. *Powder Technology,* **192**(2), pp. 178-183.

169. MEI, J., LOVELL, M.R. and MICKLE, M.H., 2005. Formulation and processing of novel conductive solution inks in continuous inkjet printing of 3-D electric circuits. *Electronics Packaging Manufacturing, IEEE Transactions on,* **28**(3), pp. 265-273.

170. MELCHELS, F.P.W., FEIJEN, J. and GRIJPMA, D.W., 2010. A review on stereolithography and its applications in biomedical engineering. *Biomaterials,* **31**(24), pp. 6121-6130.

171. SANTOS, E.C., SHIOMI, M., OSAKADA, K. and LAOUI, T., 2006. Rapid manufacturing of metal components by laser forming. *International Journal of Machine Tools and Manufacture,* **46**(12–13), pp. 1459-1468.

172. SASS, L. and OXMAN, R., 2006. Materializing design: the implications of rapid prototyping in digital design. *Design Studies,* **27**(3), pp. 325-355.

173. SINGAMNENI, S., ROYCHOUDHURY, A., DIEGEL, O. and HUANG, B., 2012. Modeling and evaluation of curved layer fused deposition. *Journal of Materials Processing Technology,* **212**(1), pp. 27-35.

174. SOOD, A.K., OHDAR, R.K. and MAHAPATRA, S.S., 2010. Parametric appraisal of mechanical property of fused deposition modelling processed parts. *Materials & Design,* **31**(1), pp. 287-295.

175. LEE, M., WEE, B. and HONG, J., 2015. High Performance Flexible Supercapacitor Electrodes Composed of Ultralarge Graphene Sheets and Vanadium Dioxide. *Advanced Energy Materials,* **5**(7), pp. 1401890-n/a.

176. ZHOU, R., MENG, C., ZHU, F., LI, Q., LIU, C., FAN, S. and JIANG, K., 2010. High-performance supercapacitors using a nanoporous current collector made from super-aligned carbon nanotubes. *Nanotechnology,* **21**(34), pp. 345701.

177. PORTET, C., TABERNA, P., SIMON, P. and LABERTY-ROBERT, C., 2004. Modification of Al current collector surface by sol–gel deposit for carbon–carbon supercapacitor applications. *Electrochimica Acta*, **49**(6), pp. 905-912.

178. MEHRABI-MATIN, B., SHAHROKHIAN, S. and IRAJI-ZAD, A., 2017. Silver Fiber Fabric as the Current Collector for Preparation of Graphene-Based Supercapacitors. *Electrochimica Acta*, **227**, pp. 246-254.

179. XU, Y., TAO, Y., ZHENG, X., MA, H., LUO, J., KANG, F. and YANG, Q., 2015. A Metal-Free Supercapacitor Electrode Material with a Record High Volumetric Capacitance over 800 F cm− 3. *Advanced Materials*, **27**(48), pp. 8082-8087.

180. YU, J., WU, J., WANG, H., ZHOU, A., HUANG, C., BAI, H. and LI, L., 2016. Metallic fabrics as the current collector for high-performance graphene-based flexible solid-State supercapacitor. *ACS applied materials & interfaces*, **8**(7), pp. 4724-4729.

181. KUMAGAI, S., MUKAIYACHI, K. and TASHIMA, D., 2015. Rate and cycle performances of supercapacitors with different electrode thickness using non-aqueous electrolyte. *Journal of Energy Storage*, **3**, pp. 10-17.

182. TSAY, K., ZHANG, L. and ZHANG, J., 2012. Effects of electrode layer composition/thickness and electrolyte concentration on both specific capacitance and energy density of supercapacitor. *Electrochimica Acta*, **60**, pp. 428-436.

183. YOON, S., JANG, J.H., BOK, H.K. and OH, S.M., 2005. Complex capacitance analysis on rate capability of electric-double layer capacitor (EDLC) electrodes of different thickness. *Electrochimica Acta*, **50**(11), pp. 2255-2262.

184. ZHAO, S., WU, F., YANG, L., GAO, L. and BURKE, A.F., 2010. A measurement method for determination of dc internal resistance of batteries and supercapacitors. *Electrochemistry Communications*, **12**(2), pp. 242-245.

185. KIM, H.S., KANG, J.S., PARK, J.S., HAHN, H.T., JUNG, H.C. and JOUNG, J.W., 2009. Inkjet printed electronics for multifunctional composite structure. *Composites Science and Technology*, **69**(7–8), pp. 1256-1264.

186. Yuan, Y. and Lee, T.R., 2013. Contact angle and wetting properties. In *Surface science techniques* (pp. 3-34). Springer Berlin Heidelberg.

Appendix A

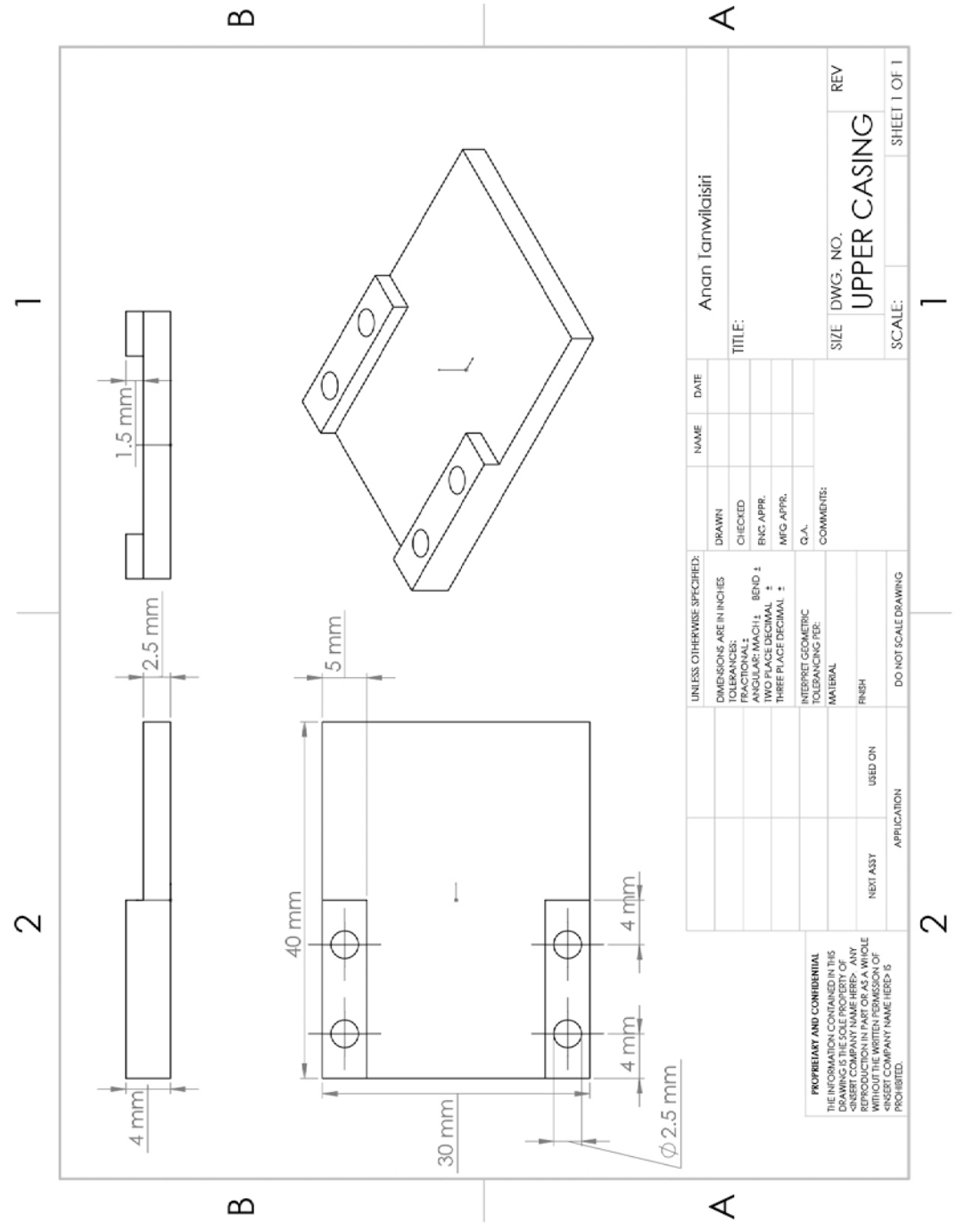

Technical Drawing of the design specification of Pilot sample 1 (upper casing)

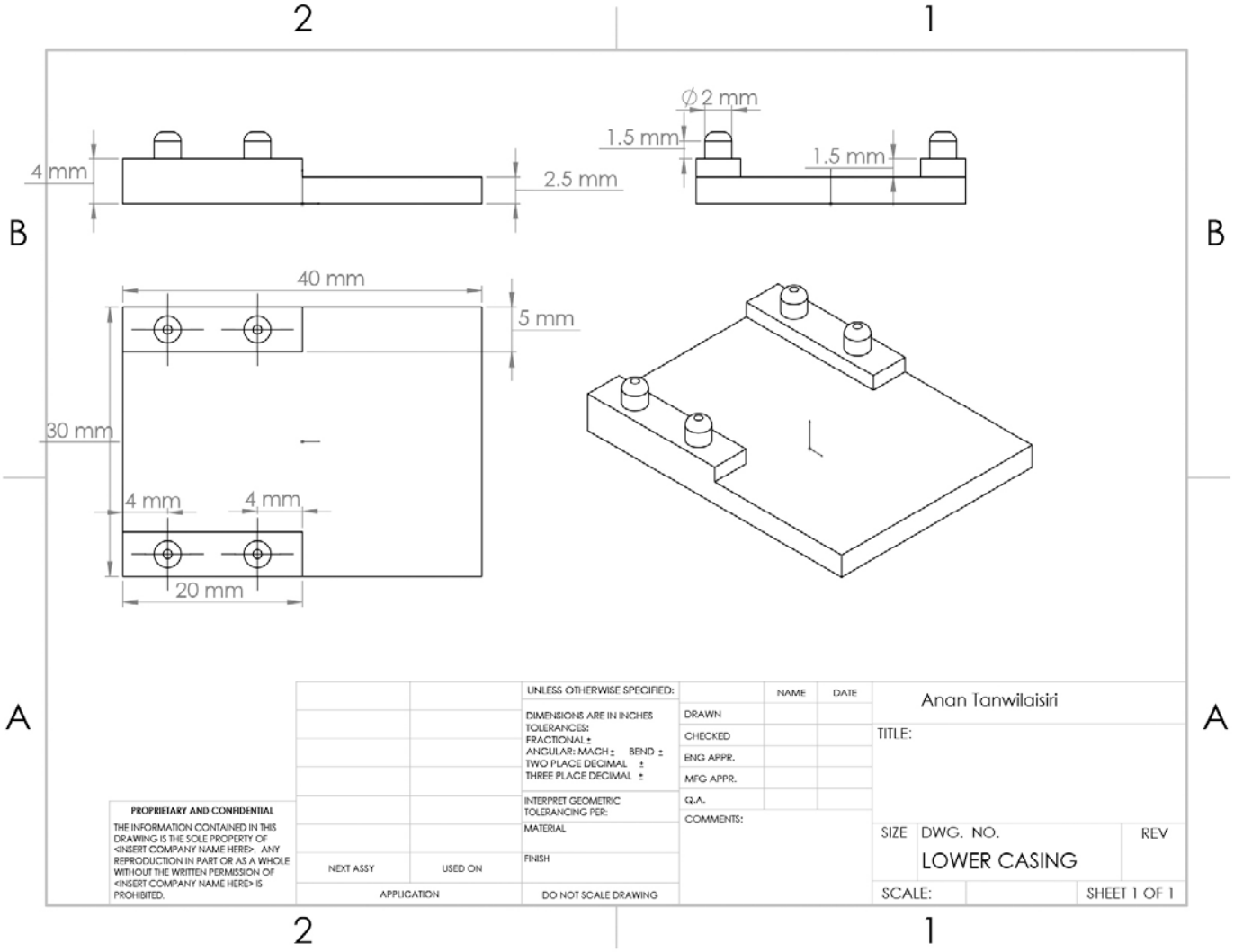

Technical Drawing of the design specification of Pilot sample 1 (lower casing)

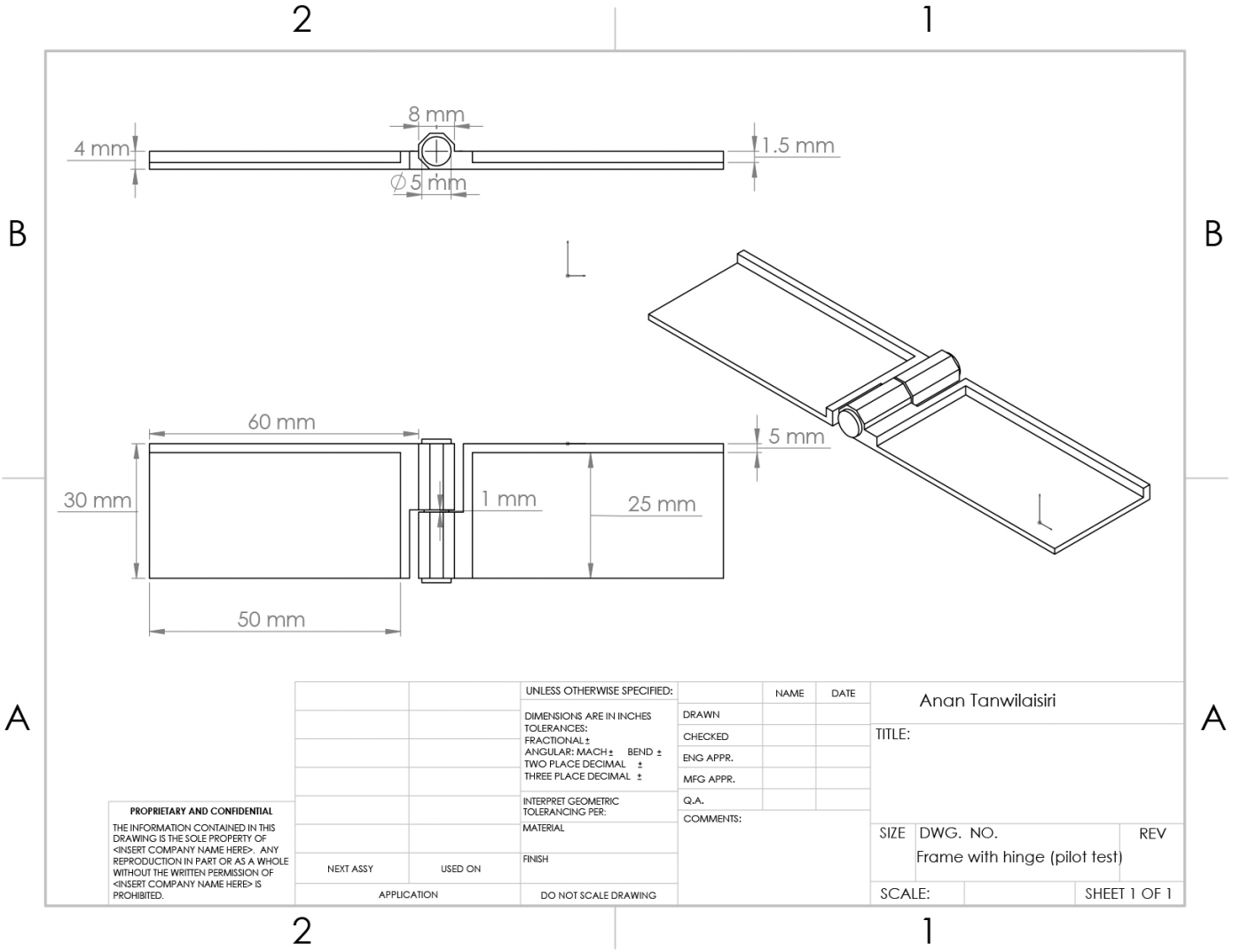

Technical Drawing of the design specification of Pilot sample 2

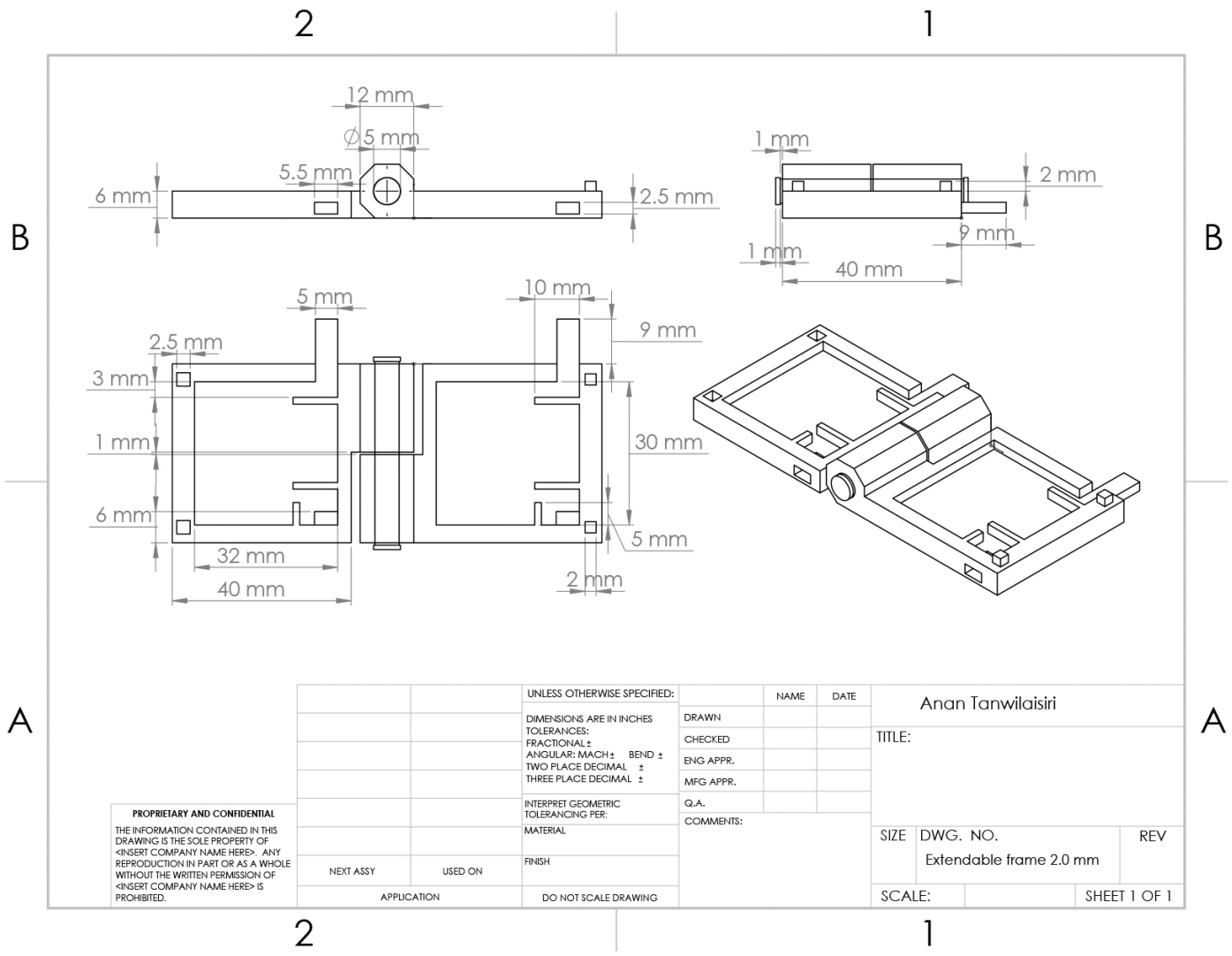

Technical Drawing of the design specification of extendable sample

Appendix B

Bare Conductive®

Electric Paint®

Application Notes

PRODUCT DESCRIPTION

Electric Paint is available in 10ml tubes and 50ml jars. It is a nontoxic, water based, water soluble, electrically conductive paint, intended for applications with circuits using low DC voltages at low currents. **Electric Paint** adheres to a wide variety of substrates and is easily removed with water. It is black in color and can be painted over with any material compatible with a water-based paint. Please see the **Electric Paint** MSDS for precautionary information.

ADVANTAGES / PRODUCT BENEFITS

- Electrically conductive
- Nontoxic
- Water-soluble
- Works with low voltage DC power sources at low currents (see "Power Sources" p.2) Powers small devices
- Can be used as a potentiometer
- Compatible with many standard printing processes

TYPICAL PROPERTIES

Color /	Black
Viscosity /	Highly viscous and shear sensitive (thixotropic)
Density /	1.16 g/ml
Sheet Resistance /	55Ω/sq at 50 micron film thickness or approximately 32Ω/Sq when applied using a brush (see p.3)
Vehicle /	Water-based
Shelf Life /	6 months after opening
Drying Temperature /	**Electric Paint** should be allowed to dry at room temperature for 5 – 15 minutes. Drying time can be reduced by placing **Electric Paint** under a warm lamp or other low intensity heat source.

Bare Conductive Ltd
First Floor, 98 Commercial St
London E1 6LZ
United Kingdom

First Floor, 98 Commercial St
London E1 6LZ, United Kingdom
+44 0 207 650 7977
info@bareconductive.com

APPLICATION TIPS

Electric Paint is a unique material that can be applied in many different ways, from a paintbrush to common printing processes like screen-printing. To achieve consistent electrical performance it is best to apply **Electric Paint** in an even layer. If you're interested in screen printing **Electric Paint**, it is best to use a textile-type screen in order to achieve a generous layer thickness. We tend to use a 43T screen. **Electric Paint** is not inkjet printer compatible. For more application tips visit **www.bareconductive.com/tutorials**

POWER SOURCES

Electric Paint is intended for use with low voltage DC power sources at low currents and has not been tested with sources exceeding 12VDC at 50mA. Higher voltages are not recommended.

SUBSTRATES

Electric Paint is a water-based paint and acts much like other poster paints. **Electric Paint** adheres well to wood, paper products, some plastics, corks, textiles and metal. Hydrophobic materials such as some glass and plastics will exhibit poor adhesion, though this can be improved by roughing the surface with sandpaper or similar.

DRYING TIPS

Electric Paint is fast drying at room temperature. This material dries rather than cures and gives off no fumes during the drying process. Drying time can be moderately reduced by placing the material near a low intensity heat source such as an incandescent lamp. Subjecting **Electric Paint** to a high temperature environment will negatively affect both physical and electrical performance.

FLEXIBILITY

Electric Paint is somewhat flexible, but this flexibility depends on two factors, the layer thickness and choice of substrate. Regardless of substrate, a consistently thin layer of paint creates the most flexible circuitry. Areas of paint with wide variation in thickness tend to produce fracturing. Substrates which are flexible, but not stretchy (such as paper) work better than materials like Lycra which stretch in multiple dimensions.

COLD SOLDERING

Electric Paint works well as a cold solder joint. Whether used to solder a surface mount or through-hole component onto a circuit board, or to adhere a component to a piece of paper, this material is non-permanent and almost infinitely repairable.These unique properties mean that components can be harvested from projects, cleaned and reused.

RESISTANCE SAMPLES

The aim of these application notes is to give you as much information as you need to get your work moving forward. As there are so many ways to apply **Electric Paint**, raw technical data is not always the most useful way to present the product. Presenting sheet resistances at thicknesses not achievable with screen printing are not helpful for someone wanting to experiment in a loose manner, yet still be able to make meaningful calculations.

Page 3 showcases a series of samples which indicate the amount of electrical resistance (measured end to end) that you might expect from a given area of **Electric Paint**. This assumes a reasonably thin layer of material (i.e. carefully painted with a brush or home screen printed). The areas of paint below are shown full size.

See next page for visual.

Bare Conductive Ltd
First Floor, 98 Commercial St
London E1 6LZ
United Kingdom

First Floor, 98 Commercial St
London E1 6LZ, United Kingdom
+44 0 207 650 7977
info@bareconductive.com

RESISTANCE SAMPLES VISUAL

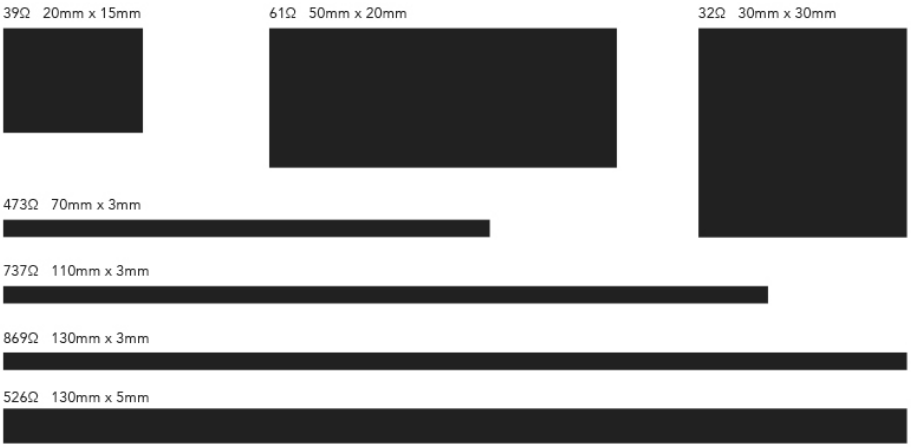

RESISTANCE GRAPH

Electric Paint presents a wholly unique way of exploring electrical resistance. In general, the resistance of a sample of conductive material is defined by the dimensions of the sample being tested, and resistance is inversely proportional to cross sectional area (i.e. given a set length and depth, a wider sample will have less resistance than a thin one). Thus, the resistance can be defined by the ratio of length/width.

The diagram below plots the proportional ratio of a sample of **Electric Paint** against its approximate resistance. This diagram assumes that **Electric Paint** has been applied with a brush. You can calculate an estimated resistance for any proportion over 1, based on the equation: **Resistance=19.77(Ratio)+12**

Example one is illustrated by a blue point on the diagram. This point is associated with a shape with a ratio of 1 (dimensions of 10mm x 10mm i.e. 10 x 10 =1). The resistance associated with this ratio is 32Ω. The nature of the ratio number means that this shape could have the dimensions of 100mm x 100mm and the resistance would still be 32Ω.

Example two shows a shape of ratio 125. In this example the shape has the dimensions of 1250mm x 10mm (1250/10=125). The resistance associated with this shape is 2500Ω.

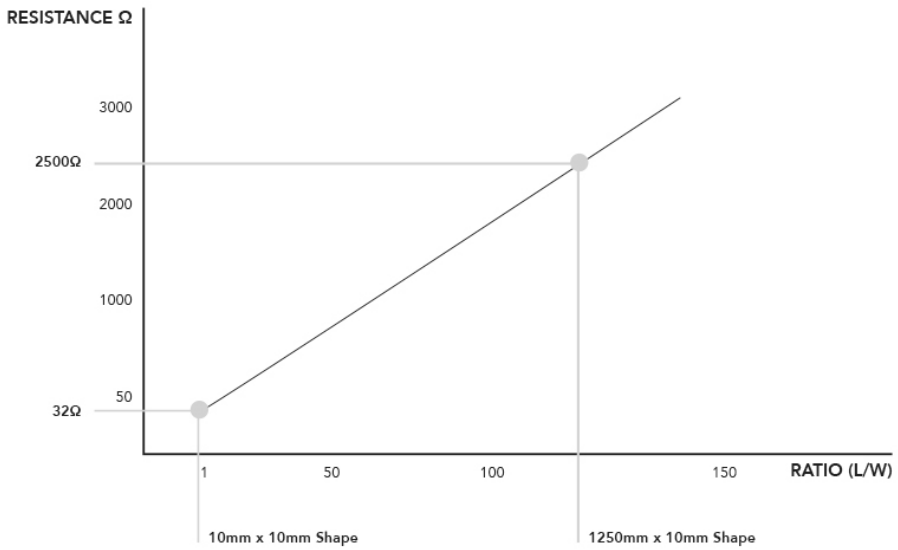

Bare Conductive® Electric Paint®

Safety Data Sheet

ACCORDING TO EC-REGULATIONS
1907/2006 (REACH) & 1272/2008 (CLP)

1. IDENTIFICATION OF THE SUBSTANCE / MIXTURE AND OF THE COMPANY / UNDERTAKING

1.1	**Product identifier**	
	GHS Product Identifier	**Bare Conductive Paint**
	Chemical Name	*Water-based dispersion of carbon pigment in Natural resin*
	Other names	
	CAS No.	Mixture — Not applicable
	EINECS No.	Mixture — Not applicable

1.2	**Relevant identified uses of the substance or mixture and uses advised against**	
	Identified use(s)	Electrically conductive paint
	Uses advised against	None

1.3	**Details of the supplier of the safety data sheet**	
	Company Identification	Bare Conductive Limited First Floor 98 Commercial Street London E1 6LZ
	Telephone	+44 (0)20 3432 5385
	E-Mail (competent person)	**info@bareconductive.com**

1.4	**Emergency telephone number**	
	Emergency Phone No.	**+44 (0)20 3432 5385 / Technical manager**

2. HAZARDS IDENTIFICATION

2.1	**Classification of the substance or mixture**	
2.1.1	**Regulation (EC) No. 1272/2008 (CLP)**	
2.1.2	**Directives 1999/45/EC**	Preparation is not classified as hazardous according to Directives 1999/45/EC.
2.2	**Label elements**	
2.2.1	**Label elements**	According to Regulation (EC) No. 1272/2008 (CLP)
2.2.2	**Label elements**	According to Directive 1999/45/EC
	Hazard Symbol	Not applicable
	Risk Phrases	Not applicable
	Safety Phrases	Not applicable
2.3	**Other hazards**	
2.4	**Additional Information**	

3. COMPOSITION / INFORMATION ON INGREDIENTS

3.1 Substances

EC Classification No. 1272/2008

Ingredients	%W/W	CAS No.	EC No.	Hazard statement(s)
Water		7732-18-5	231-791-2	Not classified.
Natural Resin		Trade secret	Trade secret	Not classified.
Conductive carbon		Trade secret	Trade secret	Not classified.
Humectant		Trade secret	Trade secret	Not classified.
Processing aids and preservatives		Trade secret	Trade secret	Individual levels below 1% do not give rise to classification

EC Classification No. 67/548/EEC

Hazard statement(s)	%W/W	CAS No.	EC No.	Classification and Risk Phrases
None				

3.2 Substances

For full text of R/H/P phrases see section 16.

4. FIRST AID MEASURES

4.1	**Description of first aid measures**	
	Inhalation	Remove patient from exposure. Give oxygen if breathing difficult. Apply artificial respiration if necessary. Obtain medical attention if ill effects occur.
	Skin Contact	Wash affected skin with plenty of soap and water. Remove contaminated clothing and wash before reuse. Obtain medical attention if ill effects occur.
	Eye Contact	If substance has got into the eyes, immediately wash out with plenty of water for at least 15 minutes. Obtain medical attention.
	Ingestion	If swallowed, rinse mouth with water (only if the person is conscious). Do not induce vomiting. Obtain medical attention.
4.2	**Most important symptoms and effects, both acute and delayed**	Unlikely to cause harmful effects under normal conditions of handling and use.
4.3	**Indication of the immediate medical attention and special treatment needed**	None

5. FIRE-FIGHTING MEASURES

5.1	**Extinguishing media**	
	Suitable Extinguishing Media	As appropriate for surrounding fire.
	Unsuitable Extinguishing Media	As appropriate for surrounding fire.
5.2	**Special hazards arising from the substance or mixture**	Combustion or thermal decomposition will evolve toxic and irritant vapours. (Nitrogen oxides)
5.3	**Advice for fire-fighters**	Self-contained breathing apparatus to be worn if involved in fire. Water spray should be used to cool containers.

6. ACCIDENTAL RELEASE MEASURES

6.1	**Personal precautions, protective equipment and emergency procedures**	Put on protective clothing.
6.2	**Environmental precautions**	Do not allow to enter drains, sewers or watercourses. If substance has entered a watercourse or sewer advise police and water authority.
6.3	**Methods and material for containment and cleaning up**	Adsorb spillages onto sand, earth or any suitable adsorbent material. Transfer to a lidded container for disposal. Clean area afterward with water and detergent
6.4	**Reference to other sections**	See Section: 8 (Exposure controls / PPE) & 13 (Disposal)

7. HANDLING AND STORAGE

7.1	**Precautions for safe handling**	Avoid contact with skin and eyes. Natural ventilation is adequate.
7.2	**Conditions for safe storage, including any incompatibilities**	Keep in the original container in a cool, dry place.
	Storage Temperature	Maximum temperature 25 degC. Product may be refrigerated but do not freeze
	Storage Life	Six months at 25 degC. After opening, use within two months
	Incompatible materials	Strong oxidising agents.
	Other information	Product may settle on storage Stir thoroughly before use

8. EXPOSURE CONTROLS / PERSONAL PROTECTION

8.1	**Control parameters**	
8.1.1	**Occupational Exposure Limits**	**WEL: Workplace Exposure Limit (UK HSE EH40)**
	LTEL (8 hr TWA mg/m³)	Not listed
	LTEL (8 hr TWA mg/m³)	Not listed
8.2	**Exposure controls**	
8.2.1	**Appropriate engineering controls**	Ventilation recommended. Follow the principles of good occupational hygiene to control personal exposures.
8.2.2	**Personal protection equipment**	
	Eye/face protection	Safety spectacles recommended.
	Skin protection (Hand protection/ Other).	Plastic or rubber gloves recommended
	Respiratory protection	No personal respiratory protective equipment normally required.
	Other	General hygiene measures for the handling of chemicals are applicable. Wash hands before breaks and after work. Wash contaminated clothing before reuse.
8.2.3	**Environmental Exposure Controls**	Do not allow to enter drains, sewers or watercourses.

9. PHYSICAL AND CHEMICAL PROPERTIES.

9.1	**Information on basic physical and chemical properties (Solution)**	
	Appearance	Liquid
	Colour	Black
	Odour	Slight
	Odour Threshold (ppm)	Not applicable
	pH (Value)	5-7
	Melting Point (°C) / Freezing Point (°C)	Approx -10 degC
	Boiling point/boiling range (°C)	Approx 102 – 105 degC
	Flash Point (°C) [Closed cup]	Not applicable. (Not combustible)
	Evaporation rate (Water = 1)	1
	Explosive limit ranges	Not applicable
	Vapour Pressure (mmHg)	17 mmHg at 20 degC (Water)
	Vapour Density (Air=1)	Not applicable
	Density (g/ml)	1.2 – 1.25 at 25 degC
	Solubility (Water)	Partially soluble
	Solubility (Other)	Partially soluble in organic solvents
	Partition Coefficient (n-Octanol/water)	Not applicable
	Auto Ignition Temperature (°C)	Not applicable
	Decomposition Temperature (°C)	> 100 degC (Partly Evaporates)
	Viscosity	Viscous liquid
	Explosive properties	Not explosive
	Oxidising properties	Not oxidising
9.2	**Other information**	

10. STABILITY AND REACTIVITY

10.1	**Reactivity**	Oxidises
10.2	**Chemical stability**	Stable under normal conditions
10.3	**Possibility of hazardous reactions**	Possibility of highly exothermic reaction with strong oxidizing agents
10.4	**Conditions to avoid**	High temperatures
10.5	**Incompatible materials**	Strong oxidising agents
10.6	**Hazardous Decomposition Product(s) Nitrogen oxides**	

11. TOXICOLOGICAL INFORMATION

11.1	**Information on toxicological effects**	
11.1.1	**Substances**	
	Acute toxicity	
	Ingestion	LD50 :>10 000 mg/kg (rat) (Calculated as product)
	Inhalation (4 hrs)	Not applicable
	Skin Contact	LD50 :> 10 000 mg/kg (rabbit) (Calculated as product)
	Skin corrosion / irritation	Unlikely to cause skin irritation
	Serious eye damage / irritation	Product is slightly irritant to eyes. Contains low concentrations (< 0.5%) of corrosive ingredients
	Respiratory or skin sensitization	Product is not sensitizing
	Mutagenicity	There is no evidence of mutagenic potential
	Carcinogenicity	No evidence of carcinogenicity
	Reproductive toxicity	No evidence of reproductive toxicity
	STOT-single exposure	**Inhalation:** Irritation of the respiratory tract. Coughing. Unlikely route of exposure.
		Ingestion: Nausea, vomiting
	STOT-repeated exposure (91 days)	NOAEL > 10 000 mg/kg/day(rat)(Calculated as product)
11.2	**Other information**	

12. ECOLOGICAL INFORMATION

12.1	**Toxicity**	
	(Fish) (96hrs)	LC50 > 1000 mg/l (Calculated as product)
	(Daphnia magna) (48hrs)	EC50 > 1 000 mg/l (Calculated as product)
	(Algae) (72hrs)	EC50 > 1 000 mg/l (Calculated as product)
12.2	**Persistence and degradability**	The organic ingredients are Biodegradable
12.3	**Bioaccumulative potential** (96 hrs)	The product has no potential for bioaccumulation.
12.4	**Mobility in soil**	The substance is predicted to have high mobility in soil.
12.5	**Results of PBT and vPvB assessment**	Not classified as PBT or vPvB.

13. DISPOSAL CONSIDERATIONS

13.1	**Waste treatment methods**	Do not empty into drains. Dispose of this material and its container at waste collection centre. Dried paint may be disposed of by landfill in accordance with local regulations.
13.2	**Additional Information**	The waste is considered to be non hazardous.
12.6	**Other adverse effects**	

14. TRANSPORT INFORMATION

14.1	**Land transport (ADR/RID)** UN number	Not classified as dangerous for transport.
14.2	**Sea transport (IMDG)** UN number	Not classified as dangerous for transport.
14.3	**Air transport (ICAO/IATA)** UN number	Not classified as dangerous for transport.

15. REGULATORY INFORMATION

15.1	**Safety, health and environmental regulations/legislation specific for the substance or mixture**	
15.1.1	**EU regulations** Authorisations and / or restrictions on use.	Not applicable
15.1.2	**National regulations**	Not applicable
15.2	**Chemical Safety Assessment**	No Chemical Safety Assessment (CSA) has been carried out

16. OTHER INFORMATION

References	European Chemicals Agency
	European Chemicals Bureau
	European Regulations and Directives
	Published chemical directories
	Suppliers' safety data sheets
	UK Health and Safety Executive
Risk Phrases	
Safety Phrases	
Hazard statement(s)	

Additional Information

Information contained in this publication or as otherwise supplied to Users is believed to be accurate and is given in good faith, but it is for the Users to satisfy themselves of the suitability of the product for their own particular purpose. **Bare Conductive Limited** gives no warranty as to the fitness of the product for any particular purpose and any implied warranty or condition (statutory or otherwise) is excluded except to the extent that exclusion is prevented by law. **Bare Conductive Limited** accepts no liability for loss or damage (other than that arising from death or personal injury caused by defective product, if proved), resulting from reliance on this information. Freedom under Patents, Copyright and Designs cannot be assumed.

Prepared by:
Edmund Fowles
EF Chemical Consulting Ltd
17 Kings Crescent East
Chester CH3 5TH
UK

T: +44 (0)1244 351644
E: edmund@efchemicalconsulting.co.uk

Bare Conductive® Electric Paint®

Technical Data Sheet

PRODUCT DESCRIPTION

Electric Paint is a nontoxic, water based, water soluble, electrically conductive paint. It can be used in circuits as a painted resistor element, a capacitive electrode or can function as a conductor in designs that can tolerate high resistivity. It is intended for applications with circuits using low DC voltages at low currents. **Electric Paint** adheres to a wide variety of substrates and can be applied using screen printing equipment. Its major benefits include low cost, solubility in water and good screen life. It is black in colour and can be over-painted with any material compatible with a water-based paint.

ADVANTAGES / PRODUCT BENEFITS

- High sheet resistance
- Nontoxic
- Water-soluble
- Can be used to create capacitive touch and proximity sensors
- Can be used as a potentiometer or resistive circuit element
- Compatible with many standard printing processes
- Low cost

TYPICAL PROPERTIES

Colour /	Black
Viscosity /	Highly viscous and shear sensitive (thixotropic)
Density /	1.16 g/ml
Sheet Resistance /	55Ω/sq at 50 micron film thickness
Vehicle /	Water-based
Drying Temperature /	**Electric Paint** should be allowed to dry at room temperature for 5 – 15 minutes. Drying time can be reduced by placing Electric Paint under a warm lamp or other low intensity heat source.

See below summary table of typical properties.

PROCESSING AND HANDLING

Screen Printing Equipment /	Manual
Screen Types /	Polyester, stainless steel (43T – 90T gauge mesh)
Typical Cure Conditions /	Room temperature (24˚C) for 15 minutes
Typical Circuit Line Width /	0.5 – 10mm (43T-mesh stainless steel screen)
Clean-up Solvent /	Warm water and soap
Sheet Resistance /	Approximately 32Ω/sq when using a brush or manual screen printing
Shelf Life /	6 months after opening
Storage /	**Electric Paint** should be stored, tightly sealed in a clean, stable environment at room temperature. Composition should be thoroughly mixed prior to use.

See below graph to predict resistance using manual screen printing.

Bare Conductive Ltd
First Floor, 98 Commercial St
London E1 6LZ
United Kingdom

First Floor, 98 Commercial St
London E1 6LZ, United Kingdom
+44 0 207 650 7977
info@**bareconductive.com**

TYPICAL PROPERTIES TABLE

TABLE 1 TYPICAL PHYSICAL PROPERTIES	
TEST	**PROPERTIES**
Sheet Resistance at 50 micron film thickness (Ω/sq)	55
Density (g/ml)	1.16
TABLE 2 COMPOSITION PROPERTIES	
Viscosity	Thixotropic
Thinner	Water

Table 1 and 2 show anticipated physical properties for **Electric Paint** based on specific controlled experiments in our labs when applied highly accurately. For more realistic values for application of the paint with brushes and screen printing see the below graph and equation. Further notes on working with **Electric Paint** can be found in **Application Notes**.

PROCESSING GRAPH AND EQUATION

When processed using manual screen printing one can expect a sheet resistance of approximately 32Ω/sq. The below graph illustrates how resistance changes with line shape and a simple equation can be applied to roughly predict surface resistance:

Resistance = 19.77(length/width) + 12

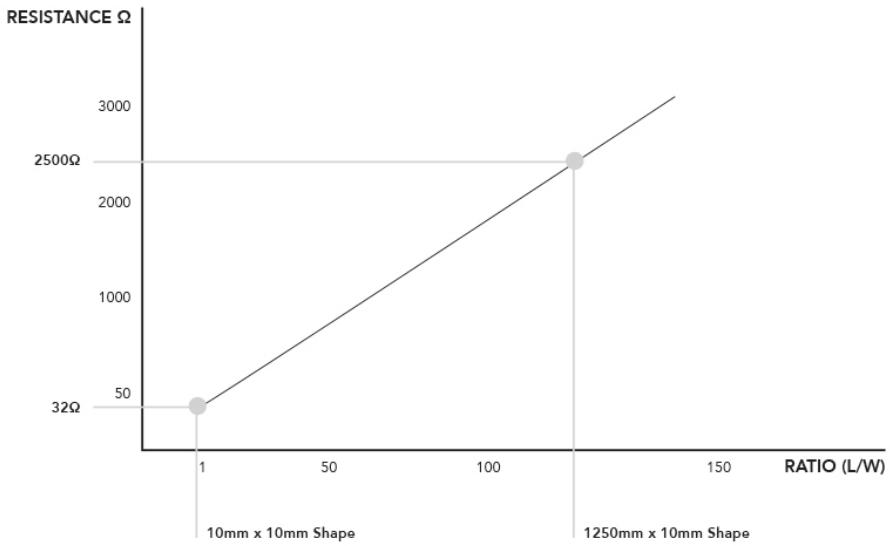

Bare Conductive Ltd
First Floor, 98 Commercial St
London E1 6LZ
United Kingdom

First Floor, 98 Commercial St
London E1 6LZ, United Kingdom
+44 0 207 650 7977
info@bareconductive.com